



University
of Glasgow

Khan, Saima Ishfaque (2016) The optical properties of metamaterials.
PhD thesis.

<http://theses.gla.ac.uk/7781/>

Copyright and moral rights for this thesis are retained by the author

A copy can be downloaded for personal non-commercial research or
study, without prior permission or charge

This thesis cannot be reproduced or quoted extensively from without first
obtaining permission in writing from the Author

The content must not be changed in any way or sold commercially in any
format or medium without the formal permission of the Author

When referring to this work, full bibliographic details including the
author, title, awarding institution and date of the thesis must be given



University
of Glasgow

The Optical Properties of Metamaterials

Saima Ishfaque Khan

Submitted in fulfilment of the requirements for
the degree of Doctor of Philosophy (Ph. D)

School of Engineering
College of Science and Engineering
University of Glasgow

June 2016
© S. I. Khan

Abstract

This thesis studies the parametric investigation, polarisation dependence and characterization of fishnet structure at near infrared wavelengths. Detailed simulations are performed to understand the behaviour of the structure at near infrared and optical wavelengths. Simulations are performed to obtain negative refractive index of the fishnet structure formed from nanoimprint lithography (NIL) by taking into account the effect of substrate and polymethyl methacrylate (PMMA) beneath it. Two different structures have been designed and fabricated of varying dimensions using NIL and their resonant wavelength measured in the near infrared at 1.45 μm and 1.88 μm . Simulations suggest that a negative refractive index real part with the magnitude -0.24 is found at 1.53 μm and this decrease to a maximum magnitude of -0.57 at 1.9 μm . The PMMA and suppressed pillars are here responsible for the increasing material losses and limiting the value of negative refractive index.

An analytical approach has been suggested to characterise fishnet structures at oblique incidence. The expressions for an absorbing medium are rewritten for an alternative definition of refractive index. The expressions are initially validated for a dielectric slab and a metal film. These results provide the possibility that this proposal may yield a general algorithm for obtaining the complex reflection and transmission coefficients for artificial structures. FDTD simulations have been extensively used in this thesis to understand the optical metamaterials and their characterization.

Acknowledgement

I humbly thank my God, the most gracious and the most merciful, who blessed me much more than I wished.

I pay my heartfelt gratitude and deep regards to my supervisor Dr. Nigel P Johnson for his continuous guidance, dynamic supervision and attentive support. Throughout my research, he has provided me support and encouragement. He has not only supported academically but motivated me in the most difficult years of my life. I am grateful to him from the bottom of my heart for considering me his PhD student.

Prof. Richard De La Rue has been a great source of inspiration and admiration. Despite his extraordinary professional commitments, he has always been very generous in finding time to me and discusses my work. There is many a time when words fall short of feelings. It is difficult to express my thoughts for both Prof. De la Rue and Dr. Nigel P Johnson. They did a lot for me.

I would like to thank Prof. John Arnold and Dr. Timothy Drysdale for helping me to learn simulation. I would like to say thanks to my colleagues and particularly Ifeoma & Dr. Graham Sharp for many fruitful discussions.

It is fair to admit that all my accomplishments, large or small, are possible because of my parents love, support and constant prayers for me. This is true that this thesis could not be written without my husband's generous support. It is no exaggeration that I owe a huge amount of my success to him. For this I will be forever grateful. It would be injustice not to mention my daughters Maryam & Sarah. They have encouraged me so very much and have been very helpful during difficult times.

I would like to acknowledge the financial support from HEC, Pakistan in the form of a doctoral scholarship.

Publications

- [1] Graham J. Sharp, S. I. Khan, A.Z. Khokhar, R. M. De La Rue and N. P. Johnson, “Negative index fishnet with nanopillars formed by direct nanoimprint lithography,” *Material Research Express*, 1(4), 045802.
- [2] S.I. Khan, G. J. Sharp, R. M. De La Rue, T. D. Drysdale and N. P. Johnson, “Modelling angle resolved complex reflection and transmission coefficients from fishnet structure formed from nanoimprint lithography,” In: *SPIE Photonics Europe*, Brussels, Belgium, 14-17 Apr 2014.
- [3] S.I. Khan, G. J. Sharp, R. M. De La Rue, T. D. Drysdale and N. P. Johnson, “Electromagnetic parameter retrieval at oblique incidence,” In: *Metamaterials VIII*, Prague, Czech Republic, 17-18 Apr 2013, 877118.
- [4] G. J. Sharp, S. I. Khan, A. Z. Khokhar, R. M. De La Rue and N. P. Johnson, “Negative index fishnet structure formed by nanoimprint lithography,” In: *SPIE Photonics Europe*, Brussels, Belgium, 14-17 Apr 2014.
- [5] N. P. Johnson, G. J. Sharp, S. I. Khan, I.G. Mbonson, S.G. McMeekin, B. Lahiri, and R.M. De La Rue, “Progress in metamaterial fishnet formed by nanoimprint lithography and asymmetric split ring resonators (A-SRRs) for sensing,”. In: *2014 16th International Conference on Transparent Optical Networks (ICTON)*, Graz, Austria, 6-10 Jul 2014, pp. 1-3.
- [6] R. M. De La Rue, I. G. Mbomson, S. I. Khan, G. J. Sharp, B. Lahiri and N. P. Johnson, “Molecular band Fano resonances in organic thin films enhanced by (A) SRR arrays,” In: *Active Photonic Materials VI*, San Diego, CA, USA, 17 Aug 2014, 916212-1-916212-4.
- [7] S.I. Khan, G. J. Sharp, R. M. De La Rue, T. D. Drysdale and N. P. Johnson, “Angle resolved reflection and transmission coefficients,” In: *Europmeta Conference*, University of Glasgow, UK, 2013.

Contents

| | |
|---|-----------|
| Abstract | i |
| Acknowledgement | ii |
| List of Publications | iii |
| Contents | iv |
| List of Figures | ix |
| List of Tables | xv |
| | |
| 1. Introduction | 1 |
| 1.1 Historical Overview | 4 |
| 1.2 The recent interest in metamaterials | 5 |
| 1.3 Numerical Modeling of metamaterials | 10 |
| 1.4 Thesis outline | 11 |
| 1.5 References | 13 |
| | |
| 2. Characterization of Metamaterials | 20 |
| 2.1 Introduction | 20 |
| 2.2 Electromagnetic Characterization theory | 21 |
| 2.3 Electromagnetic classification of artificial materials | 22 |
| 2.3.1 Classification of metamaterials | 23 |
| 2.4 Characteristic and effective material parameters | 23 |
| 2.5 Locality | 24 |
| 2.5.1 Locality requirements | 25 |
| 2.6 Dynamic retrieval approach | 26 |
| 2.6.1 Homogenization | 26 |
| 2.6.2 Pre-Requisites of homogenization | 27 |
| 2.6.3 Theoretical and heuristic homogenization of particle arrays. | 27 |
| 2.6.4 Characteristic material parameters of nanostructured materials | 28 |

| | | |
|-----------|---|-----------|
| 2.7 | Retrieval methods | 29 |
| 2.7.1 | Variable Angle Spectroscopic Ellipsometry | 30 |
| 2.8 | The NRW method | 32 |
| 2.8.1 | Determination of Effective parameters of metamaterials from reflection and transmission coefficients. | 33 |
| 2.8.2 | Electromagnetic parameter retrieval | 34 |
| 2.8.3 | Material parameter retrieval for inhomogeneous periodic structures | 37 |
| 2.8.4 | Analysis of retrieved parameters | 38 |
| 2.9 | Summary | 39 |
| 2.10 | References | 40 |
| 3. | Modifications in the Split-Ring Resonator | 44 |
| 3.1 | Introduction | 44 |
| 3.2 | First magnetic atom | 45 |
| 3.2.1 | Different topologies of Split Ring Resonator | 46 |
| 3.2.2 | Split ring resonator | 47 |
| 3.2.3 | Electric and magnetic coupling of SRR | 49 |
| 3.2.4 | Saturation of the magnetic response of SRR | 50 |
| 3.3 | Wire pair as magnetic atoms | 52 |
| 3.3.1 | Cut wire pair | 52 |
| 3.3.2 | Electric and magnetic coupling of the wire pair | 54 |
| 3.3.3 | Wide cut slab pair | 56 |
| 3.3.4 | Disadvantage of wire pair | 57 |
| 3.4 | Slabs & continuous wires | 59 |
| 3.5 | Optimized design | 63 |
| 3.6 | Summary | 64 |
| 3.10 | References | 64 |
| 4. | Metamaterials fishnet structures | 69 |

| | | |
|-----------|---|------------|
| 4.1 | Introduction | 69 |
| 4.2 | Numerical modeling of the fishnet structure | 70 |
| 4.2.1 | Simulation set up | 71 |
| 4.3 | Polarization dependence of the fishnet | 73 |
| 4.4 | Parametric investigation of fishnet structure | 75 |
| 4.4.1 | LC Circuit Model | 75 |
| 4.4.2 | The neck contribution in electromagnetic response of the fishnet | 78 |
| 4.4.3 | The slabs width contribution in electromagnetic response of the fishnet | 79 |
| 4.4.4 | The slabs length contribution in electromagnetic response | 80 |
| 4.4.5 | Discussion | 81 |
| 4.5 | Modelling of metallic constituent of the fishnet structure | 82 |
| 4.5.1 | Numerical Example | 83 |
| 4.6 | Fishnet at Visible frequency | 88 |
| 4.7 | Choice of metal | 91 |
| 4.8 | Effect of substrate | 96 |
| 4.9 | Multilayer fishnet structure | 96 |
| 4.9.1 | Simulation setup | 96 |
| 4.10 | Summary | 99 |
| 4.11 | References | 99 |
| 5. | Metamaterial fishnets formed from nanoimprint lithography | 102 |
| 5.1 | Introduction | 102 |
| 5.2 | Fabrication challenges | 103 |
| 5.2.1 | Electron-beam lithography | 104 |
| 5.2.2 | FIB milling | 104 |
| 5.2.3 | Nanoimprint lithography | 105 |
| 5.3 | Fabrication of fishnet using NIL | 106 |

| | | |
|-----------|--|------------|
| 5.3.1 | Stamp fabrication | 106 |
| 5.3.2 | Sample fabrication | 107 |
| 5.4 | Numerical modelling of fishnets formed from NIL | 109 |
| 5.4.1 | Simulation setup | 109 |
| 5.4.2 | Unit Cell | 111 |
| 5.5 | Reflection and transmission | 113 |
| 5.5.1 | Depth parameter | 114 |
| 5.5.2 | Measurements at infrared wavelength | 117 |
| 5.6 | Refractive index calculations | 120 |
| 5.7 | Figure of merit calculations | 125 |
| 5.8 | Field plots | 126 |
| 5.9 | Summary | 128 |
| 5,10 | References | 129 |
| | | |
| 6. | Angle Resolved Reflection and Transmission Coefficients | 134 |
| 6.1 | Introduction | 134 |
| 6.2 | Reflection and Transmission Coefficients at normal incidence | 136 |
| 6.2.1 | The NRW method at Oblique incidence | 139 |
| 6.2.2 | Reflection and transmission coefficients for an absorbing film | 141 |
| 6.3 | Numerical Examples | 147 |
| 6.3.1 | Dielectric slab | 147 |
| 6.3.2 | Metal film | 150 |
| 6.4 | Validity of results at normal incidence | 153 |
| 6.4.1 | Validity of results at oblique incidence | 157 |
| 6.4.2 | Numerical Example | 159 |
| 6.5 | Summary and conclusive remarks | 161 |
| 6.7 | References | 162 |
| | | |
| 7. | Conclusions and Future Work | 164 |

| | |
|--------------------|-----|
| 7.1 Thesis Summary | 164 |
| 7.2 Conclusions | 167 |
| 7.3 Future work | 168 |
| Appendix | |

List of Figures

| | | |
|-----------------|--|----|
| Fig. 1.1 | Parameter space for ϵ and μ . The two axes correspond to the real part of permittivity and permeability respectively. | 2 |
| Fig. 1.2 | Orientation of the field quantities E , H , Poynting vector S and wave vector k in (a) metamaterials and (b) conventional materials. | 3 |
| Fig. 1.3 | Three dimensional photonic metamaterials are shown. This Figure is taken from reference [36]. a) Split ring resonator. b) Single layer fishnet metamaterials. c) Stereo or chiral metamaterials d) Double negative index metamaterials with several layers. e) SRR oriented in all three directions fabricated through membrane projection lithography f) chiral metamaterials g) Connected cubic symmetry negative index metamaterials structure. h) Metal clusters of cluster visible frequency magnetic metamaterial. | 8 |
| Fig. 2.1 | Classification of metamaterials [12] | 24 |
| Fig. 2.2 | Illustration of NRW method used for the determination of effective material parameters from reflection and transmission data. | 33 |
| Fig. 3.1 | A single unit cell of double concentric Split Ring Resonator. | 45 |
| Fig. 3.2 | Different topologies of Split Ring Resonator. | 46 |
| Fig. 3.3 | The equivalent LC circuit used for the description of split ring resonator | 47 |
| Fig. 3.4 | Simulated transmittance and reflectance spectra for Split Ring Resonator for TE and TM polarizations. The geometric parameters are taken from reference [13]. The thickness of the gold film is 20 nm, width $w = 90$ nm, length l of the SRR is 320 nm, and the gap d between the arms is 70 nm. The lattice constant is $a = 450$ nm. | 50 |
| Fig. 3.5 | A wire-pair structure with its equivalent RLC circuit is shown where l is the length of the short wire pairs, w is the width, t_s is the separation between short wire pairs and t_m is the metal thickness. | 53 |

- Fig. 3.6** Simulated Reflectance (blue) and Transmittance (red) obtained from the 55
wire pair structure for two different lengths (a) $l = 500$ nm, (b) $l = 400$
nm. The geometric parameters for the Figure 3.5 are $w = 150$ nm, $t = 20$
nm, $d = 80$ nm, lattice constants $a_x = 500$ nm and $a_y = 1050$ nm. The
polarisation configuration for electric field component of
electromagnetic wave (*TE* Polarisation) is also shown [31].
- Fig. 3.7** Simulated Reflectance (blue) and Transmittance (red) obtained from the 56
wire pair structure for two different lengths (a) $l = 500$ nm, (b) $l = 400$
nm. The geometric parameters are same for Figure 3.6. The polarisation
configuration for electric field component of electromagnetic wave (*TM*
Polarisation) is also shown [31].
- Fig. 3.8** a) The electric permittivity ϵ and b) magnetic permeability μ obtained 58
from the simulated reflection and transmission coefficients [31]. The
geometric parameters are same for Figure 3.6.
- Fig. 3.9** Real (blue) and imaginary (red) part of refractive index retrieved from 59
simulated reflection and transmission coefficients [31]. The geometric
parameters are same for Figure 3.6.
- Fig. 3.10** A 3D view of short wire-pair and continuous wire-pair is shown. 60
- Fig. 3.11** Simulated reflection and transmission coefficients obtained from slabs 61
and continuous wire pair shown in Figure 3.10. The geometric
parameters are taken from reference [34] for structure shown in Figure
3.10.
- Fig. 3.12** Retrieved material parameters (a) real and imaginary part of electric 62
permittivity (b) real and imaginary part of magnetic permeability. The
geometric parameters are taken from reference [34] for structure shown
in Figure 3.10.
- Fig. 3.13** Real and imaginary part of refractive index. The geometric parameters 63
are taken from reference [34] for structure shown in Figure 3.10.

- Fig. 4.1** Unit cell of perforated fishnet structure with dielectric spacer MgF_2 embedded in between two metal Ag layers. The thickness of metal films $t_m = 30$ nm and dielectric spacer $t_d = 40$ nm are kept constant. 72
- Fig. 4.2** Sketch of the fishnet structure, a_x and a_y are the unit cell sizes along x and y directions respectively. w_x and w_y show the hole size. t_m and t_d are the thickness of metal films and dielectric spacer respectively. The dimensions of geometric parameters are given in Table 4.1. 72
- Fig. 4.3** Simulated Reflection/Transmission/Absorption obtained from a fishnet structure. The polarisation configuration is also shown. 74
- Fig. 4.4** Simulated reflection/transmission/absorption coefficients obtained from TM Polarisation 74
- Fig. 4.5** The equivalent RLC circuit used for the description of fishnet structure shown in Figure 4.1. 76
- Fig. 4.6** Simulated reflection spectra of fishnet structure for different widths of neck w_y . The geometric parameters are shown in Table 4.1 for the structure shown in Figure 4.1. The results are shown for three different neck widths of the fishnet structure i.e., 250 nm, 150 nm and 100 nm. 78
- Fig. 4.7** Simulated reflection spectra for fishnet structure for different widths of slab a_y . The geometric parameters are shown in Table 4.1 for the structure shown in Figure 4.1. The results are shown for three different slab widths of the fishnet structure i.e., 600 nm, 500 nm and 400 nm. 79
- Fig. 4.8** Simulated reflection spectra for fishnet structure for different lengths of slab w_x . The geometric parameters are shown in Table 4.1 for the structure shown in Figure 4.1. The results are shown for two different slab widths of the fishnet structure i.e., 300 nm, 200 nm. 80
- Fig. 4.9** Comparison of real and imaginary parts of refractive index for gold with Johnson-Christy data, Drude A, Drude B. a) Real part of refractive index $\text{Re}(n)$ b) Imaginary part of refractive index $\text{Im}(n)$. 84
- Fig. 4.10** Retrieved electromagnetic parameters for the fishnet structure. The geometric parameters are shown in Table 4.1. a) Real and imaginary part 86

- of ϵ b) Real and imaginary part of μ c) Real and imaginary part of n .
- Fig. 4.11** Comparison of Drude model (B) and Johnson & Christy data for the fishnet structure a) Real and imaginary part of n b) Real and imaginary part of μ . 87
- Fig. 4.12** Comparison of the Figure of Merit for the fishnet structure for three different material data sets for gold. 88
- Fig. 4.13** Reflection/transmission/absorption coefficient obtained from fishnet structure at visible frequency region. The geometric parameters are given in Table 4.2. 89
- Fig. 4.14** Retrieved electromagnetic material parameters for the fishnet structure at visible frequency range a) Real and imaginary part of ϵ b) Real and imaginary part of μ c) Real and imaginary part of n . 90
- Fig. 4.15** Comparison of real and imaginary part of refractive index for gold (Au), silver (Ag), copper (Cu), aluminium (Al). 91
- Fig. 4.16** Comparison of a) real and b) imaginary part of refractive index n for fishnet structures in visible frequency range for gold (Au), silver (Ag), copper (Cu), and aluminium (Al). 92
- Fig. 4.17** Comparison of a) real and b) imaginary part of μ for fishnet structure at visible frequency range for gold (Au), silver (Ag), copper (Cu) and aluminium (Al). The geometric parameters are given in Table 4.2. 93
- Fig. 4.18** Comparison of FOM for fishnet structure at visible frequency range for different metals. The geometric parameters are given in Table 4.2. 94
- Fig. 4.19** Simulated a) Reflection b) Transmission obtained from a multilayer fishnet structure. The results are in agreement with the reference [24]. The geometric parameters are given in Table 4.3. 98
- Fig. 5.1** An angled micrograph of a SiC stamp used for imprinting showing etched pillars 1 μm in height 107
- Fig. 5.2** Angled *SEM* micrograph of structure B showing, in detail, the interlocking Ag–MgF₂–Ag wires, and imprinted nano-pillars pushed into *PMMA*. The dark region located between the fishnet and 108

imprinted nano-pillar is *PMMA*

- Fig. 5.3** 3D model of an ideal single unit cell of the fishnet with pillars, detailing 111
 dimensions and material thickness (not to scale). The depth of the PMMA
 layer at its thickest, d_z is 1000 nm. This is the thickness of the PMMA
 when it is spun on to the SiO₂ substrate and same thickness is used for
 modelling. The thickness of SiO₂ substrate is kept as semi-infinite in the
 simulations. The fishnet sits on the top of the sample with the pillars
 pressed down into the PMMA layer. The imprinted depth of the pillars in
 the PMMA is denoted by d_i , which equals 300 nm for both designs. The
 metal-dielectric-metal tri-layer of silver-magnesium fluoride-silver (Ag-
 MgF₂-Ag) is denoted by *m-d-m* and has a total thickness of 110 nm (30
 nm Ag, 50 nm MgF₂, 30 nm Ag). Light incident normally on the top of
 the fishnet is polarized as shown. The electric field component is parallel
 to thin wire tracks of the structure and perpendicular to the wide tracks
- Fig. 5.4** Sketch of the NIL fishnet metamaterials slab used for the retrieval of 112
 negative refractive index.
- Fig. 5.5** Simulated transmission and reflectance spectra of fishnets and 115
 nanopillars of varying dimensions. The spectra are obtained from
 structures patterned to the specifications detailed in Figure 5.4. The data
 used to obtain these results is shown in Table 5.2.
- Fig. 5.6** Simulated transmission and reflectance spectra of fishnets and nano- 116
 pillars of varying dimensions. The spectra are obtained from structures
 patterned to the specifications detailed in Figure 5.4. The data used to
 obtain these results is shown in Table 5.3.
- Fig. 5.7** Measured and simulated transmission and reflectance spectra of fishnets 117
 and nanopillars of varying dimensions, with a micrograph of each
 structure inset. The scale bar is 2 μ m in both instances. The spectra are
 obtained from structures patterned to the specifications detailed in Figure
 5.4. The shaded regions on both plots indicate the wavelengths at which
 n is negative [27].

- Fig. 5.8** Experimental transmission spectra of an unpatterned, 1mm thick fused quartz substrate without PMMA. It is the same type as used for measurements of the fabricated structures. This data is taken from reference [27]. 119
- Fig. 5.9** Real and imaginary values of refractive index n obtained from simulations modelling the fishnet and pillars structure supported on PMMA for the dimensions of (a) structure A (b) structure B. The discontinuities observed are taking scaling of dimensions into consideration, consistent with those previously reported by Koschny et al [34] and Zhou et al [39]. 123
- Fig. 5.10** Real and imaginary values of refractive index n obtained from simulations modelling fishnets only without the PMMA, metal-dielectric-metal pillars and SiO₂ substrate. Values are obtained using dimensions measured from the fabricated fishnets and with the structure suspended in air. (a) Real and imaginary part of refractive index obtained from structure A. (b) Real and imaginary part of refractive index obtained from structure B. 124
- Fig. 5.11** (a) The FOM calculated for the structure A (b) The FOM calculated for the structure B. 125
- Fig. 5.12** Field plot showing a unit cell of the fishnet and nanopillar on the x - y plane from normal incidence. The electric field distribution of a single unit cell of structure B at resonant wavelength 1.88 μm , has shown the top silver layer of the fishnet and aperture on the x - y plane. The wide metal tracks exhibit a strong electric field induced by the magnetic field of the incident wave. 126
- Fig. 5.13** Field plots showing the electric field across two different planes of structures, with incident light as polarized in Figure 5.3. An outline of the structure has been added for clarity. Axis values are in microns and indicate the dimension of each structure. (a) A cross section of the structure A (x - z) plane showing the electric field distribution of the Ag- 127

MgF₂-Ag in the fishnet, pillars and supporting PMMA at a wavelength of 1.44 μm. (b) The *x-z* plane cross section field plot of structure B at a wavelength of 1.88 μm. The field plots in Figures 5.10(a) and (b) show electromagnetic coupling between the fishnets and pillars, through the PMMA

- Fig. 6.1** An illustration of The NRW retrieval procedure applied to a finite thickness lattice of small particles at oblique incidence 139
- Fig. 6.2** An absorbing film situated between two dielectric media. The thickness of the absorbing film is h and refractive index is n_2 . The refractive indices of dielectric media are n_1 and n_3 . 141
- Fig. 6.3** a) Reflectance and b) Transmittance of a dielectric slab for TE polarization. 148
- Fig. 6.4** a) Reflectance and b) Transmittance of a dielectric slab for TM polarization. 149
- Fig. 6.5** a) Reflectance and b) Transmittance of a finite thickness metal film as a function of wavelength for TE polarization. 151
- Fig. 6.6** a) Reflectance and b) Transmittance of a finite thickness metal film as a function of wavelength for TM polarization. 152
- Fig. 6.7** a) Reflectance and b) Transmittance of a dielectric slab for normal incidence as a function of wavelength. 154
- Fig. 6.8** a) Reflectance and b) Transmittance c) Absorbance of a metal film for normal incidence 156
- Fig. 6.9** Reflectance and Transmittance of a metal film of a finite thickness metal film as a function of wavelength. 160

List of Tables

| | | |
|------------------|---|-----|
| Table 4.1 | Table listing the geometric parameters for the unit cell of fishnet structure shown in Figure 4.1. | 73 |
| Table 4.2 | Table listing the geometric parameters for the unit cell of fishnet structure shown in Figure 4.1 for visible range. | 89 |
| Table 4.3 | Table listing the geometric parameters for the unit cell of multilayer fishnet structure shown in Figure 4.1 | 97 |
| Table 5.1 | Table listing measured dimensions of the two fabricated structures. The same dimensions are used for modelling. | 112 |
| Table 5.2 | Table listing measured dimensions of the fabricated structures. These dimensions are used for understanding the behaviour of the structure shown in Figure 5.3. | 113 |
| Table 5.3 | Table listing depth parameter of the simulated structures. These dimensions are used for understanding the behaviour of the structure shown in Figure 5.3. | 114 |

1. Introduction

The notion of metamaterials includes a wide range of engineered structures with designed properties. The useful and unusual properties of metamaterials are offered by the specific response of their constituents and their arrangement [1-5]. The structural units of these rationally designed structures can be tailored in both shape and size. To achieve new functionality, inclusions can be designed and placed at desired locations. The desired properties of these materials mainly depend upon their geometry rather than their composition. Metamaterials were introduced about a decade ago and they represent a broad class of micro or nanostructures composed of tailored building blocks. These sub-wavelength building blocks can be densely packed in to an effective material. This deceptively simple, powerful and truly revolutionary concept allows the synthesis of novel, and unusual properties. These properties include magnetism at optical frequencies, negative refractive indices, large positive refractive indices, zero reflection *via* impedance matching, perfect absorption, giant circular dichroism, or enhanced nonlinear optical properties. The possible applications of metamaterials comprise ultrahigh-resolution imaging systems, compact polarization optics, and cloaking devices.

The existence of homogeneous substances with negative permittivity ϵ and/or permeability μ in nature was first discussed in 1967 by Veselago. There are four kinds of substances according to the values of ϵ and μ which are considered theoretically. All the electromagnetic materials with all possible combinations of ϵ and μ can be placed in a parameter space. Materials found in the first quadrant, where both ϵ and μ have positive values are conventional materials or known to be transparent. A negative value of ϵ (μ) indicates that the direction of the electric (magnetic) field induced inside the material is in the opposite direction to the incident field. Noble metals at optical frequencies are good examples of for materials with negative ϵ . A negative μ can be found in ferromagnetic media near a resonance [6]. No propagating waves can be supported in materials represented by the second and fourth quadrants, where one of the two parameters is negative and the index of refraction becomes purely imaginary. All conventional materials are confined to an extremely narrow zone around a horizontal line at $\mu=1$ in the space as shown in Figure1.1

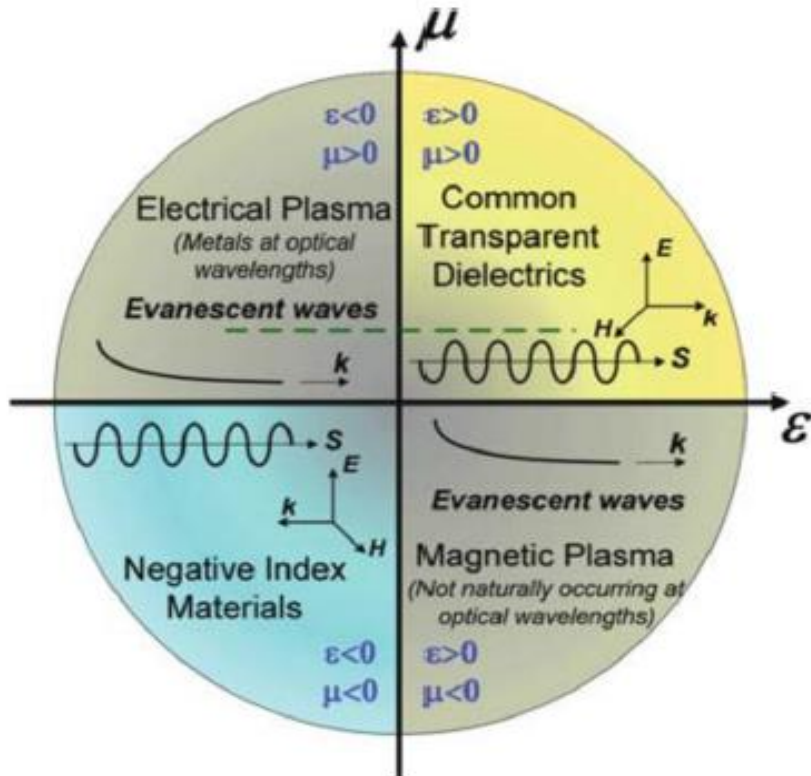


Figure 1.1: The parameter space for ϵ and μ . The two axes correspond to the real part of permittivity and permeability respectively [10].

In an anisotropic medium, the field vectors E and D are not necessarily parallel to each other; hence the permittivity must be in the form of a tensor rather than a scalar value. Anisotropic and strongly dispersive features generally occur in most of metamaterials. For this reason, one should always specify the frequency and direction under consideration while addressing effective parameters in a metamaterial. Various kinds of passive artificial media are under consideration, and these media can be divided into two large classes. In the first class the spatial period of the inclusions in the hosting material is small compared to the wavelength. It means that the spatial dispersion effects are weak. In the second case there are structures in which those characteristic sizes are comparable with the wavelength known as photonic crystals [7]. This is a situation of strong spatial dispersion, and the usual material description in terms of ϵ and μ loses their sense.

The word meta means beyond in Greek, so the name metamaterials refers to beyond conventional materials. This term is widely used and can have different meanings from different point of views [8, 9]. Several other names for these materials are also in use. It is mentioned in the literature that this term should be used for three-dimensional volumetric or

bulk structures. Media with only one negative parameter are sometimes called single-negative *SNG*, specifically either ϵ -negative *ENG* or μ -negative *MNG* media. Many authors use the term left-handed media.

To understand the properties of metamaterials one need to revise the basic laws of electromagnetism. The refractive index of the material is defined as

$$n = \sqrt{\epsilon\mu}$$

where ϵ is the dielectric permittivity of the material and μ is the magnetic permeability of the material. Since the refractive index of the material depends upon the ϵ and μ of the material it is possible for a material to possess a negative refractive index by having simultaneously negative permittivity and negative permeability. For centuries people had believed that refractive index can only be positive until negative index was introduced by Vaselago.

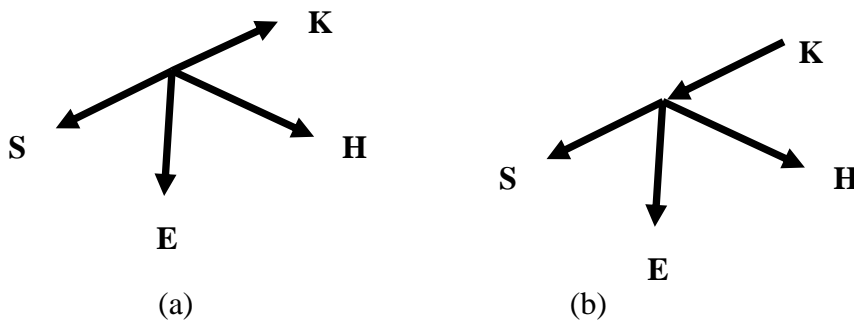


Figure 1.2: Orientation of the field quantities E , H , Poynting vector S and wave vector k in (a) metamaterials with left handed behaviour and (b) conventional materials.

Light has an unmatched speed and it can transmit data in a signal of zero mass. It is an electromagnetic wave that is composed of electric and magnetic fields; its propagation is determined by both the electric and magnetic responses of the medium. In isotropic media the electric and magnetic responses are characterized by dielectric permittivity and magnetic permeability. Light remains one handed when interacting with atoms of conventional material because from the two field components of light, only the electric component interacts the material properly whereas the magnetic component remains relatively unused because the interaction of atoms with the magnetic field component is normally weak. But artificially designed materials can allow both field components of light to be coupled to atoms of the metamaterials, enabling new exciting properties.

In the case of $\mu > 0$ and, $\varepsilon > 0$ the vectors E , H and k form a right-handed triplet, and if $\mu < 0$ and $\varepsilon < 0$, they form a left-handed set. The vector k is in the direction of the phase velocity, it is clear that left-handed substances are substances with negative group velocity, which occurs in particular in anisotropic substances or when there is spatial dispersion. Orientation of the field quantities E , H , and wave-vector k in conventional material and metamaterials are shown in Figure 1.2.

The negative refractive index is one among the many fascinating properties. It provides the basis for the negative index materials *NIM*. The existence of negative index materials brings the concept of refractive index into a new domain and revolutionizes present day optoelectronics. The existence of *NIM* provides an opportunity for scientists to revise the interpretation of basic laws because the index of refraction enters into basic formulae for optics.

The refractive index is a complex number

$$n = n' + n''$$

where n'' is the imaginary part that characterizes light extinction. The real part gives the factor by which the phase velocity is decreased in a material as compared with the vacuum. Hence the phase velocity is directed against the flow of energy in *NIM*, also the vectors E , H , and k form a left handed system.

1.1 Historical Overview

The earliest publication on backward waves and on negative refraction was that of lecture notes of Prof. I.I. Mandelshtam [11]. Backward waves were observed in mechanical system by Lamb in 1904 [7] and by H.Pocklington [12]. The logic of Mandelshtam was simple. He mentioned that in the case of negative dispersion the wave in the medium is backward and negative refraction should occur at interface with such a medium. The possibility of negative refraction was also mentioned by A. Schuster in [13]. However he meant the anomalous dispersion and not negative one as a possible reason of the negative refraction [13]. Mandelshtam who gave examples of fictitious 1D media with negative group velocity form acoustic waves presented an example of a 3D structure supporting backward electromagnetic waves [14]. It was an inhomogeneous material with permittivity

periodically varying in space. This work predicted the negative refraction in photonic crystals later discovered by M. Notomi [15].

In 1946-1959 L. Brillouin [16] and J.R. pierce [17] developed the theory of backward wave microwave tubes utilizing the RLC circuit model and pointed out the antiparallel phase/group velocities propagation. In 1951 G.D. Malyuzhinets generalized this concept to the 3D case in hypothetical backward wave media [18]. An equivalent 1D analogue of this media was artificial transmission lines depicted by Malyunzhinets [19].

Materials with negative parameters such as backward wave materials were mentioned by D.V. Sivukhin in 1957[20]. He was the first one who noticed the media with negative parameters are continuous and homogeneous backward wave media. He stated that media with $\mu < 0$ and $\varepsilon < 0$ are not known and the question on the possibility of their existence has not been clarified [20].

In 1960s 1D backward wave structures were studied in connection with the design of microwave tubes and slow wave periodic systems [21-23]. The negative refraction phenomenon in periodical 2D media was discussed by R. A. Silin [24-25]. The historical overview of metamaterials is taken from references [2, 3].

1.2 The recent interest in metamaterials.

The paper published by Veselago in 1967 provoked considerable interest at the time. Surprisingly, however, real metamaterial research did not start until about three decades later, when several seminal papers were published [26-28]. The idea of having negative effective material parameters and thus a negative refractive index was stunning, but it lacked practical applications. In 1999, Pendry et al. [29] showed that microstructures built from nonmagnetic conducting sheets exhibit an effective magnetic permeability μ , which can be tuned to values not accessible in naturally occurring materials. An example of such a structure is an array of non-magnetic thin sheets of metal, planar metallic split-rings [29].

The Split-Ring Resonator *SRR* continues to be a paradigm example [30]. The incident light field can induce a circulating and oscillating electric current in the ring, leading to a magnetic dipole-moment normal to the ring. The realisation of a material with a negative refractive index was shown by Smith in 2000 in the paper [27]. Veselago had been looking

for such a material for many years. But unfortunately he did not find the proper way. He had intended to build the metamaterial as a mixture of natural materials with electric and magnetic anisotropy. The problem was always with high losses and the resonance of magnetically and electrically anisotropic materials at different frequencies. The idea of Smith et al. was different because it utilized a composite material, not a homogeneous one. A great number of research groups started to work in this novel and promising directions after the publication of seminal papers [27-28]. Many different approaches and areas of particular interest appeared. The magnetic-dipole resonance of the *SRR* has reminded the optics community that light is an electromagnetic wave. If one aims at obtaining complete control over an electromagnetic light wave inside a material, one needs to be able to independently control both the electric and the magnetic fields. The newly achieved magnetic control has opened one half-space of optics which is still not considered in many text books.

There has never been shortage of new ideas in the field of metamaterials. Several conditions must be fulfilled to make the transition from a curious scientific finding to a real world material usable by the optics industry.

- First the operational frequency must be brought to the optical including visible range.
- Second, the structures should have several or even many layers of truly three dimensional unit cells to approach the bulk *3D* limit and to qualify as a “material”.
- Third the losses should be reasonably low.

An increase of the operational frequency has become possible by miniaturizing and redesigning the magnetic *SRRs*. However it is required to achieve negative electric permittivity and negative permeability simultaneously and hence negative refractive index at the same frequency. *SRRs* along with the long metal wires could not provide negative electric permittivity and negative permeability at the same frequency [31, 32]. To overcome this problem the structure was redesigned. This redesign has led to the so called double fishnet negative index structure [33]. To qualify as a material, it is required to see how many layers are sufficient for convergence of metamaterials when going from a single layer to many layers. The next obvious step was to stack an integer number of functional layers of the double fishnet to eventually achieve a bulk *3D* negative index metamaterials [34].

The optical properties of a few-monolayers of a thin film are significantly different from those of a 50-nm film, although the fact that the total thickness is much smaller than one optical wavelength in both cases. The situation in metamaterial is more complex, because the building blocks can interact strongly. Therefore, one must study how the effective optical parameters changes as the number of layers increases. Thus, there is no unique answer to the above question. In some cases, a single functional layer may be sufficient; in other cases, a few layers are needed. The answer strongly depends on the spacing between neighbouring unit cells and coupling between adjacent layers. If the distance between adjacent functional layers is small, the coupling is strong; the convergence of the optical properties is slow. It requires at least four functional layers [35].

If one aims at achieving functionalities other than negative refractive indices, flexibility in tailoring the metamaterials unit cell interior is another crucial factor. For instance, strong chirality which is the prerequisite for large optical activity and circular dichroism requires the lack of a mirror plane parallel to the substrate.

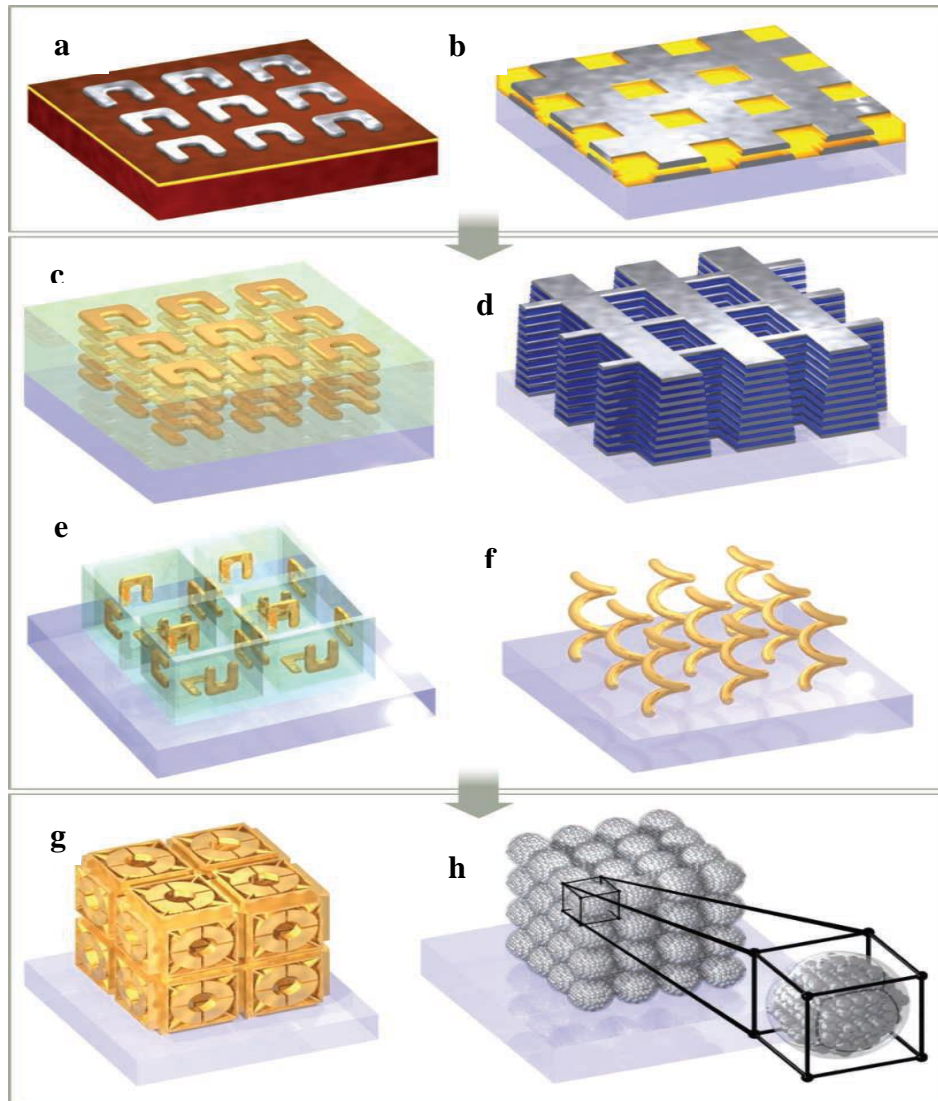


Figure 1.3: Three dimensional photonic metamaterials are shown. This Figure is taken from reference [36]. a) Split ring resonator. b) Single layer fishnet metamaterials. c) Stereo or chiral metamaterials d) Double negative index metamaterials with several layers. e) SRR oriented in all three directions fabricated through membrane projection lithography f) chiral metamaterials g) Connected cubic symmetry negative index metamaterials structure. h) Metal clusters of cluster visible frequency magnetic metamaterial.

Chiral structures have led to huge circular dichroism and optical activity at optical frequencies [37, 38], but not yet to negative refractive indices in contrast to microwave [39-41] and far-infrared frequencies [42-43]. Tunable chiral metamaterials have been experimentally fabricated, and exhibit tunable optical activity and a tunable refractive index [44].

Isotropy remains as a goal for some of the metamaterials shown in Figure 1.3. Indefinite or hyperbolic metamaterials rely on intentional anisotropy. The notion hyperbolic metamaterials stems from the resulting hyperbolic shape of the iso-frequency surfaces in wave vector space [45]. These anisotropic systems can be used to achieve broadband all-angle negative refraction and super lens imaging [46, 47].

All of the above metamaterials lead to large inherent losses at optical or even at infrared frequencies. It is also interesting to ask whether purely dielectric materials might offer effective magnetic or negative index metamaterials properties. Mie resonances of dielectric particles play a key role in achieving a negative magnetic permeability [48-55].

Metamaterial losses become an increasingly important issue while moving from single metamaterials layers or metasurfaces towards bulk metamaterials. The level of losses can be quantified by a figure of merit *FOM*. It is defined as

$$FOM = |\text{Re}(n)/\text{Im}(n)|$$

This dimensionless number allows comparison of metamaterials operating in different wavelength regimes in a meaningful manner. These large losses are due to the fact that the region of $n < 0$ is near to the resonance of the single unit cell where $\text{Im}(n)$ is large. Thus, $\text{Im}(n)$ and hence losses can be reduced by moving $n < 0$ further away from resonance. An actual desired increase in *FOM* by several orders of magnitude appears to be out of reach at optical frequencies even though future design optimizations may lead to certain improvements.

An obvious approach is to introduce gain materials in the metamaterials structure to compensate for the loss. Large magnitude gain coefficients are hard to obtain in practice. This challenge may be hard to solve but not impossible. Recent experiments on single layer of double negative index structures in which the intermediate dielectric layer spacer was doped with dye molecules have raised hopes [56].

Electromagnetic materials have come a long way from microwave frequencies to visible throughout this decade. They have become truly bulk *3D* materials at optical frequencies, for certain propagation directions and/or for certain polarizations of light. But none of these intricate *3D* structures is yet available in gram quantities. Thus, one of the future challenges is to fabricate large- scale *3D* isotropic metamaterials. Some nanofabrication technologies

have specifically been developed for this purpose or have been modified accordingly. This comprises stacked electron-beam lithography, membrane projection lithography, direct laser writing and electroplating, as well as particular bottom-up self-assembly approaches [57,58].

Much of the photonic metamaterial research has been inspired by the fascinating and far reaching vision of the perfect lens. This concept was introduced by John Pendry and is based on the idea of lossless isotropic negative index materials. This may never come true but it has fuelled an entire field. One should not forget that the field of electromagnetic metamaterials is still very young when it comes to applications or products. However the conceptual and technological progress has truly been dramatic.

1.3 Numerical Modelling of metamaterials

Numerical approaches are vital for the design and analysis of metamaterials. We use analytic solutions for the analysis of electromagnetic problems but if they are not available, semi-analytic solutions are a good alternative because they can quickly complete solutions to a very high accuracy. However, sometimes semianalytic solutions are not useful because of geometry or material considerations. The processing power of modern computing has been increasing linearly. The advances in the computer technology have directly affected scientific research. Multicore central processing units *CPU* allow multitasking procedures and vast amount of memory is now accessible.

In general, numerical techniques can be divided in time and frequency domain. The frequency domain method can solve Maxwell's equation for only one particular frequency at a time. They are not appropriate to simulate devices, where their performance over a broad frequency spectrum is highly desirable. However they produce very accurate and stable results for complicated structures, which cannot be analysed using analytical techniques. The most important frequency domain methods are Finite Element Method (*FEM*) and Method of Moments (*MOM*).

In contrast, the time domain techniques solve Maxwell's equations for the whole frequency spectrum with single simulation. However, these methods can easily become unstable, especially when computationally large and complicated electromagnetic problems are considered. The most widely used time domain methods are the Finite-Difference Time

Domain Method (*FDTD*), Finite Integral Method (*FIM*), and the Transmission Line Methods (*TLM*).

The *FDTD* method has been proven to be one of the most effective numerical methods in the study of metamaterials. This method is widely used because it is simple to implement numerically. It provides a flexible means for directly solving Maxwell's time dependent curl equations by using finite differences to discretize them. Developments of *FDTD* schemes that are more accurate and computationally efficient are continuing and the method is still evolving.

The aim of numerical modelling is to achieve fast, reliable and accurate characterisation of electromagnetic metamaterials. Lumerical Solutions based on *FDTD* method is used in this thesis to simulate characterize and optimize metamaterials at optical frequencies. The *FDTD* method is most appropriate technique for the accurate and efficient modelling of these structures. It is essential to simulate metamaterials to predict their performance. They give the opportunity to optimize designs because design optimization is challenging and results are not always intuitive.

It is really challenging to simulate metamaterials because they can have feature sizes an order of magnitude smaller than the wavelength. It is difficult to model thin layers of metal which are dispersive in nature. Mostly silver and gold are used in this work. A very fine mesh is used to accurately model the metal patches of the metamaterials studied in this thesis. The Drude model is used to describe the properties of metal. Lumerical solutions offer Multi-Coefficient Model (*MCM*) for describing material properties. Most metamaterials are periodic structures so one unit cell with periodic boundary conditions are simulated. If the structure has symmetry then it is possible to reduce the simulation volume by replacing periodic boundary conditions with symmetric/antisymmetric boundary conditions depending upon the polarization of source. A perfectly matched layer (*PML*) boundary condition is used in the direction of propagation of the electromagnetic source.

1.4 Thesis Outline

Chapter1: The definition of metamaterials along with historical overview is briefly discussed. The recent interest in metamaterials and progress in the development of this research area is briefly discussed.

Chapter2: This chapter presents an important aspect of metamaterials research. It is of prime importance to define and specify the applicability domain and physical meaning of material parameters that are used to characterize metamaterials. Because a broad class of applications is based upon the specialized electromagnetic materials, the difference between characteristic and effective material parameters is established. The effects of spatial dispersion and locality requirements are discussed. The most widely used method for the characterization of metamaterials, the *NRW* method is discussed in detail. This chapter is concluded by providing the analysis of the retrieved material parameters obtained by the *NRW* method.

Chapter3: Firstly, the elementary units of negative index materials are discussed. Different topologies of *SRRs* are also briefly discussed. The knowledge of basic magneto-statics has been employed to create this structure. The design provides negative magnetic permeability at microwave frequency. The reasons for the saturation of magnetic resonance frequency are summarized. Further, the conventional *SRR* has been flattened to result in a wire-pair arrangement. Simulation results are shown for both *TE* and *TM* modes. As both of these structures do not provide negative refractive index, the two additional wires are placed on either side of the short wires. Hence, there is always room for improvement by optimizing the details of geometrical parameters and by choosing the most successful of various designs. Finally, the optimization rules are summarized to obtain high quality metamaterials at optical frequencies.

Chapter4: In this chapter the fishnet structure which is an optimized design to obtain negative refractive index is discussed in detail. Parametric investigation of the structure is performed with the help of an *LC* equivalent circuit. The polarisation dependence of the structure is shown with the help of simulations and the response of the structure for the visible frequency range is provided. Detailed simulations are performed for different choices of metal and material data with effect of substrate and dielectric spacer explained. Multilayer fishnet structure is simulated and convergence of negative refractive index n is shown.

Chapter5: Aiming at development of high quality 3D optical metamaterials, the fishnet is fabricated by NIL and optically characterized. The fabrication challenges are briefly outlined. After a short description of fabrication techniques, the steps involved for the fabrication of fishnet by NIL are briefly discussed. The structure is designed and simulated using Lumerical Solutions. Simulation results are shown for the reflection/transmission properties of the structure in comparison with the measurements results. The structure is characterized by using the Standard Retrieval Method. A negative refractive index is obtained for the structure by taking into account the effect of substrate which is PMMA in this instance. Simulation suggest that negative refractive index real part with a magnitude as large as 5, with the figure of merit *FOM* of 2.74 can be obtained.

The fabrication and measurements of fishnet structure formed from nanoimprint lithography are done by Dr. Graham Sharp (University of Glasgow).

Chapter6: The *NRW* method has the potential to be extended towards the oblique incidence. Here, an idea is put forward to extend *NRW* method for the oblique incidence. The reflection/transmission coefficients for a dielectric slab at oblique incidence are obtained with the help of Parameter Sweep Method by using Lumerical Solutions. The results are also obtained by analytical expressions to validate the simulation results. The reflection and transmission coefficients for thin metal film at oblique incidence are obtained with the help of Parameter Sweep Method. The analytical expressions for thin metal film are rewritten for an alternative definition of refractive index which matches the simulation results. The research work is still in progress and needs further analysis to be comprehensively explained.

Chapter7: This chapter draws an overall conclusion of the research. Suggestions have been made for the future research work.

1.6 References

- [1] W. Cai, V. Shalaev *Optical metamaterials: Fundamentals and applications*, Springer (2010).
- [2] F. Capolino *Metamaterials Handbook vol 1 Theory and Phenomena of Metamaterials* (Boca Raton, FL: CRC Press) (2009).
- [3] F. Capolino *Metamaterials Handbook vol 2 Applications of Metamaterials* (Boca Raton, FL: CRC Press) (2009).
- [4] V.M Shalaev, “Optical negative index metamaterials,” *Nature Photonics*. 1 41-48 (2007).
- [5] S. A. Ramakrishna “Physics of negative refractive index materials,” *Rep. Prog. Phys.* 68 449 (2005).
- [6] G. Thomson, “Unusual waveguide characteristics associated with the apparent negative permeability obtainable in ferrites,” *Nature*, Vol. 175, pp. 1135–1136 (1995).
- [7] J. D. Joannopoulos, S. G. Johnson, R. D. Meade, and J. N. Winn. “*Photonic Crystals: Molding the Flow of Light*,” Second edition. Princeton Univ. Press, (2008).
- [8] A. Sihvola “Metamaterials in electromagnetics (invited review),” *Metamaterials*, Vol. 1, pp. 2-11. (2007).
- [9] A. Sihvola and I. Lindell “On the three different denotations of handedness in wavematerial interaction,” *Pisa: URSI International Symposium on Electromagnetic Theory*, pp. 84-86. (2004).

- [10] G. Parisi, "Propagation of Electromagnetic Waves in Fishnet Metamaterials," (2012).
- [11] L. Mandelshatm, 15, 476 (1945).
- [12] H. C. Pollington, *Nature*, 71 607-608 (1905).
- [13] A. Schuster, *An Introduction to the Theory of Optics*, 2nd edn, London: E. Arnold (1909).
- [14] L. I. Mandelshatm, "Lectures on some problems of the theory of oscillations," pp.428-467 (1950).
- [15] M. Notomi, "Theory of light propagation in strongly modulated photonic crystals: Refraction like behaviour in the vicinity of photonic band gap," *Phys. Rev. B*, 62 10696 (2000).
- [16] L. Brillouin, "Wave propagation in periodic structures," New York McGraw-Hill, (1946).
- [17] J.R. Pierce, "Travelling wave tubes," NewYork: Van Nostrand, (1950).
- [18] G.D. Malyuzhinets, 21, 40. (1951).
- [19] A. Grbic and G. eleftheriades, "Periodic analysis of 2D negative refractive index transmission line structure," *IEEE Trans. Antennas propagate*, 51, 2604-2611 (2003).
- [20] C. Caloz and T.Itoh, "Transmission line approach of left handed (LH) materials and microstrip implementation of an artificial LH transmission line," *IEEE Trans. Antennas Propagat*, 52, 1159-1166 (2004).
- [21] D.V. Sivukhin, *Opt Spectroscopy*, 3, 308, (1957).

- [22] R.G. E. Hutter, *Beam and wave electronics in microwave tubes*, Princeton, (1960).
- [23] J.L. Altman, *Microwave circuits*, Princeton, (1964).
- [24] R. A. Silin and V. P. Sazonov, *Slow-Wave Structures*, Moscow: Soviet Radio, (1966).
- [25] R. A. Sillin, 4, Moscow: Soviet Radio, (1959).
- [26] D. R. Smith, W. J. Padilla, D. C. Vier, S. C. Nemat-Nasser, and S. Schultz, “Composite medium with simultaneously negative permeability and permittivity,” *Phys. Rev. Lett*, Vol. 84, pp. 4184–4187, (2000).
- [27] J. B. Pendry, “Negative refraction makes a perfect lens,” *Phys. Rev. Lett.*, Vol. 85, pp. 3966–3969. (2000).
- [28] D. R. Smith, N. Kroll, “Negative refractive index in left-handed materials,” *Phys. Rev. Lett.*, Vol. 84, pp. 2933–2936, (2000).
- [29] J. B. Pendry, A.J. Holden, D. J. Robbins, and R. J. Stewart, “Magnetism from conductors and enhanced nonlinear phenomena *IEEE Trans. Microwave Theory Tech*, Vol. 47, pp. 2075–2084. (1999).
- [30] J. B. Pendry, A.J. Holden, D. J. Robbins, and R. J. Stewart, “Photonic band gap effects and magnetic activity in dielectric composites,” *IEEE Trans. Microw. Theory* 47, 2075-2084 (1999).
- [31] V. M. Shalaev, W. Cai, U. Chettiar, H.-K. Yuan, and A. K. Sarychev, V. P. Drachev, and A. V. Kildishev, “Negative index of refraction in optical metamaterials,” *Opt. Lett.* 30, 3356-3358 (2005).

- [32] C. M. Soukoulis, S. Linden, and M. Wegener, “Negative refractive index at optical wavelengths,” *Science* 315, 47-49 (2007).
- [33] S. Zhang, W. Fan, B. K. Minhas, A. Frauenglass, K. J. Malloy, and S. R. J. Brueck, “Mid-infrared resonant magnetic nanostructures exhibiting a negative permeability,” *Phys. Rev. Lett.* 94, 037402 (2005).
- [34] S. Zhang, W. Fan, N. C. Panoiu, K. J. Malloy, R. M. Osgood and S. R. J. Brueck, “Optical negative-index bulk metamaterials consisting of 2D perforated metal-dielectric stacks,” *Opt. Express* 14, 6778-6787 (2006).
- [35] J. F. Zhou., Th. Koschny, M. Kafesaki, and C.M Soukoulis, “Negative refractive index response of weakly and strongly coupled optical metamaterials,” *Phys. Rev. B* 80, 035109 (2009).
- [36] C. M. Soukoulis, M. Wegner, “Past achievement and future challenges in the development of three dimensional photonic metamaterials”, www.nature.com/nature photonics, July, (2011).
- [37] M. Decker, “Strong optical activity from twisted-cross photonic metamaterials,” *Opt. Lett.* 34, 2501-2503 (2009).
- [38] M. Decker, R. Zhao, C. M. Soukoulis, S. Linden, and M. Wegener, “Twisted split-ring-resonator photonic metamaterial with huge optical activity,” *Opt. Lett.* 35, 1593-1595 (2010).
- [39] E. Plum, “Metamaterial with negative index due to chirality,” *Phys. Rev. B* 79, 035407 (2009).
- [40] J. F. Zhou, “Negative refractive index due to chirality,” *Phys. Rev. B* 79, 121104 (2009).

- [41] F. Z. Li, "Chiral metamaterials with negative refractive index based on four "U" split ring resonators," *Appl. Phys. Lett.* 97, 081101 (2010).
- [42] S. Zhang, "Negative Refractive Index in Chiral Metamaterials," *Phys. Rev. Lett.* 102, 023901 (2009).
- [43] X. Xiong, "Construction of a chiral metamaterial with a U-shaped resonator assembly," *Phys. Rev. B* 81, 075119 (2010).
- [44] J. Zhou, R. Zhao, C. M. Soukoulis, A. J. Taylor, and J. O'Hara, "Chiral THz metamaterial with tunable optical activity," *Proceedings of the Conference on Lasers and Electro-Optics, CTuF* (2010).
- [45] A. Fang, Th. Koschny, C. M. and Soukoulis, "Optical anisotropic metamaterials: Negative refraction and focusing," *Phys. Rev. B* 79, 241104 (2009).
- [46] S. Kawata, A. Ono, and P. Verma, "Subwavelength colour imaging with a metallic nanolens," *Nature Photon.* 2, 438-442 (2008).
- [47] C. F. Bohren, D. R. & Huffman, "Absorption and scattering of light by small particles," (Wiley, 1983).
- [48] S. O'Brien, J. B. Pendry, "Photonic band-gap effects and magnetic activity in dielectric composites," *J. Phys.: Condens. Mat.* 14, 4035-4044 (2002).
- [49] L. Peng, "Experimental observation of left-handed behaviour in an array of standard dielectric resonators," *Phys. Rev. Lett.* 98, 157403 (2007).
- [50] A. J. Schuller, R. Zia, T. Taubner, & M. L. Brongersma, "Dielectric metamaterials based on electric and magnetic resonances of silicon carbide particles," *Phys. Rev. Lett.* 99, 107401 (2007).

- [51] K. Vynck, "All-dielectric rod-type metamaterials at optical frequencies," *Phys. Rev. Lett.* 102, 133901 (2009).
- [52] C. L. Holloway, E. F. Kuester, J. Baker-Jarvis, & P. Kabos, "A double negative (DNG) composite medium composed of magnetodielectric spherical particles embedded in a matrix," *IEEE Tran. Antenn. Propag.* 51, 2596-2603 (2003).
- [53] A. Ahmadi, and H. Mosallaei, "Physical configuration and performance modeling of all-dielectric metamaterials," *Phys. Rev. B* 77, 045104 (2008).
- [54] X. Cai, R. Zhu, and G. Hu, "Experimental study of metamaterials based on dielectric resonators and wire frame," *Metamaterials* 2, 220-226 (2008).
- [55] S. Xiao, "Loss-free and active optical negative-index metamaterials," *Nature* 466, 735-738 (2010).
- [56] G. M. Whitesides, and B. Grzybowski, "Self-assembly at all scales," *Science* 295, 2418-2421 (2002).
- [57] R. M. Erb, H. S. Son, B. Samanta, V. M. Rotello, and B. B. Yellen. "Magnetic assembly of colloidal superstructures with multipole symmetry", *Nature* 457, 999-1002 (2009).
- [58] N. Lui, "Planar metamaterial analogue of electromagnetically induced transparency for plasmonic sensing", *Nano Lett.* 10, 1103-1107 (2010).

2. Characterization of Metamaterials

2.1 Introduction

Characterization in material science refers to the use of external techniques to probe the internal material structure (geometric characterization) and the properties of materials such as elemental content, chemical properties, electric conductivity, static permeability and hysteresis, mechanical thermal properties etc. The problem of the electromagnetic characterization of nanostructured materials has been only scantily studied and methods and the techniques of this characterization are not sufficiently developed in spite of the fast development of nanoscience and nanotechnologies. There are several reasons for this. Among them is a significant part of known nanostructures are not materials in the common meaning of the term. It is difficult to characterize an artificial material because artificial materials are extended heterogeneous structures comprising a huge number of interactive constitutive elements. It is not only unclear how to calculate or how to measure their electromagnetic characteristic parameters. Even a list of these characteristic parameters has not been conclusively established.

It is of prime importance to define and specify the applicability domain and physical meaning of every material parameter that is used to characterize a structured material. The parameters that describe the material properties in a condensed way consistently and unambiguously can be called characteristic material parameters. The effective material parameters results from a homogenization procedure. An adequate homogenization model guarantees that the effective material parameter fit the concept of electromagnetic characterization. It gives an accurate and practically useful description of the material response to electromagnetic waves.

The electromagnetic parameters of artificial materials are of primary concern because a broad class of application is based upon the specialized electromagnetic materials. This chapter presents an important aspect of metamaterials research. After a short introduction of electromagnetic characterization theory, classification of artificial structures and

metamaterials is explained. The difference between characteristic and effective material parameters is established. Effects of spatial dispersion and locality requirements are discussed in detail. Pre-requisites of homogenization and the difference between theoretical and heuristic homogenization is discussed.

The two main retrieval methods, The Nicholson-Ross-Weir (NRW) method and Variable Angle Spectroscopic Ellipsometry (VASE) are explained. The NRW method is discussed in detail as it is most widely used method for the characterization of metamaterials. The procedure for the retrieval of effective material parameters from reflection and transmission coefficients is given. However this method is not trivial in general so the applicability limits of these material parameters is also discussed in detail.

2.2 Electromagnetic Characterization theory

Characterization in material science refers to the use of external techniques to probe the internal material structure (geometric characterization) and the properties of materials such as elemental content, chemical properties, electric conductivity, static permeability and hysteresis, mechanical thermal properties etc. The results of the characterization of a bulk metamaterial by definition do not depend upon the sample shape and measuring setup, whereas for interface and surface phenomena the geometry is taken into account. The electromagnetic characteristic material parameters are not parameters specific for one kind of wave incidence or one kind of sample geometry.

The problem of electromagnetic characterization of nanostructured materials, and methods and techniques of electromagnetic characterization are not sufficiently developed. To characterize the electromagnetic properties of nanostructured materials, researchers encounter a very basic difficulty. It is difficult to characterize an artificial material rather than a device because artificial materials are extended heterogeneous structures comprising a huge number of interacting constitutive elements.

It is not only unclear how to calculate their electromagnetic characteristic parameters, even a list of these constitutive parameters has not been established yet. One researcher characterizes the nanostructured material by dielectric permittivity. Another one claims for the same material with some permeability. The third one claims that these characteristic material parameters have no physical meaning. Still further researcher claims that these material

parameters must be complemented with some additional material parameters. It is difficult to judge which approach is correct.

2.3 Electromagnetic classification of artificial materials

The possibilities of combining nanosized inclusions are infinite. Metamaterials are most interesting from the point of view of electromagnetic properties. They are defined as artificial structural elements designed to achieve advantageous and unusual electromagnetic properties. One can find many types of nanostructured materials which satisfy the definition of metamaterials. It is instructive to introduce a classification of these materials to show the place of metamaterials among all these nanostructured materials. Different type of nanostructured materials should be described by different sets of electromagnetic parameters. This classification takes in to account the internal geometry of nanostructured materials. It also takes into account linear electromagnetic properties of constituents and effective medium formed by them.

The first criterion of the classification is the dimension of unit cell which forms the nanostructured materials. Three dimensional or bulk materials correspond to structures with the large number of unit cells in any direction. Two dimensional materials correspond to the artificial material which is including only 1-3 constitutive elements. These types of metamaterials are called as metasurfaces [1, 2] and metafilms [3-5].

The second criterion of the classification is the optical size of the unit cell in the optical and near-IR frequency range. Several known nanostructures usually operate in this range and possess useful and unusual electromagnetic properties. The structures which possess large optical size or are optically sparse cannot be characterized by local material parameters. The structures which are optically dense can be characterized by local electromagnetic parameters and can be referred as metamaterials. An important example of artificial structures is photonic crystals which are optically sparse nanostructures. They cannot be referred as metamaterials since they do not fit the concept of effectively continuous materials. The third criterion is the presence or absence of properties which allow us to refer or not to refer an optically dense material to metamaterials.

2.3.1 Classification of metamaterials

Metamaterials are classified based on their material properties and their electromagnetic behaviour. Artificial dielectric media with optically dense nanocomposites can have unusual permittivity. It can have permittivity close to zero or -1. They can have very high permittivity in the visible range where normal materials except some very lossy semiconductors and liquid crystals that have low permittivity

Artificial structures possessing negative magnetic permeability in the visible range are also called as metamaterials. Media with $\mu = 0$ or even $\mu = 2$ in the optical range are also called as metamaterials. The most known type of metamaterials is the media with both negative permittivity and permeability. Material with $\epsilon = 0$ and $\mu = 2$ in the visible range should be referred as magneto-dielectric metamaterials. Optically dense nanocomposites with plasmonic inclusions refer to metamaterials for both cases of regular and random arrangements. Regular plasmonic composites do not possess additional scattering losses and are more promising for applications. They can also behave as resonant multipole media and resonant bianisotropic media formed by nanoparticles. The number of material parameters describing such media is larger than two.

2.4 Characteristic and effective material parameters

The characteristic material parameters (*CMP*) of composite media are those material parameters satisfying basic physical limitations and applicable to different wave processes. In contrast the traditional concept of effective material parameters (*EMP*) are parameters retrieved from reflection R and transmission T coefficients of composite layers.

The electromagnetic (*CMP*) of a given material should be applicable to different wave processes in the sample and for different samples filled with the same material. In a maxima list approach the term (*CMP*) can be granted to only those parameters which do not depend upon the sample shape and size and they are independent of the external sources and therefore do not depend on the electromagnetic field distribution in the sample. Such (*CMP*) would give a fully condensed description of linear electromagnetic properties of the material sample from which the sample is prepared, where the electromagnetic parameters of materials cannot be measured directly, the retrieval of (*CMP*) from measured data is

necessary. Not only composite media, but (*CMP*) of natural media are also measured indirectly.

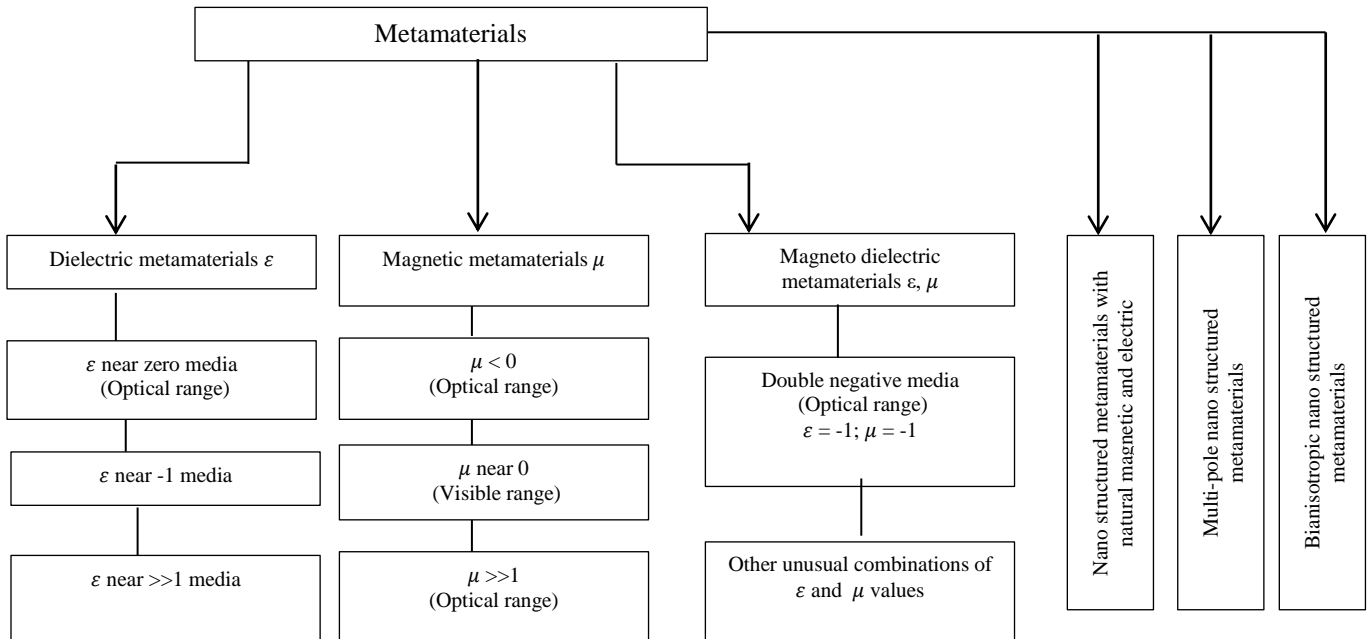


Figure 2.1: Classification of metamaterials [12].

The effective material parameters (*EMP*) can be in principle retrieved from scattering parameters assuming that the effective medium formed by atoms or molecules is continuous. One can conclude that (*EMP*) retrieved from the field scattered by the sample of natural materials fit the concept of (*CMP*) if the (*EMP*) of natural materials describe their electromagnetic properties for any shape of the macroscopic sample and for any angle of the incidence of plane wave. But this is not true for all composite media.

2.5 Locality

If the material parameters of a medium depend only on the frequency and possibly, the medium is called a local isotropic medium. It is also useful in some situations to be able to assume that the spatial variation in the medium is slow by comparison with the wavelength of the electromagnetic wave but this assumption is not valid in photonic crystals or metamaterials structures. If the medium is isotropic, the properties of the local medium do not vary with the orientation of the electric and magnetic fields or the propagation direction of electromagnetic waves.

The local medium assumption practically means that the material parameters;

- are independent of the spatial distribution of the wave fields excited in the material sample by a source.
- are independent of the geometrical size and shape of the sample.

Spatial dispersion is the name of an effect based on non-locality of the electromagnetic response of material. It is one of the key notions in the theory of artificial electromagnetic materials. The spatial dispersion is negligible when the inclusions forming a composite material as well as distance between them are small. The composite behaves as a normal material. If the homogeneity scale is on the order of a wavelength or larger as in the case for instance, in photonic crystals the material cannot be described using effective material parameters. In order to have pronounced artificial magnetism the inhomogeneity should not be too small or nor too large in order to allow for an effective medium description to be valid.

2.5.1 Locality requirements

The locality requirement is respected for bulk *EMPs* only if the following conditions are fulfilled [7, 8].

- **Passivity** For the temporal dependence of $e^{-i\omega t}$ it implies that $\text{Im}(\epsilon) > 0$ and $\text{Im}(\mu) > 0$ at all frequencies, for $e^{j\omega t}$ the sign of both $\text{Im}(\epsilon) > 0$ and $\text{Im}(\mu)$ should be negative. The violation of passivity is equivalent to the violation of second law of thermodynamics. The signs of real parts of ϵ and μ are subject to no physical restriction. Any non-steady process in an actual body is to some extent thermodynamically irreversible. The electric and magnetic losses in a variable electromagnetic field therefore always occur to some extent. That is the functions $\epsilon''(\omega)$ and $\mu''(\omega)$ are not exactly zero for any frequency other than zero. It therefore follows that the imaginary parts of ϵ and μ are always positive. [9,10]
- **Causality** For media with negligible losses it corresponds to the conditions $\frac{\partial(\omega\epsilon)}{\partial\omega} > 1$ and $\frac{\partial(\omega\mu)}{\partial\omega} > 1$. This in practice means that in the frequency regions where losses are small material parameters obviously grow versus frequency:

$$\frac{\partial \text{Re}(\epsilon)}{\partial \omega} > 0 \quad \text{and} \quad \frac{\partial \text{Re}(\mu)}{\partial \omega} > 0.$$

- The independence of the material parameters on the wave propagation direction. It means the independence for incidence angles for planar slabs [11].

If these mandatory locality requirements are not respected for material parameters retrieved from reflection R and transmission T coefficients over the essential frequency range, this indicates the dependence of these parameters on the spatial field distribution, and these extracted material parameters are redundant. It is, therefore, of prime importance to define and specify the applicability area and the physical meaning of every parameter that is used to characterize a material and to answer following questions.

- How to introduce effective material parameters of the composite media. What is the physical meaning of them and in which electrodynamics problems are such material parameters applicable?
- What are the frequency bounds in which these retrieved effective material parameters keep their meaning and applicability?
- What are the physical limitations that should be imposed on these effective material parameters, and can be used as a check of calculations, measurements, and finally in practical applications? [11].

In the literature devoted to electromagnetic characterization of composite media, all these questions are not answered properly.

2.6 Dynamic retrieval approach

2.6.1 Homogenization

The introduction of effective electromagnetic parameters of a material is called homogenization. Homogenization means that material parameters of an artificial material are obtained and constitutive relations in which these parameters are known. In the homogenization approach a heterogeneous structure is replaced by an effectively homogeneous one. Any homogenization theory is an approximation because it employs a finite number of parameters to describe samples with huge number of molecules. In the case of artificial materials these molecules are inclusions. In the case of metamaterials the response of these inclusions is dispersive. This means that effective parameters significantly depend on the frequency of excitation. The only alternative approach to this macroscopic

description is directly solving the microscopic Maxwell equations where each and every electron should be accounted for separately. This is absolutely not realistic in any practical situation when we deal with material samples containing huge number of molecules or small particles, in the case of metamaterials and other nanostructures.

In order to design a new electromagnetic material, one should find the optimal shape and chemical content of inclusions, their optimal size and mutual arrangement, the optimal distance between them. This means that many realizations of the material should be considered before the optimal design is obtained. The homogenization allows one to avoid the exact simulation of each realization, each size and each shape of material samples.

2.6.2 Pre-Requisites of homogenization

The description of the medium composed of particles as continuous medium (possibility of homogenization) is determined by the following conditions [12].

The first condition requires that the composite media can be represented as an array of lattice with geometrically identical or at least nearly identical unit cells. The nearly identical unit cells refer to media where particles in the unit cells can deviate from their statistically averaged positions. However in the majority of unit cells these deviations are small enough so that the number of particles per unit cell is almost constant. This condition allows the homogenization in terms of the spatially uniform material parameters.

The second condition of homogenization is that the microscopic spatial distributions of fields and polarization currents are slowly varying between adjacent unit cells. The small variation of microscopic field distribution from cell to cell is the key pre-requisite for homogenization. If the wave phase shift qa (where q is the wave number and a is the lattice period) between any two adjacent unit cells is much smaller than π , then homogenization is possible. It is difficult to determine the exact frequency bounds of homogenization for particular metamaterial experimentally; however they can be estimated theoretically [12].

2.6.3 Theoretical and heuristic homogenization of particle arrays

The procedure of introducing material parameters for media of particles is called homogenization. There are two main approaches to the homogenization of lattices resulting in material parameters. One approach is theoretical and it starts from the averaging of

microscopic fields and microscopic polarization/magnetization which satisfy microscopic Maxwell's equations and the continuity equation. The averaging results in the material equations and the relations for material parameters entering these equations. These relations express material parameters through susceptibilities of individual particles and other parameters of the original heterogeneous structure. Every theoretical model does not guarantee that material parameters resulting from it give a condensed description of the material response to electromagnetic waves, i.e. that these material parameters are *CMP*. It is necessary to analyse the properties of waves of different polarizations, propagating at different directions in the lattice to assess whether the material parameters are representative of the characteristic parameters.

The applicability of these material parameters should also be checked and the same set of material parameters should describe eigen waves propagating at different angles with respect to the lattice axes. If these material parameters are suitable for describing the wave reflection and transmission at the interface at different angles of incidence, then one can finally conclude that this set of material parameters fits the characterization concept. These material parameters represent the set of *CMP* [13].

Many researchers working with metamaterials prefer a simplistic approach to their material parameters suggested in [14-16] which can be called heuristic homogenization. In this approach the sample formed by artificial particles in the dielectric matrix is heuristically replaced by a sample of the same shape and size filled with uniform continuous magneto-dielectric medium with unknown ϵ and μ . These two complex quantities can be retrieved from measurement or from exact numerical simulation of two scattering parameters at a specific angle of the wave incidence and polarization. These material parameters are effective material parameters and are not *CMP* i.e. the sample composed of the actual metamaterial will have all scattering characteristics identical to those of the effective continuous magneto-dielectric medium with these retrieved parameters. It is not shown in any known result that effective material parameters retrieved in this way for any metamaterial are applicable to many angles of incidence and for both *TE* and *TM* polarizations of the incident wave. These *EMP* do not fit the concept of *CMP* because they are only applicable to the same case of the wave incidence in which they were retrieved.

2.6.4 Characteristic material parameters of nanostructured materials

It is not a realistic task to define a unique set of *CMP* which would give description suitable for the whole spatial spectrum of electromagnetic waves produced by all possible external sources. It is possible to use one set of material parameters applicable for propagating waves and another set of parameters for evanescent waves. A set of *EMP* deserves to be called as *CMP* if they are applicable to describe the interaction of the sample with plane waves in a certain interval of incidence angles (say 0-60°). But it is essential to remember that *EMP* retrieved for one special angle of incidence (normal incidence) does not fit the concept of *CMP* if these *EMP* are inapplicable for all other incidence angles.

The nanostructured metamaterials can be realized as layers of inclusions where their tangential size is much larger than the wavelength of the incidence electromagnetic wave at which they operate and are also much larger than the layer thickness. As a rule metamaterial layers are designed so that they comprise an integer number N of unit cells across them. This common practice has softened the restrictive requirement of the independence of *CMP* on the sample shape and now only the independence of *CMP* on N is required. In other words, *CMP* of bulk metamaterial should not depend on the number N of unit cells across the layer.

Material parameters of a continuous medium, once extracted from the specific wave processes are applicable to all wave processes. They are unique for any sample shape, unique for all incidence angles, and even unique for all evanescent waves. The *NRW* method applied to composite media is exactly heuristic homogenization.

2.7 Retrieval methods

In order to understand the properties of these artificial materials and to evaluate the applicability of a structure to the target applications, one should first determine if a particular structure can be described by a few parameters. The sample of the composite material under consideration is shaped as a planar slab. It is necessary to take into account few more things. First it is necessary to see whether the sample is a piece of an effectively homogeneous material or a complicated mesoscopic structure i.e. the sample changes its properties from sample to sample depending on its size, shape and environment. The second important aspect of the retrieval is to see the effects of spatial dispersion. Third, it is required to determine the type of material for instance isotropic, anisotropic, bianisotropic, chiral or gyrotropic. After determining the type of a material, the numerical values of

constitutive parameters are determined as a function of frequency. There are two main methods of the electromagnetic characterisation of composite media.

- Variable Angle Spectroscopic Ellipsometry (VASE)
- The Nicholson-Ross-Wier method (The *NRW* method)

2.7.1 Variable Angle Spectroscopic Ellipsometry

Ellipsometry is the method of choice for the experimental determination of the permittivity of thin and bulk materials [17, 18]. Ellipsometry measures obliquely incident reflected and transmitted polarization ratios. Oblique incidence lifts the polarization degeneracy and expands the number of measurable parameters to four complex values for both reflection and transmission coefficients [19]. Ellipsometry uses the ratio of polarized reflection coefficients. In the Jones formalism one defines the polarization states as orthogonal electric field components E_p and E_s . Reflection of an incident light ray from a surface is expressed by the Jones matrix [19].

$$\begin{bmatrix} E_{rp} \\ E_{rs} \end{bmatrix} = \begin{bmatrix} r_{pp} & r_{ps} \\ r_{sp} & r_{ss} \end{bmatrix} \begin{bmatrix} E_{ip} \\ E_{is} \end{bmatrix} \quad (2.1)$$

Where matrix elements are the reflection co-efficients and the subscripts r and i denote the reflected and incident rays. The ratios between the electric fields of the incident and reflected waves of the same polarization are denoted by $r_{ss, pp}$ and the ratio of cross-polarized reflected electric field to the corresponding incident fields by $r_{sp, ps}$.

In isotropic materials the off diagonal elements r_{ps} and r_{sp} are zero. The diagonal elements r_{pp} and r_{ss} may then be simply written r_p and r_s , the ratio of which defines the ellipsometric angles ψ and Δ as [19].

$$\rho = \frac{r_p}{r_s} \equiv \tan \psi e^{i\Delta} \quad (2.2)$$

The angles ψ and Δ correspond to the amplitude ratio and the phase difference of the reflection coefficients, respectively. Linearly polarized obliquely incident light beams are used to probe the electromagnetic properties of layers. The polarization plane is chosen so that the amplitudes of the electric fields in the incidence plane and the electric field in the orthogonal plane are equal. The reflection coefficients for the two polarizations are different for oblique angles.

Ellipsometry can measure the complex ratio of reflection coefficients r_{pp}/r_{ss} at different angles. Modern setups can measure also reflection and transmission amplitudes $|r_{ss}|^2$ and $|t_{pp}|^2$. If the sample is transparent it is possible to measure the same ratios as well as amplitudes for respective transmission coefficients. After assuming that sample layer under test is isotropic or anisotropic, the permittivity can be derived from the Fresnel formulas [17, 18]. This technique works very well for the normal materials where the sample under consideration behaves as effectively continuous. But it runs into fundamental problems if the structure needs more advanced model to describe its electromagnetic properties.

It is a serious technical challenge to measure the complex reflection and transmission coefficients. If the film and or/substrate are optically anisotropic, and the measurement is not performed along an optical axis, a proportion of p polarized light is converted into s polarized light and vice versa and the off diagonal elements of the Jones matrix are non-zero. They may be determined by using the generalized ellipsometry.

This method is a combination of the ellipsometry and spectroscopy and is applicable to characterize layers of anisotropic media whose complex permittivity is described a tensor. The known modifications of ellipsometric method are called as Variable Angle Spectrometric Ellipsometry VASE [20, 21]. It has been recognized as most useful and highly accurate method of experimental determination of material parameters from the data of optical measurements. Measurements are made at several incidence angles of light. The angle of incidence is controlled by a computer which varies between 50° - 180° but this is dependent upon the sample type [22]. The spectrometer measures the ratio of s and p components for different angles. The existing software [23] fit the angular dependence of these results to the mathematically generated model of this angular dependence expected for a uniaxial layer of a given thickness. This fitting delivers the most suitable values of both components of the complex permittivity tensor at a given wavelength. The data is measured over the entire wavelength range. The analysis of the frequency dispersion of the permittivity allows one to judge on the applicability of this technique to the nanostructures. This method is not applicable if the dispersion turns out to be non-physical i.e. it violates fundamental physical limitations. This method can provide useful information about resonances of metamaterials structures although it cannot be directly used as an inversion calculation method due to the complexity of fitting tensor components and missing possibility to vary the angle of

incidence due to spatial dispersion [24, 25]. This method is also used to investigate the angular dependent optical modes of fishnet metamaterials fabricated by nanoimprint lithography [19]. This method is also used to characterize negative index photonic crystal metamaterials [26]. Spectroscopic ellipsometry can be used as a valuable tool for future design and characterization of large area metamaterials and needs further consideration. Since this method is based on experimental characterization not available here, it is beyond the scope of the work presented here.

2.8 The NRW method

The Nicholson-Ross-Weir (*NRW*) method [27, 28] principally operates by analysing the transmission and reflection coefficients for the calculation of the dielectric and also magnetic properties of bulk layers. Its main advantage is that it can be applied in a wide frequency range providing a broadband description of the medium's dispersive properties. This is the standard RT-retrieval method also called as S-parameter retrieval method. It is the most commonly used characterization method for nanostructures and metamaterials.

If an inhomogeneous structure can be replaced conceptually by a continuous material, ideally there would be no distinction in the scattering characteristics of two. A procedure for the assignment of effective material parameters to the inhomogeneous structure consists of comparing the complex transmission and reflection coefficients from a slab of the inhomogeneous material to those scattered from a hypothetical continuous material. The inversion of scattering parameters is an established method for the experimental characterization of unknown materials [27, 28].

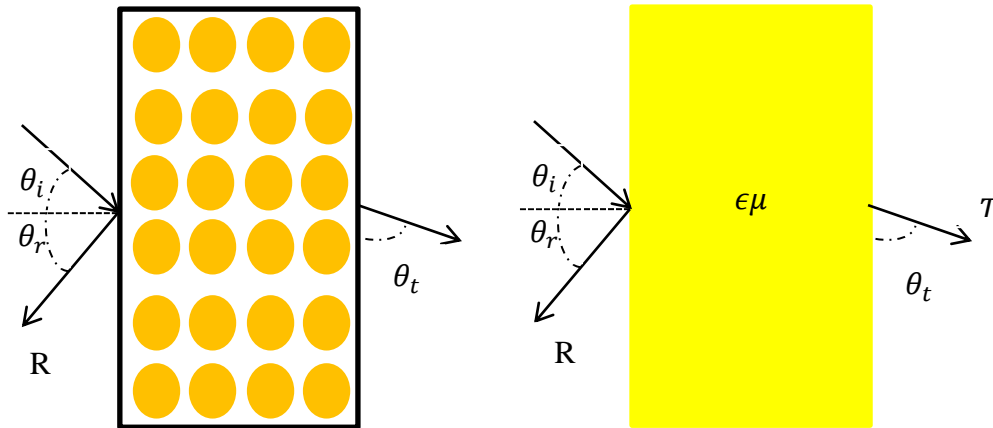


Figure 2.1: Illustration of NRW method used for the determination of effective material parameters from reflection and transmission data.

Soukoulis demonstrated that the traditional procedure of obtaining material parameters from reflection and transmission data can be successfully applied to metamaterials with a few ambiguities in it. He derived an algorithmic approach for the assignment of effective medium parameters to a periodic structure [27]. This approach utilizes the transmission and reflection coefficients known as S parameters calculated for a wave normally incident on a finite slab of metamaterial. By knowing the phases and amplitudes of the wave transmitted and reflected from the slab, one can retrieve the values for the complex refractive index n and wave impedance z .

2.8.1 Determination of Effective parameters of metamaterials from reflection and transmission coefficients

The scattering parameter retrieval methods have become the principle means of characterizing artificially structured metamaterials. It has been proposed that electromagnetic metamaterials formed from periodic or random arrays of scattering elements should respond to electromagnetic radiation as a continuous material at least in the long wavelength limit [29].

The electromagnetic properties of an inhomogeneous structure can be determined exactly by solving Maxwell's equations, which relate the local electric and magnetic fields to the local charge and current densities. The macroscopic forms of Maxwell's equations is applied when

the particular details of the inhomogeneous structure are unimportant to the behaviour of relevant fields of interest, the local field, charge, and current distributions are averaged [3]. The electric permittivity and magnetic permeability encapsulate the specific local details of the composite medium. It has been demonstrated that there are certain metamaterial configurations which exhibit scattering behaviour consistent with the assumption of approximate frequency dependent forms for ε and μ [3,6].

Kyriazidou et al have used homogenization methods that have been extended beyond the traditional regime where effective medium theories would be valid by distilling the complexity of an artificial medium into bulk electromagnetic parameters [9]. It has been demonstrated that the scattering elements whose dimensions are an appreciable fraction of a wavelength ($> \lambda /10$) can be described by the effective medium parameters ε and μ . Artificial materials or metamaterials with negative refractive index have been designed and characterized by following the assumption that effective medium theory applies [30]. These metamaterials have successfully been shown to interact with the electromagnetic radiation in the same manner as would homogeneous materials with equivalent material parameters [11]. The most common method of characterizing the electromagnetic scattering properties of homogeneous material is to find its impedance z and refractive index n . It is often more convenient to choose a second set of variables that completely describes the material i.e. dielectric permittivity and magnetic permeability.

2.8.2 Electromagnetic parameter retrieval

To outline the general approach to the retrieval of material parameters from S parameters for homogeneous materials, the transfer matrix is required [31]. The one dimensional transfer matrix relates the fields on one side of a planar slab to the other.

The transfer matrix is defined as

$$F' = TF \quad (2.3)$$

Where,

$$F = \begin{pmatrix} E \\ H \end{pmatrix} \quad (2.4)$$

Where E and H are the complex electric and magnetic field amplitudes on the right hand side and left hand side of the slab. The analytic form of the transfer matrix for a homogeneous 1D slab has the form.

$$T = \begin{bmatrix} \cos(nkd) & -\frac{z}{k} \sin(nkd) \\ \frac{k}{z} \sin(nkd) & \cos(nkd) \end{bmatrix} \quad (2.5)$$

Where n is the refractive index, z is the wave impedance of the slab, k is the wave number, d is the thickness of slab. The electric permittivity ϵ and magnetic permeability μ can be related to n and z as follows,

$$\epsilon = \frac{n}{z} \quad (2.6)$$

$$\mu = nz \quad (2.7)$$

The total field amplitudes cannot be conveniently measured but the scattered field amplitudes and phases can be measured easily. A scattering matrix relates the incoming field amplitudes to the outgoing field amplitudes and they are directly related to the experimentally determined quantities. The elements of the S matrix can be found from the element of the T matrix as follows [32]

$$S_{21} = \frac{2}{T_{11} + T_{22} + \left(ikT_{12} + \frac{T_{21}}{ik} \right)} \quad (2.8)$$

$$S_{11} = \frac{T_{11} - T_{22} + \left(ikT_{12} + \frac{T_{21}}{ik} \right)}{T_{11} + T_{22} + \left(ikT_{12} + \frac{T_{21}}{ik} \right)} \quad (2.9)$$

$$S_{21} = \frac{2\det(T)}{T_{11} + T_{22} + \left(ikT_{12} + \frac{T_{21}}{ik} \right)} \quad (2.10)$$

$$S_{22} = \frac{T_{22} - T_{11} + \left(ikT_{12} - \frac{T_{21}}{ik} \right)}{T_{11} + T_{22} + \left(ikT_{12} + \frac{T_{21}}{ik} \right)} \quad (2.11)$$

It is noted that for a slab made up of homogeneous material, the elements of the transfer matrix has the following form,

$$T_{11} = T_{22} = T_s \quad (2.12)$$

with $\det(T) = 1$, and the scattering matrix is symmetric which gives,

$$S_{12} = S_{21} = \frac{1}{T_s + \frac{1}{z} \left(ikT_{12} + \frac{T_{21}}{ik} \right)} \quad (2.13)$$

$$S_{11} = S_{22} = \frac{\frac{1}{z} \left(\frac{T_{21}}{ik} - ikT_{12} \right)}{T_s + \frac{1}{z} \left(ikT_{12} + \frac{T_{21}}{ik} \right)} \quad (2.14)$$

By substituting the elements of the transfer matrix, scattering parameters can be calculated as follows

$$S_{12} = S_{21} = \frac{1}{\cos(nkd) - \frac{i}{2} \left(z + \frac{1}{z} \right) \sin(nkd)} \quad (2.15)$$

$$S_{11} = S_{22} = \frac{i}{2} \left(\frac{1}{z} - z \right) \sin(nkd) \quad (2.16)$$

$$S_{11} = S_{22} = \frac{i}{2} \left(\frac{1}{z} - z \right) \sin(nkd) \quad (2.17)$$

The refractive index n and wave impedance z can be calculated by the inversion of scattering parameters

$$\cos(nkd) = \left[\frac{1}{2S_{21}} (1 - S_{11}^2 + S_{21}^2) \right] \quad (2.18)$$

$$n = \frac{1}{kd} \cos^{-1} [1 - S_{11}^2 + S_{21}^2] \quad (2.19)$$

$$z = \sqrt{\frac{(1+S_{11})^2 - S_{21}^2}{(1-S_{11})^2 - S_{21}^2}} \quad (2.20)$$

Above two equations completely characterize the slab made up of homogeneous material. The application of equations (2.19) and (2.20) ^Ato metamaterials is complicated because the multiple branches associated with the inverse cosine and square root makes the unambiguous determination of the material parameter difficult.

It becomes difficult to determine the correct solution when the metamaterials are composed of resonant elements because there is always a frequency region over which the branches associated with the inverse cosine becomes very close together.

2.8.3 Material parameter retrieval for inhomogeneous periodic structures

If the unit cell is not uniform then a unit cell is divided into N slab regions, each with different material properties. The total thickness of the unit cell is given by

$$d = d_1 + d_2 + \dots + d_N$$

The transfer matrix of the composite can be found by multiplying the transfer matrix for each constituent slab. If the unit cell is periodic then the properties of a periodic structure associated with the single unit cell can be determined by the transfer matrix. The fields on one side of a unit cell of a periodic structure are related to the fields on the other side by a phase factor.

A well-known result for a periodic 1D photonic crystal [31] is derived for a binary system composed of two repeated slabs with different material properties.

The validity of the results for refractive index n and wave impedance z is not clear when the unit cell is asymmetric. If there is an asymmetry along the propagation direction then S_{11} and S_{22} will differ, and the retrieval procedure will produce results depending on the direction of propagation of the incoming plane wave. Depending on the direction of propagation of the incident wave with respect to the unit cell, the refractive index is defined by either

$$\cos(nkd) = \left[\frac{1}{2S_{21}} (1 - S_{11}^2 + S_{21}^2) \right] \quad (2.21)$$

or

$$\cos(nkd) = \left[\frac{1}{2S_{21}} (1 - S_{22}^2 + S_{21}^2) \right] \quad (2.22)$$

which gives the different values as S_{11} and S_{22} are not the same for asymmetric structures.

An effective index can be recovered from the modified S parameter retrieval procedure that utilizes all elements of the S matrix. The standard retrieval procedure can be applied to find the effective index for an inhomogeneous structure using an average of S_{11} & S_{22} . It is noted that retrieval procedures for homogeneous and symmetric inhomogeneous unit cells are identical because $S_{11} = S_{22}$

It is necessary to determine the impedance z for the inhomogeneous medium to determine the values of permittivity and permeability. The impedance z for a continuous material is defined as an intrinsic parameter which is the ratio of electric to magnetic fields for a plane wave. But for an inhomogeneous material this ratio will vary throughout the medium which leads to the ambiguous definition of z .

An inhomogeneous periodic structure does not have well defined impedance, as the ratio of electric to magnetic fields vary throughout the structure. This variation can be decreased by keeping the size of the unit cell very small relative to the wavelength. The lack of unique definition of z indicates that there is an ambiguity in the retrieved values of electric permittivity and magnetic permeability.

2.8.4 Analysis of retrieved parameters

It is possible to retrieve these effective material parameters incorrectly due to several reasons. The first reason is that the structure can be spatially dispersive in the frequency range where the retrieval of material parameter is done. Many metamaterials behave as spatially dispersive structures within some narrow frequency intervals lying inside the resonance band of inclusions but outside this band they behave as continuous media. It is possible to properly retrieve the effective material parameters outside these regions. But within this region it is impossible and retrieved parameters have no physical meaning. Another reason can be an incorrect retrieval method. One can try to characterize an anisotropic medium by ϵ and μ . This approach delivers the wrong material parameters because the scattering by anisotropic layers obey different laws than the scattering by isotropic layers. It also delivers wrong material parameters if the retrieval procedure which is valid for only natural materials is applied to an array of resonant elements. Also the effective material parameters retrieved at one angle of incidence are not applicable to all other angles. The applied retrieval procedures for nanostructured materials are not adequate if they do not meet certain conditions.

In order to analyse whether the effective material parameters obtained make physical sense and can be used to describe material of the sample one should check following key points.

1. The retrieved parameters do not depend on the thickness or shape of the sample or on the environment [33].
2. Energy conservation is not violated. The imaginary parts of permittivity and permeability do not change signs and the real part of effective impedance is positive [34].
3. The Causality principle is not violated. The model does not allow any response before the corresponding stimulus has been applied. For the material to be causal the real and imaginary parts of the parameters satisfy the Krammers-Kronig relations and in the low-loss regions and well below resonances the permittivity and permeability grow with increasing frequency [35].
4. Retrieved parameters have non-zero imaginary parts in the absence of dissipation [36].
5. The retrieved parameters do not depend on the angle of incidence and sample thickness otherwise they do not characterize material but only this material for a particular excitation of source [37].

If the retrieval procedure successfully converges, this means that the sample under consideration can be characterized by effective parameters. These parameters can be used in the device design because the parameters describe the properties of material, which do not depend on the size and shape of the sample.

2.9 Summary

The conclusion is that the retrieved material parameters have a limited region of validity. They have sometimes unconventional physical meaning. However in studies of metamaterials, compromises often have to be made. In many instances there are no better ways to describe material response other than using these material parameters. They can

successfully provide some qualitative description of physical phenomena in the sample, but care should be taken in understanding the limitations of their use.

2.10 References

- [1] Metamaterials Handook. Volume 1. *Theory and phenomena of metamaterials*, F. Capolino, Editor, Boca Raton-London-New York: CRC Press, (2009).
- [2] Metamaterials Handook. Volume 2. *Applications of metamaterials*, F. Capolino, Editor, Boca Raton-London-New York: CRC Press, (2009).
- [3] E.F. Kuester, M.A. Mohamed, M. Piket-May, C.L. Holloway, "Averaged transition conditions for electromagnetic fields at a metafilm," *IEEE Trans. Antennas Propag.* 51 2641 (2003).
- [4] C.L. Holloway, M.A. Mohamed, E.F. Kuester, and A. Dienstfrey, "Reflection and transmission properties of a metafilm: With an application to a controllable surface composed of resonant particles," *IEEE Trans. Electromagn. Compat.* 47 853 (2005).
- [5] C.L. Holloway, A. Dienstfrey, E.F. Kuester, J.F. O'Hara, A.A. Azad, A.J. Taylor, "A discussion on the interpretation and characterization of meta-films/metasurfaces: The two-dimensional equivalent of metamaterials," *Metamaterials* 3 100 (2009).
- [6] C.R. Simovski, "Analytical modelling of double-negative composites," *Metamaterials* 2 169 (2008).
- [7] A.J. Sihvola, *Electromagnetic mixing formulas and applications*, Stevenage, UK: The IEE Publishing Group, (1999).
- [8] M. Born and K. Huang, *Dynamic Theory of crystal lattices*, Oxford: Oxford Press, (1954).

- [9] L.D. Landau and E.M. Lifshits, *Electrodynamics of continuous media*, 2nd edition, Oxford: Pergamon Press, (1984).
- [10] J.D. Jackson, *Classical electrodynamics*, 3rd edition, New York: J. Wiley and Sons, (1999).
- [11] C. R. Simovski and S. A. Tretyakov, "On effective electromagnetic parameters of artificial nanostructured magnetic materials," *Photon.Nanostruct.* 8 254 (2010).
- [12] [http:// www.econam](http://www.econam) Nanostructured Metamaterials.
- [13] C. R. Simovski, "On Electromagnetic characterization and homogenization of nanostructured metamaterials," *J. Opt.* 13 013001 (2011).
- [14] S. O'Brien, and J. B. Pendry, "Magnetic activity at infrared frequencies in structured metallic photonic crystals," *J.Phys. Condens. Matter* 14 4035 (2002).
- [15] D. R. Smith, S. Schultz, P. Markos, and C. M. Soukoulis, "Determination of effective permittivity and permeability of metamaterials from reflection and transmission coefficients," *Phys. Rev. B* 65 195104 (2002).
- [16] S. O'Brein, *Artificial Magnetic Structures*, PhD Thesis (Imperial College of Science, Technology and Medicine, (2002).
- [17] R.M.A. Azzam and N.M. Bashara, *Ellipsometry and Polarized Light*, Elsevier Science Pub. Co. (1987).
- [18] A. Roeseler, *Infrared Spectroscopic Ellipsometry*, Akademie-Verlag, Berlin (1990).
- [19] T.Oates, B. Dastmalchi, G. Isic, et al. "Oblique incidence ellipsometric characterization and the substrate dependence of visible frequency fishnet metamaterials," *Optics Express*, Vol. 20, No.10, 1116 (2012).

- [20] G.E. Jellison, V.I. Merkulov, A. A. Puretzky, D. B. Geohegan, G. Eres, D. H. Lowndes, J. B. Caughman, “Characterisation of thin-film amorphous semiconductors using spectroscopic ellipsometry,” *Thin Solid Films* 313/314 193 (1998).
- [21] V.S. Merkulov, *Optics and Spectroscopy* 103 629 (2007).
- [22] J. A. Woollam, B. Johs, C. Herzinger, J. Hilfiker, R. Synowicki, and C. Bungay, “Overview of Variable Angle Spectroscopic Ellipsometry (VASE), Part I: Basic Theory and Typical Applications,” *SPIE Proceedings CR72* (1999) 3-28; Part II: Advanced Applications, *SPIE Proceedings CR72* 29-58 (1999).
- [23] G. E. Jellison, “Generalized ellipsometry for material characterisation,” *Thin Solid Films* 450 42 (2004).
- [24] T. Oates, H. Wormeester, H. Arwin, “Characterization of plasmonic effects in thin films and metamaterials using spectroscopic ellipsometry,” *Progress in Surface Science*, 86, 328-276 (2011).
- [25] B. Dastmalchi, I. Bergmair, T. Oates, et al “Spectroscopic Ellipsometry of the fishnet metamaterial” *Metamaterials’ 2011, The Fifth International Congress on Advanced Electromagnetic Materials in Microwave and Optics* (2011).
- [26] P. Dardano et al. “Ellipsometric determination of permittivity in a negative index photonic crystal metamaterials,” *Light: Science & Applications*, (2012).
- [27] A. M. Nicholson and G.F. Ross, “The measurement of the intrinsic properties of materials by time-domain techniques,” *IEEE Trans. Instrum. Meas.* 17 395 (1968).
- [28] W. Weir “Automatic measurement of the complex dielectric constant and permeability at microwave frequencies” *Proc. IEEE* 62 33 (1974).
- [29] C. Tserkezis and N. Stefanou, “Retrieving local effective constitutive parameters for photonic crystals,” *Phys. Rev. B* 81, 115112 (2010).

- [30] C. R. Simovski, "On material parameters of metamaterials," *Opt. Spectrosc.* 107 26 (2009).
- [31] D. M. Pozar, *Microwave Engineering*, 2nd ed. (1998).
- [32] D.R. Smith, D.C. Veir, Th. Koschny, and C.M. Soukoulis, "Electromagnetic parameter retrieval from inhomogeneous metamaterials," *Phys Rev E*, 71, 036617 (2005).
- [33] A.P. Vinogradov, A.M. Merzlikin, "On the problem of Homogenizing One Dimensional Systems," *Journal of Experimental and Theoretical Physics* 94 482-488 (2002).
- [34] S.M. Rytov, "Electromagnetic properties of finely stratified medium," *Sov. Phys. - JETP* 2 466-475 (1956).
- [35] D.R. Smith, S. Schultz, P. Markos, C.M. Soukoulis, "Determination of effective permittivity and permeability of metamaterials from reflection and transmission coefficients," *Phys. Rev. B* 65 195104 (2002).
- [36] J. Zhou, T. Koschny, M. Kafesaki, C.M. Soukoulis, "Size dependence and convergence of the retrieval parameters of metamaterials," *Photonics and Nanostructures* 6 96-101 (2008).
- [37] C. Menzel, C. Rockstuhl, T. Paul, F. Lederer, T. Pertsch, "Retrieving effective parameters for metamaterials at oblique incidence," *Phys Rev B* 77 195328 (2008).

3. Modifications in Split-Ring Resonator

3.1 Introduction

The research efforts over the past several years have been instrumental in proving that negative index materials can be designed, fabricated and characterized. Negative refraction has been demonstrated many times in steady state experiments. The research work done in the past decade has placed negative refractive index on solid ground. Researchers are looking forward to further develop the technology and methods that will translate these novel materials into useful applications.

This chapter presents the basic concepts and some of the main results in a fast developing and exciting field which extend electromagnetism to new realms. The main feature of these materials is that both their effective permittivity and effective permeability are negative over the same frequency region and hence can show negative refractive index. The existence and satisfactory performance of such materials has been established in the GHz and low THz region.

The first artificial structure which has shown negative effective permeability is briefly discussed. The single gap Split ring resonator (*SRR*) and reasons for the saturation of magnetic response of *SRR* at optical frequency are discussed. The *SRR* may be replaced by two-cut *SRR* or simply the wire pair. Simulation results for both these structures for both polarisations are shown. These structures cannot provide negative refractive index, further structure formed, by placing continuous wires besides short slabs can exhibit negative refractive index.

There is always room for improvement by optimizing the details of geometrical parameters and by choosing the most successful designs. There are substantial differences among the various designs as far as the optimum performance is concerned. Optimization rules are provided as the metamaterials suffer losses at high frequency. Structure optimization has been proved to be very effective way in reducing losses in metallic component of metamaterials.

3.2 First magnetic atom

The concept of metamaterials was developed by Veselago [1] decades ago. They require negative electrical permittivity, negative magnetic permeability and hence negative refractive index at a common frequency band. It has been well known that $\epsilon < 0$ material may easily be obtained from straight wire arrays [2, 3]. But the realization of $\mu < 0$ has been a challenge due to absence of naturally occurring magnetic materials with negative μ . In 1999, Pendry predicted the possibility of the realization of a $\mu < 0$ material.

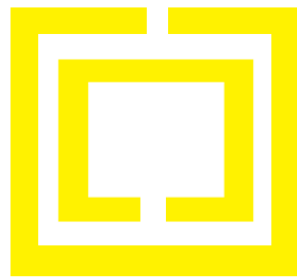


Figure 3.1: A single unit cell of double concentric Split Ring Resonator.

Pendry proposed a structure consisting of two concentric rings separated by a gap both having splits at opposite sides [4] as shown in Figure 3.1. This structure was first fabricated by Smith et al [5]. Magnetic resonance is induced by the splits at the rings and by the gap between the inner and outer rings. This structure has capacitive elements that increase the response of the material to the electromagnetic wave. The total capacitance of this structure has two main contributions. The first contribution is arising from the splits and the other from the gap between the concentric rings. Inductance arises from the conducting rings and gap between inner and outer rings. The capacitance due to the splits prevents current from flowing around the ring but the mutual capacitance between the two rings enables the flow of the current through the structure. The two splits behave like parallel plate capacitors. The total capacitance of the structure will decrease by increasing the width of the splits and hence increasing the resonance frequency of the structure [6-8]. Changing the distance between the inner and outer rings changes the mutual inductance and mutual capacitance between the rings. The magnetic resonance frequency of the structure increases by increasing the gap distances between the two rings. The metal width also affects capacitances and inductances and hence magnetic resonance of the structure [7].

3.2.1 Different topologies of the Split Ring Resonator

In this section the conventional *SRR* and related topologies are discussed. Most of the left handed metamaterials at GHz frequency region are based on the split ring resonators. There has been an ample proof for the existence of negative index metamaterials in the GHz frequency range [11, 24]. The *SRR* design is very useful at GHz frequencies where the sizes of the *SRRs* are of the order of 1 cm and it is relatively easy to form multi stacks and hence be able to obtain negative n response but it is not convenient at optical frequencies.

There is a need for alternative, improved and simplified designs to obtain magnetic resonance and hence negative magnetic permeability that can be easily fabricated and experimentally characterized. The conventional *SRR* structure is not easy to fabricate for operation at optical frequencies. By scaling down this structure, the dimensions of the narrow region and gaps will be very small which may lead to incomplete definition between the metallic parts. Conventional *SRRs* have been fabricated for only few THz [11-14]. It is possible to obtain magnetic resonance from individual *SRRs* as an *LC* circuit system besides the conventional *SRR* design [3] where the two concentric rings with splits oriented at opposite sides are employed [8,13].



Figure 3.2: Different topologies of Split Ring Resonator.

Theoretical and experimental studies have proved that an effective *SRR* can be built from a single ring design exploiting only the capacitance across the splits [13, 15]. This simplifies the fabrication especially for small structural sizes; potentially reducing the dielectric losses because the field becomes stronger between the splits and not between the rings. To further improve the working of single ring resonator and keeping in mind the need for higher dimensional isotropic metamaterials, additional splits were introduced thus forming two and four cut split ring resonators as shown in Figure 3.2. The addition of splits will alter the capacitance of the structure. The change in total capacitance of the structure will be larger for

structures having more splits. The magnetic resonance frequency increase drastically when additional splits are introduced in the system [16].

When the second split is placed on the ring, the capacitance will be connected in series. Therefore the total capacitance will decrease by a factor of 2. This large decrease in the capacitance of individual ring resonator will increase the magnetic resonance frequency. The 2-cut design needs to be further explored and is discussed in Section 3.2.2. The 4-cut single ring *SRR* design is favourable for its inherent symmetry [17, 18]. The highest possible resonance frequency exhibiting $\mu < 0$, strongly increases with the number of cuts in the *SRR* and depends mainly on the length scale.

All these structures provide negative permeability and at the same time negative permittivity can be achieved by placing a periodic array of thin metallic wires in close proximity. The wires actually act as electric dipoles and their overall response can give rise to negative permittivity. Combining wires with *SRRs* can give rise to negative refractive index.

3.2.2 Split ring resonator

In 1996 and 1998 John Pendry suggested that by composing artificial structures of sub wavelength dimensions in a periodic lattice, can give rise to a negative μ . He proposed an artificial material consisting of a so called split ring resonator which exhibits a band of negative μ in spite of being made of non-magnetic materials.

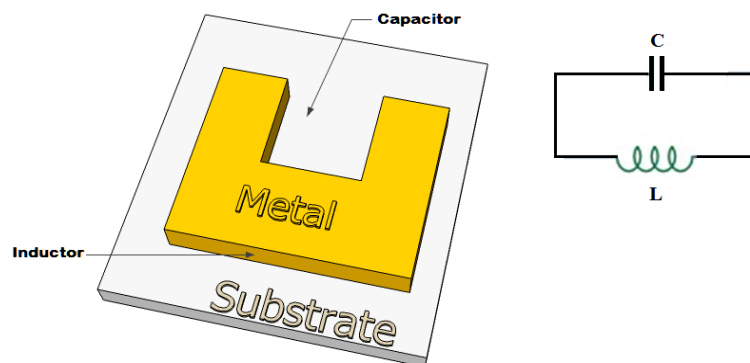


Figure 3.3: The equivalent *LC* circuit used for the description of split ring resonator.

The knowledge of basic magneto statics has been employed to create this structure. It is well known that a magnetic dipole moment can be realized by circulating ring current of a

microscopic coil. It leads to an individual magnetic moment, which can be given by the product of current and area of coil. If such a coil is combined with parallel plate capacitor, there is an increased magnetic dipole moment. Thus, this popular design mimics a usual LC circuit, consisting of a magnetic coil of inductance L and a parallel plate capacitor of capacitance C on a scale much smaller than the relevant wavelength of light. Figure 3.3 shows the analogy of conventional LC circuit and a metallic SRR on a dielectric surface.

The LC resonance frequency can be calculated by the following approach. The capacitance C of a SRR is calculated from textbook formula of a parallel plate capacitor with some standard approximations [19].

$$C \propto \frac{\text{Area of the plate}}{\text{Distance between the plates}} \quad (3.1)$$

Using the nomenclature of Fig 3.3, i-e., the width of the metal w , the metal thickness t , the gap between the arms of the capacitor d , the length of the coil l ,

$$C = \epsilon_0 \epsilon_c \frac{wt}{d} \quad (3.2)$$

Where, ϵ_c is the dielectric constant of the substrate.

The inductance L of a coil of N turns is given by, where $N=1$ is given as

$$L = \frac{\text{Area of coil}}{\text{Length}} \quad (3.3)$$

$$L = \frac{\mu l^2}{h} \quad (3.4)$$

The resonance frequency of the LC circuit is given by

$$\omega_{LC} = \frac{1}{\sqrt{LC}} \quad (3.5)$$

$$\omega_{LC} = \frac{1}{l} \frac{c_0}{\sqrt{\epsilon_c}} \sqrt{\frac{d}{w}} \quad (3.6)$$

And the LC resonance wavelength is given by

$$\lambda_{LC} = \frac{2\pi c_0}{\omega_{LC}} \quad (3.7)$$

$$\lambda_{LC} = 2\pi l \sqrt{\epsilon_c} \sqrt{\frac{w}{d}} \quad (3.8)$$

It tells us that the LC resonance wavelength is proportional to the linear dimension of the coil l , provided that the ratio w/d is fixed. This scaling is valid as long as the metal actually behaves like a metal. It is valid as long as the LC -resonance frequency is much smaller than the plasma frequency.

3.2.3 Electric and magnetic coupling of SRR

The unit cell of *SRR* and its two polarisation dependent electromagnetic responses are shown in Figure 3.4. For normal incidence with transverse electric *TE* polarisation mode, the incident electric field is across the split of the *SRR*. The electric field couples with the capacitance of the *SRR* and generates a circulating current around it. The circulating current induces a magnetic field in the base arm of the *SRR* and also interacts with the external field to generate the magnetic resonance that can be appropriately called as an *LC* resonance. When the incident light is with transverse magnetic *TM* polarisation mode, the electric field is perpendicular to the split of the *SRR*. The electric field cannot couple to the capacitance of the *SRR* and therefore generates only electric plasmon resonance.

It should be noticed that there exists a difference in the spectral position as well as the width of the plasmon peaks obtained from two different polarisation configurations. For *TE* polarisation only the base of the *SRR* is excited and produces the plasmon peak. For *TM* polarisation, both the arms of the *SRR* are excited. These two arms are coupled through the base of the *SRR* and produce a plasmon peak which is slightly red shifted as compared to the *TE* mode.

To further clarify the above arguments, simulations were performed for *SRR* structure for the two polarisations. The simulations were performed with Lumerical solutions which uses *FDTD* method [20]. The geometric parameters are taken from reference [13]. The Drude model is used to describe the metals complex dielectric constant in the infrared spectral region. The plasma frequency for gold is given by $\omega_p = 2175$ THz, and a collision frequency is given by $\omega_c = 6.5$ THz [21]. Numerical results are shown in Figure 3.4 for both *TE* and *TM* polarisation along with the polarisation configuration for the structure. Two distinct resonances are clearly visible for *TE* polarisation. The resonance around $3 \mu\text{m}$ completely disappears when the electric field vector is rotated by 90° i.e. for *TM* mode which is the *LC* resonance of the structure.

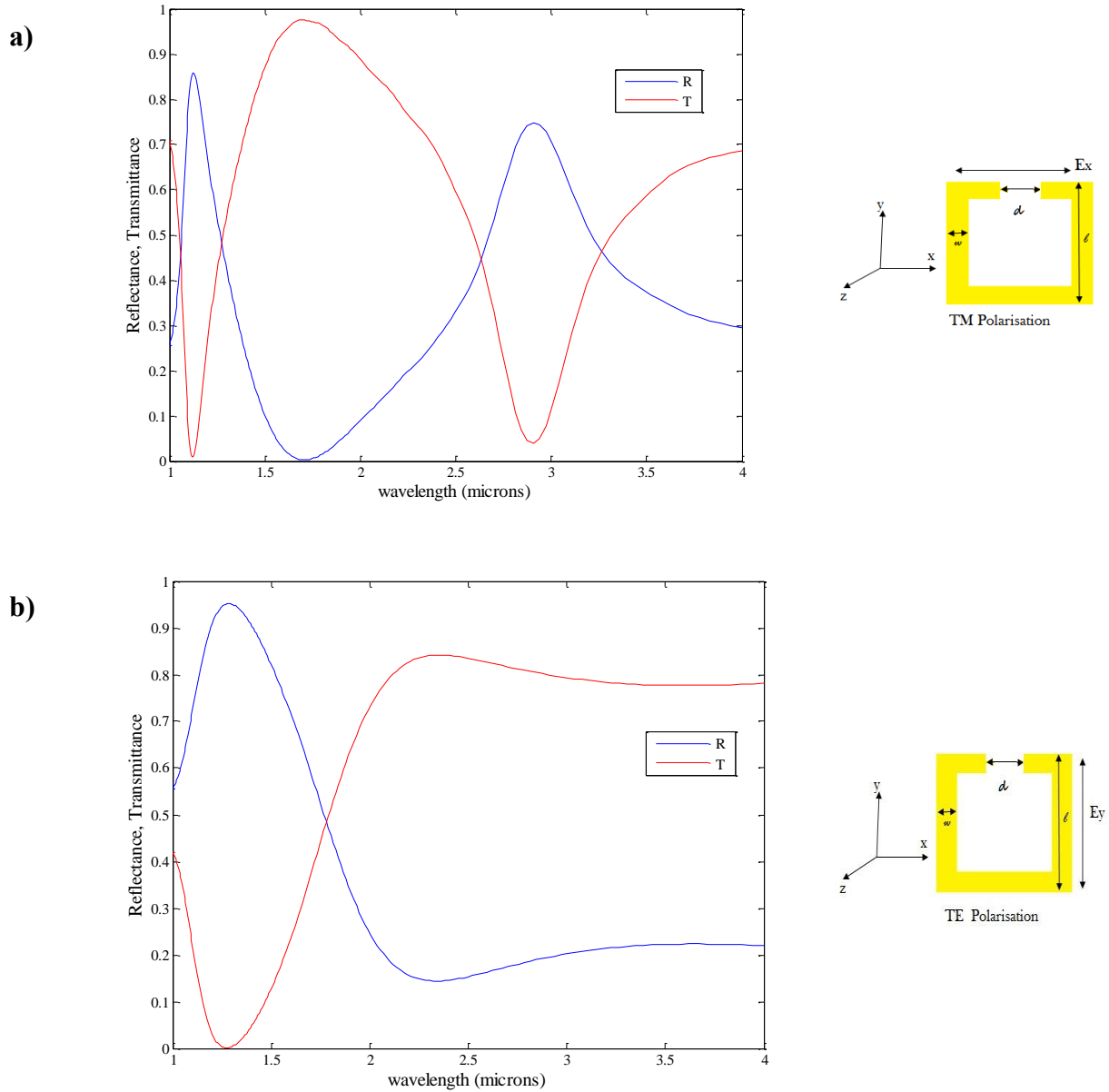


Figure 3.4: Simulated transmittance and reflectance spectra for Split Ring Resonator for *TE* and *TM* polarisations. The geometric parameters are taken from reference [13]. The thickness of the gold film is 20 nm, width $w = 90$ nm, length l of the SRR is 320 nm, and the gap d between the arms is 70 nm. The lattice constant is $a = 450$ nm.

3.2.4 Saturation of the magnetic response of SRR

There has been a sustained effort with in the metamaterials research for the better understanding and optimization of these structures. The large part of the research has been devoted to the extension of the frequency of operation of left handed metamaterials from the microwave to optical regimes. Many of the attempts to create high frequency magnetic materials are based on the scaling down of designs providing negative magnetic permeability

at microwave frequencies. These efforts determined the possibilities and limitations of this scaling approach [22-25]. The properties of metals which are involved in metamaterials are drastically different in the optical regime of electromagnetic spectrum as compared to microwave region. In the microwave region metals behaves as almost perfect conductor and the magnetic atoms in the metamaterials are not lossy.

The scientific community have led to following conclusions concerning the limitations of scaling of the *SRR* [26, 27].

1. The frequency of *SRRs* resonant magnetic response does not continuously increase. It saturates to a constant value after some length scale. This value is dependent on the *SRR* geometry employed. The magnetic response of the structure could go up to the middle visible range with proper modifications of this geometry. The saturation response of magnetic resonance frequency has been studied by Tretyakov [23]. He explained the saturation by taking into account the contribution of the kinetic energy of the electrons associated with the current inside the *SRR* ring to the magnetic energy created by the loop current.

The additional terms are introduced to the equation (3.5) [23]

$$w_{LC} = \frac{1}{\sqrt{(L+L_{add})(C+C_{add})}} \quad (3.9)$$

where,

$$L_{add} = \frac{l_{eff}}{\epsilon_0 w t \omega_p^2} \quad (3.10)$$

where l_{eff} is the effective conductor length, ϵ_0 is the permittivity of free space, w is the *SRR* width, t is the thickness, ω_p is the plasma frequency of the metal. The effective conductor or ring length is approximated as $l_{eff} = \left(\frac{\pi}{2}\right)l$. The additional capacitance C_{add} is given by

$$C_{add} = \frac{\epsilon_0 \epsilon_r w t}{l_{eff}} \quad (3.11)$$

where ϵ_r is the relative permittivity. The L and C components are approximated using round loop inductance and parallel plate inductance respectively.

$$L = \frac{\mu_0 l^2}{t} \quad (3.12)$$

$$C = \epsilon_0 \epsilon_c \frac{w t}{d} \quad (3.13)$$

where ϵ_c the dielectric constant of the substrate and d is the gap width.

2. The magnitude of magnetic permeability resonance becomes smaller and smaller by moving to smaller length-scale *SRR* structures. It ceases to reach negative value below some length scale. This weakening of the permeability is attributed to the kinetic energy of electrons at higher frequencies. The resistive losses in the metal also increase as one goes to higher frequencies. These studies are very revealing concerning the high frequency response of magnetic materials [28-30]. The influence of the dispersive response of metals does not only influence the magnetic resonance frequency. It also affects the other important features of the magnetic response such as resonance shape, damping factor, total losses and spectral width of negative permeability band [28]. The ohmic losses also play a role in the saturation of the magnetic resonance frequency.
3. In the microwave region, a negative permittivity is usually achieved by combining the *SRRs* with the thin continuous wires which provide permittivity with plasma frequency in the microwave region. This approach is not well suited for THz frequencies and because of size limitations and the absence of good conductors in this frequency region. The *SRR* itself has been shown to exhibit an electric resonance which is analogous to that of short piece of straight wire. It can provide a resonant negative effective permittivity similar to the negative effective permeability [31]. This electric resonant response of the *SRR* is much stronger than the magnetic response. But it always occurs well above the magnetic resonance frequency such that there is virtually no chance to make negative μ and ϵ regions overlap. Because the negative effective permittivity region is much stronger and wider, it is required to move negative permeability resonance into the negative permittivity region.

3.3 Wire pair as magnetic atoms

3.3.1 Cut wire pair

A pair of parallel short wires can be used as a magnetic resonator as an alternative structure to the *SRR*. This geometry can be considered as an extreme case of two-split *SRR* ring. This

geometry along with its equivalent LC circuit is shown in Figure 3.5. In this case the two continuous arms become long and finite and the split bearing arms become short and the split becomes wide. This limiting case of the two-split SRR can show both electric and magnetic resonance. The magnetic resonance is due to resonant circular ring current and electric resonance is due to resonant linear current parallel in both continuous arms. The loop inductance is greatly reduced which increases magnetic resonance frequency and can move very close to the electric resonance frequency.

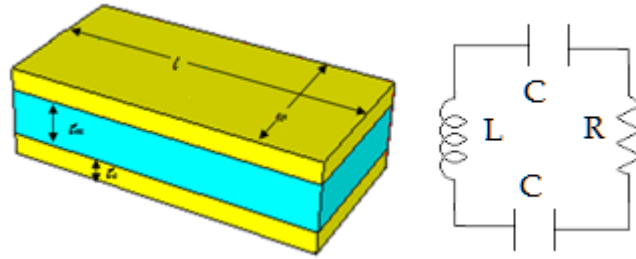


Figure 3.5: A wire-pair structure with its equivalent RLC circuit is shown where l is the length of the short wire pairs, w is the width, t_s is the separation between short wire pairs and t_m is the metal thickness.

The parallel short wires can also be considered as an LC circuit. The short wire pair will exhibit inductive response along the wires and capacitive response between the upper and lower adjacent ends of the short wires. This behaviour of the structure gives a magnetic resonance providing a negative permeability.

The inductance L of a short wire pair can be given as inductance of parallel plates, i.e.

$$L = \mu_o(l \cdot t_s)/w \quad (3.14)$$

where l is the length of short wires, w is the width and t_s is the separation between the short wires.

The capacitance C of short wire pairs can be written for lower and upper halves of short wire pair

$$C = \frac{\epsilon_r \epsilon_o (l \cdot w)}{4t_s} \quad (3.15)$$

where ϵ_o is the permittivity in vacuum, and ϵ_r is the dielectric constant of the region between the wires.

The resonance frequency is given by

$$f_m = \frac{1}{2\pi\sqrt{LC}} \quad (3.16)$$

$$f_m = \frac{1}{\pi l \sqrt{\mu_o \epsilon_r \epsilon_o}} = \frac{c_o}{\pi l \sqrt{\epsilon_r}} \quad (3.17)$$

where c_o is the speed of light in vacuum. It is straight forward to achieve such a design, by placing one cut wire on top of the other with the certain dielectric spacer layer between them as shown in Figure 3.5. The unit cell of wire pair and its two polarisations dependent electromagnetic responses are shown in Figure 3.6 along with the polarisation configuration.

3.3.2 Electric and magnetic coupling of the wire pair

To understand the behaviour of the structure, detailed simulations were performed with varying lattice constant l . The geometric parameters are taken from the reference [31]. The relevant geometric parameters are the length l of the wire pairs, the width w , metal thickness t_m and the spacing between the wires t_s . The metal patches of the structure are replaced by silver metal Ag. MgF₂ is used as a dielectric spacer between the wire pair. The Drude model is used to describe the metal with the plasma frequency by $\omega_p = 2175$ THz and by a collision frequency $\omega_c = 4.35$ THz [21]. The refractive index of MgF₂ is used as 1.38.

The simulations were performed for different lengths of the wire-pairs. It has been noticed that there exist a difference in the spectral position as well as the magnitude of the resonance with the length of the wire-pairs. The simulation results are shown in Figure 3.6. For normal incidence with transverse electric mode TE , the electric field component of the incident electromagnetic wave is parallel to the longitudinal axis of the wire pair. It generates a circular current and produces a magnetic resonance. It also produces a linear current in both wires and hence produces electric resonance as well. Therefore two distinct resonance peaks can be observed in this polarisation configuration.

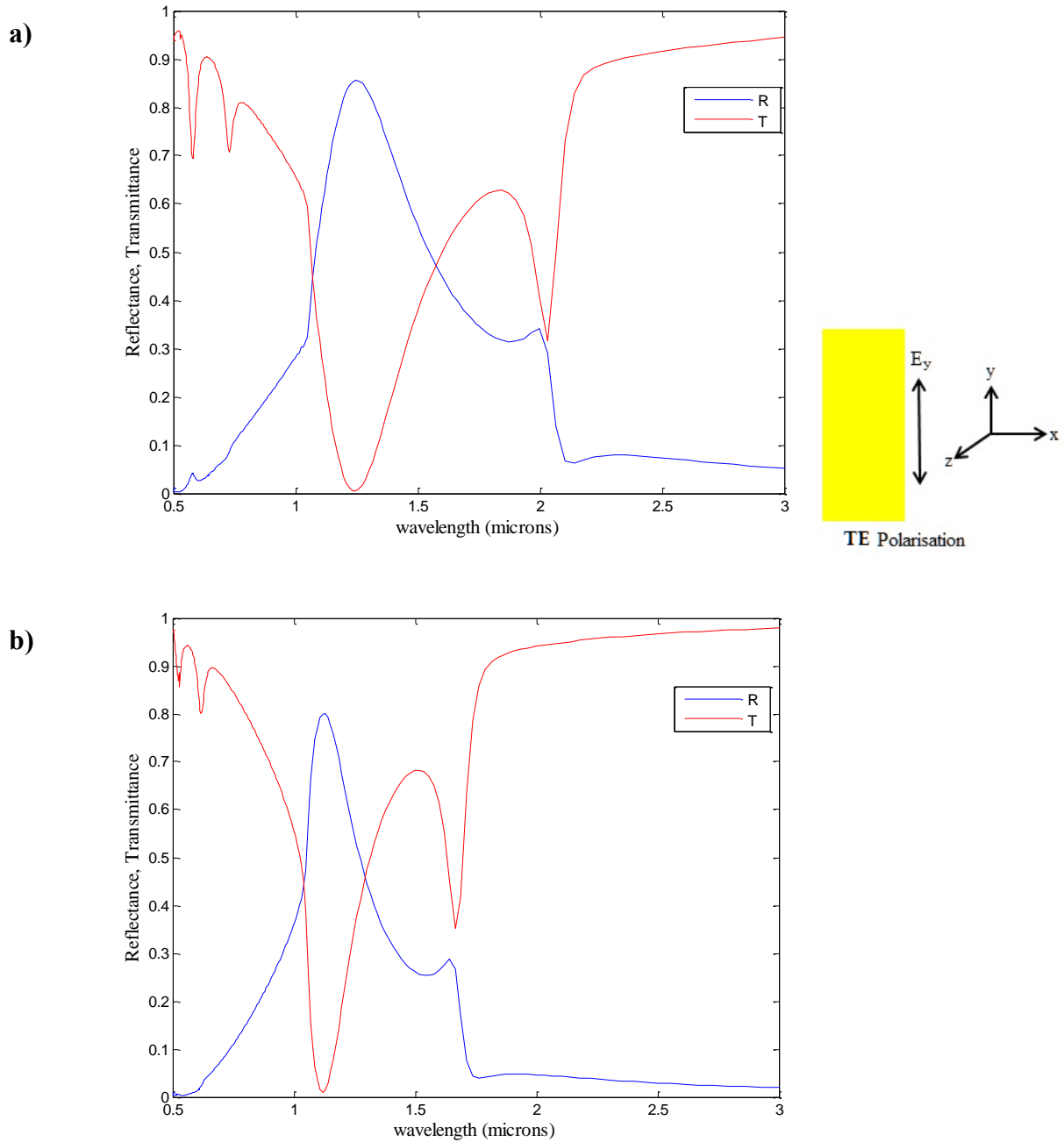


Figure 3.6: Simulated Reflectance (blue) and Transmittance (red) obtained from the wire pair structure for two different lengths (a) $l = 500$ nm, (b) $l = 400$ nm. The geometric parameters for the Figure 3.5 are $w = 150$ nm, $t = 20$ nm, $d = 80$ nm, lattice constants $a_x = 500$ nm and $a_y = 1050$ nm. The polarisation configuration for electric field component of electromagnetic wave (*TE* Polarisation) is also shown [31].

For normal incidence with transverse magnetic *TM* mode, the electric field component of the incident electromagnetic wave is perpendicular to the longitudinal axis of the wire pair and hence does not produce magnetic resonance. Therefore only electric resonance can be

observed.

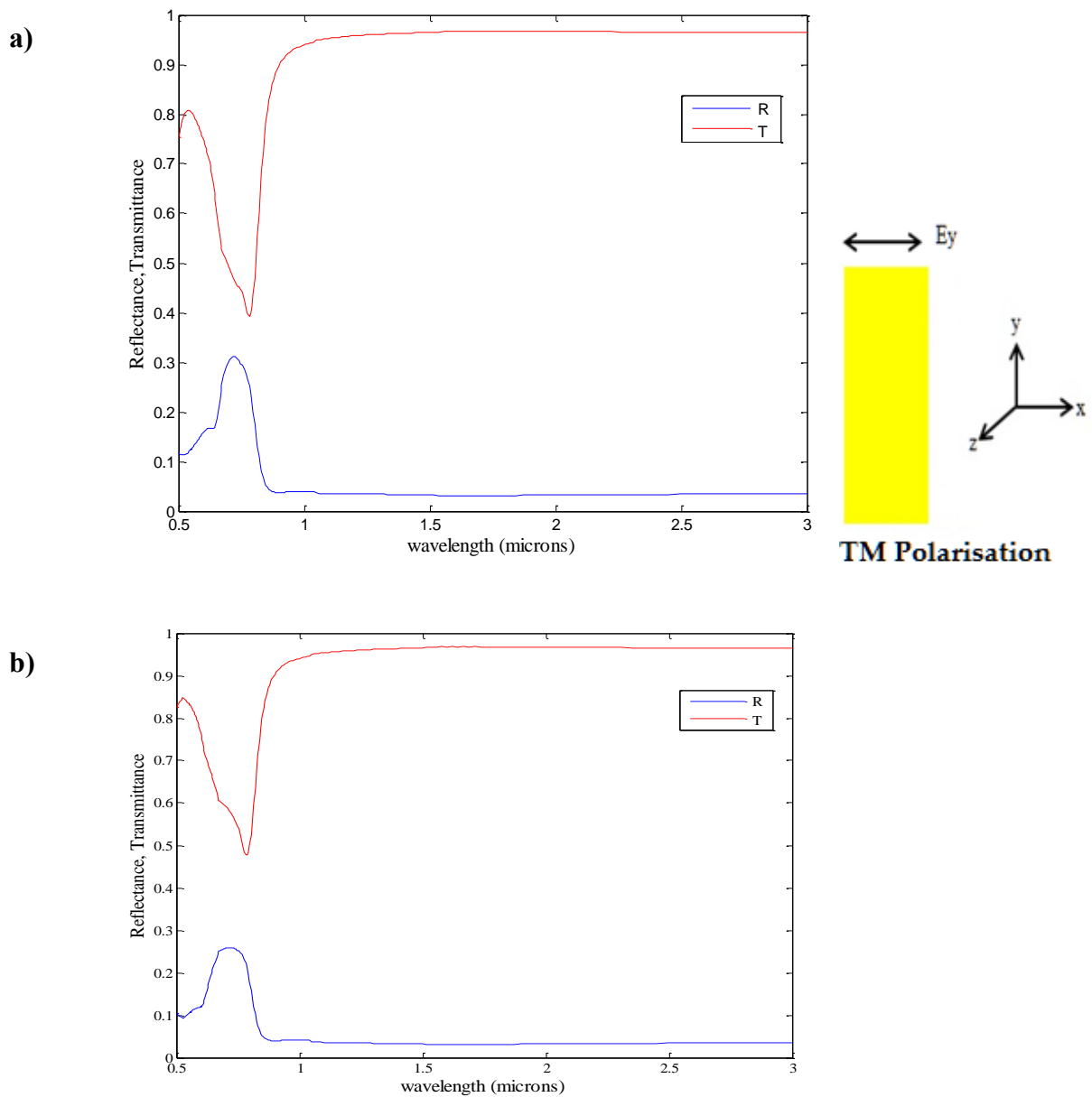


Figure 3.7: Simulated Reflectance (blue) and Transmittance (red) obtained from the wire pair structure for two different lengths (a) $l = 500$ nm, (b) $l = 400$ nm. The geometric parameters are same for Figure 3.6. The polarisation configuration for electric field component of electromagnetic wave (*TM* Polarisation) is also shown [31].

3.3.3 Wide cut slab pair

The magnetic resonance frequency of the wire pair structure scales linear to inverse lattice constant. It is shown in Figure 3.6 and 3.7 for both *TE* and *TM* polarisations. There is no dependence on the width of the slab for the spectral position of the magnetic resonance. But

strength of the magnetic resonance can be enhanced by increasing width of the wire pair structure. It has been observed that by increasing the width of the wire pair structure, the strength of the magnetic resonance frequency increases

3.3.4 Disadvantage of wire pair

The theoretical work has shown that using pairs of finite lengths wires allows replacement of the *SRRs* as magnetic resonator [31]. It can also give simultaneously a negative ϵ and negative μ in the same frequency region and therefore, negative n , without the additional need for continuous wires. But the experiments [30] have not shown evidence of negative refractive index in the short wire pair case. It is difficult to obtain a negative n with only pairs of short wires. The behaviour observed for wire pair is almost the same as for *SRR*. The reasons are almost same as discussed in section 3.2.4. The electric resonance of the short wires is usually well above the magnetic resonance frequency, thus preventing ϵ and μ from becoming simultaneously negative. Also the magnetic resonance frequency scales inversely proportional to the structure linear size at frequencies in near *IR*. But towards the optical regime this linear scaling breaks down and the magnetic resonance frequency saturates to a constant value.

Simulations were performed to obtain ϵ and μ and refractive index n for the wire pair structure. The parameter retrieval is performed by the method as described in Chapter 2. There is a negative μ but there is no negative ϵ at the same frequency region. Hence there is no negative refractive index n obtained for this structure. The qualitative behaviour of these results is in good agreement with reference [31].

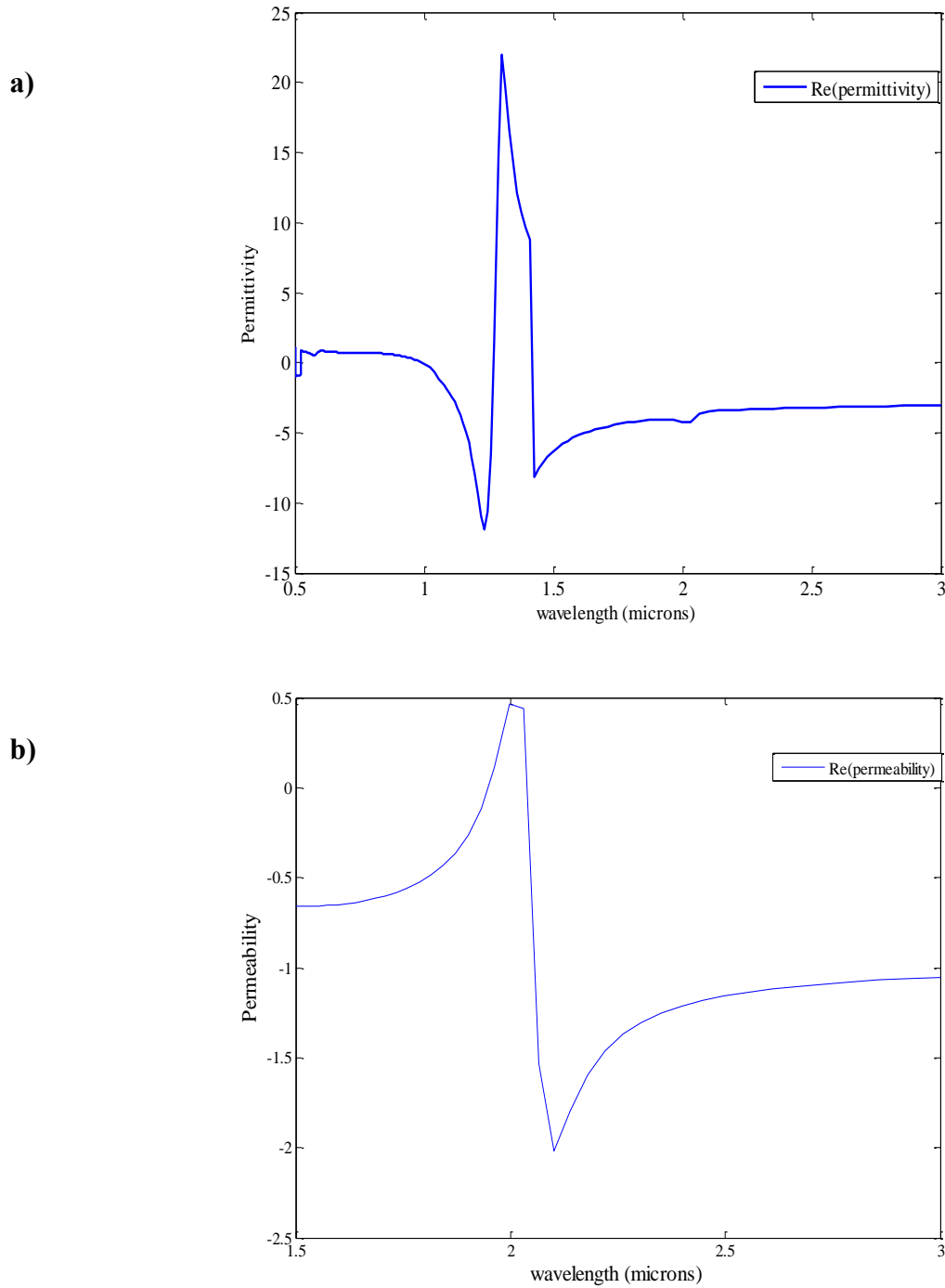


Figure 3.8: a) The electric permittivity ϵ and b) magnetic permeability μ obtained from the simulated reflection and transmission coefficients [31]. The geometric parameters are same for Figure 3.6.

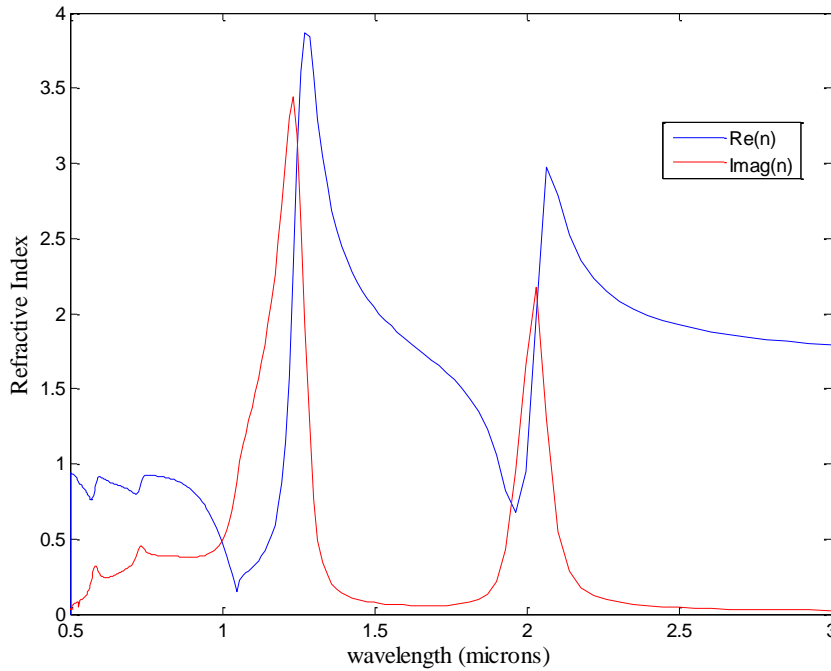


Figure 3.9: Real (blue) and imaginary (red) part of refractive index retrieved from simulated reflection and transmission coefficients [31]. The geometric parameters are same for Figure 3.6.

In Chapter 5, these results are utilized for modelling and fabricating fishnet structure formed from nanoimprint lithography. The wire pair structure/nanopillars comprising Ag-MgF₂-Ag are crushed during the imprinting while forming fishnet. These nanopillars provide negative μ , they may not deteriorate the results obtained from *NIL* fishnet structure due to the negative permeability obtained from them as shown in Figure 3.8. The details are provided in Chapter 5.

It was established by Shalaev et al [33] that a periodic array of metal-dielectric-metal nanorods can exhibit negative index of refraction. It is reported an n value of -0.3, which is in part achieved by optimising the nano-rods dimensions and periodicity.

3.4 Slabs & continuous wires.

The condition to obtain simultaneously negative ϵ and μ by pairs of metallic wires is very restrictive. An improved and simplified structure made of periodic array of pairs of short metal wires/slabs and continuous wires offer a potentially simpler approach to negative index

materials. In this structure, the conventional single gap *SRR* is replaced with a pair of short parallel wires and the continuous wires are preserved. The short wire pair is a two gap *SRR* that has been flattened to result in the wire-pair arrangement. The short wires must be combined with a continuous wire that provides the extra negative permittivity. The two additional continuous wires are placed on either side of the short wires. The presence of wire does not affect the magnetic resonance frequency of the slabs. The inductance L and capacitance C of the short slabs is given by the equations 3.7 and 3.8. The unit cell of the structure is shown in Figure 3.10.

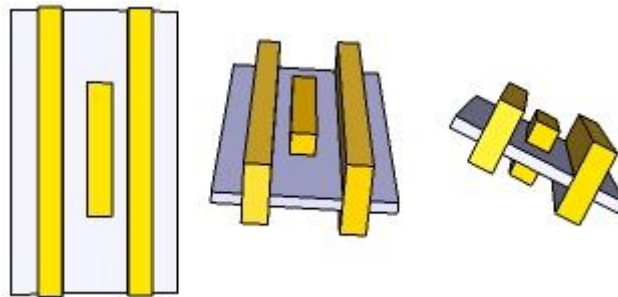


Figure 3.10: A 3D view of short wire-pair and continuous wire-pair is shown.

This structure is initially fabricated in GHz range [34] by using photolithography. The circuit board was coated on both sides with $10\mu\text{m}$ thick layers of copper. Simulations were performed to determine reflection/transmission properties of the structure. A plane wave source operating at 10-20 GHz is incident normally on the structure by keeping the electric field component parallel to the longitudinal axis of the slabs. Periodic boundary conditions are used to extend the structure in the x and y directions.

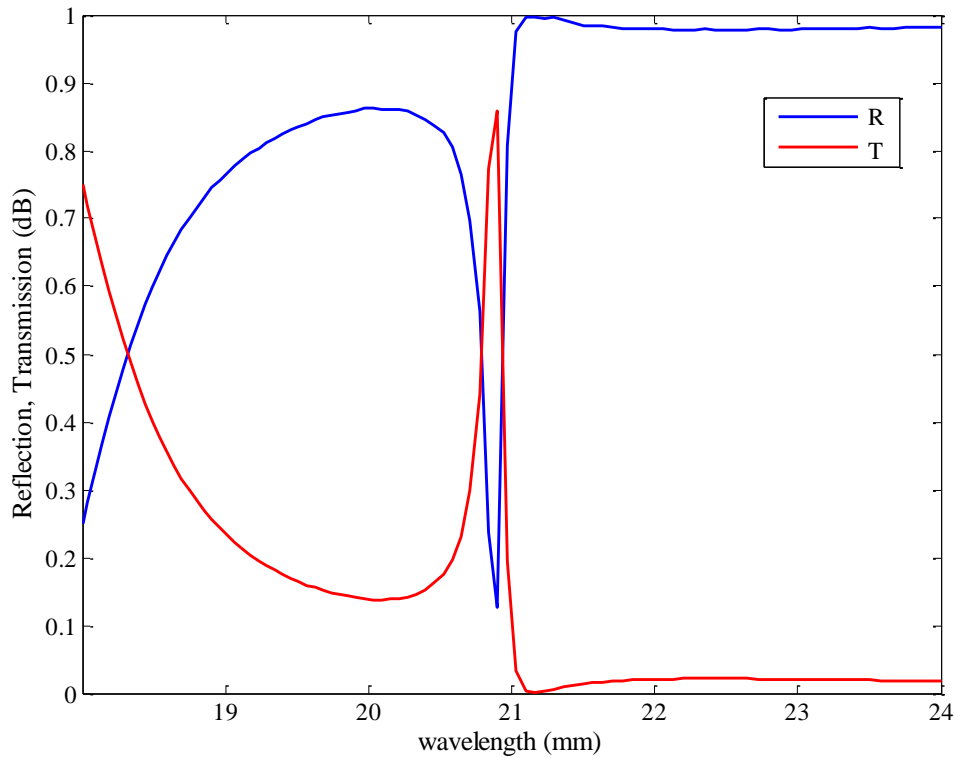


Figure 3.11 Simulated reflection and transmission coefficients obtained from slabs and continuous wire pair shown in Figure 3.10. The geometric parameters are taken from reference [34] for structure shown in Figure 3.10.

Simulations were performed to obtain, μ and refractive index n for the slabs and continuous wire structure. The parameter retrieval is done as explained in Chapter 2. There is a negative μ and ϵ over the same frequency region. Hence there is a negative refractive index n obtained for this structure. The qualitative behaviour of these results shown in Figure 3.12 and 3.13 is in good agreement with reference [34].

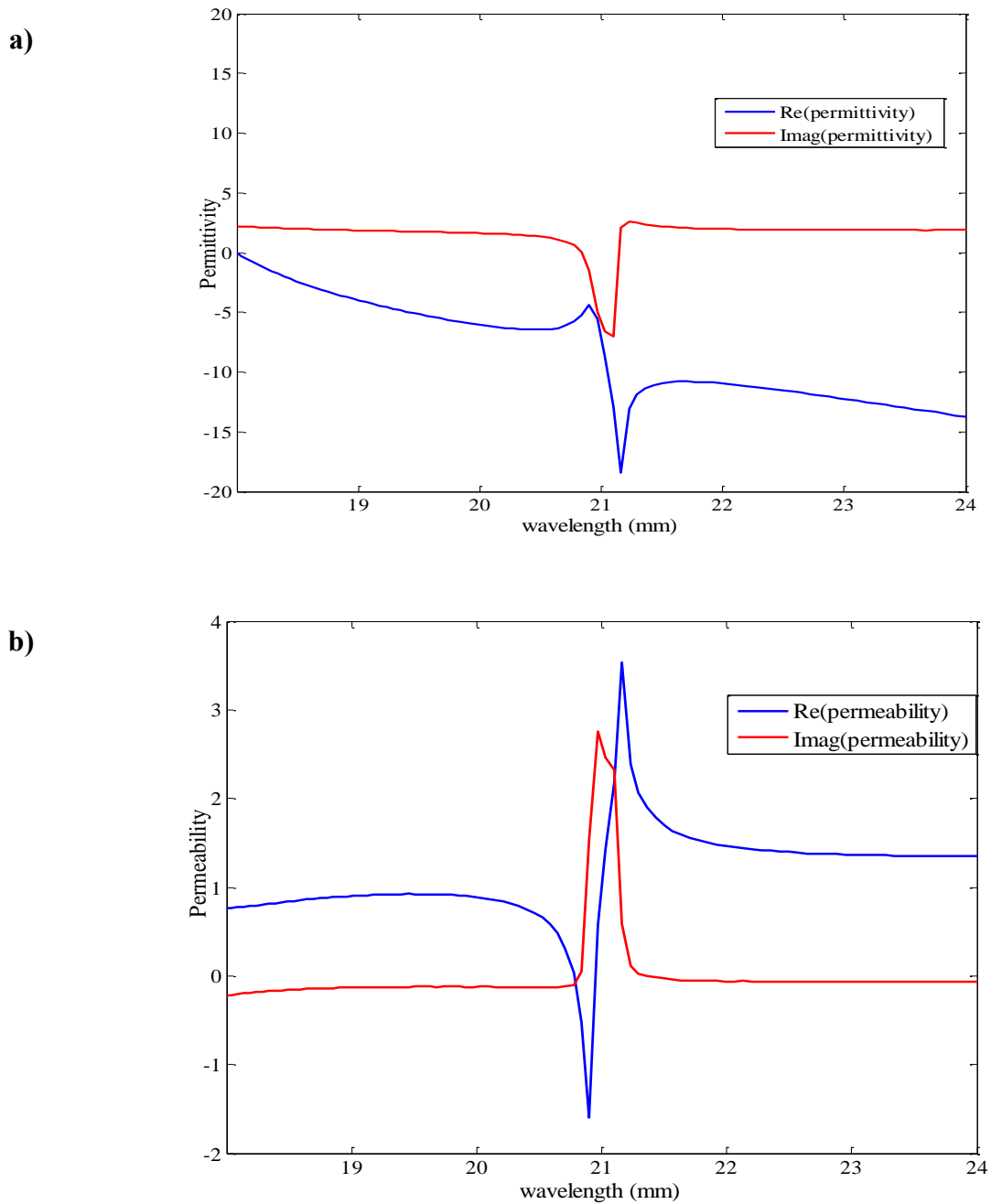


Figure 3.12: Retrieved material parameters (a) real and imaginary part of electric permittivity (b) real and imaginary part of magnetic permeability. The geometric parameters are taken from reference [34] for structure shown in Figure 3.10.

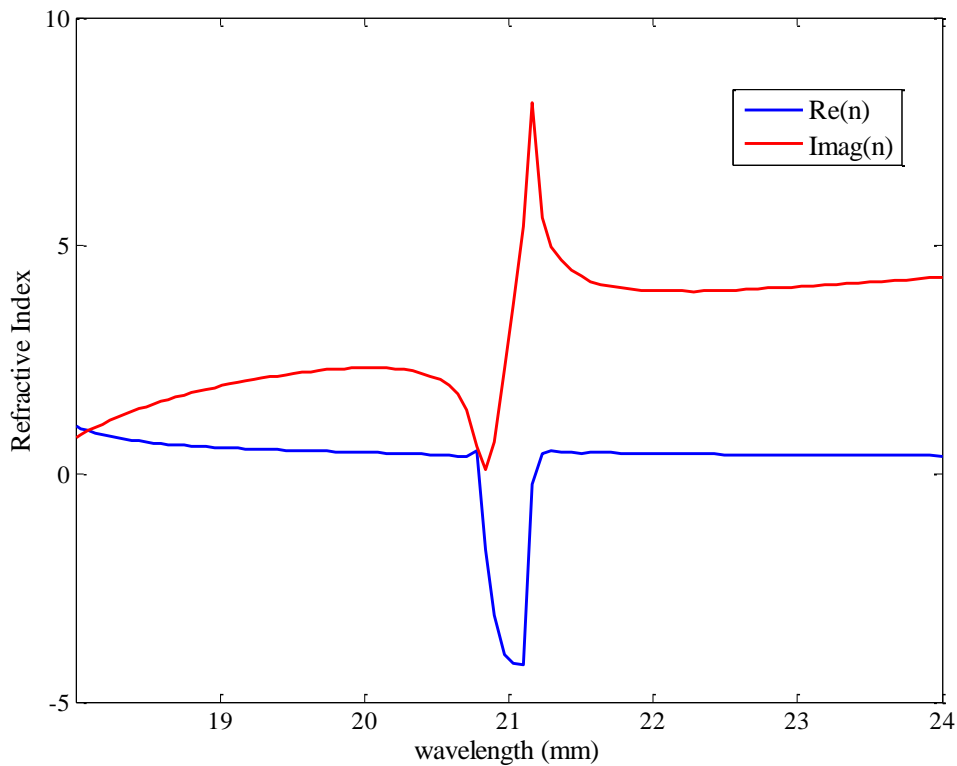


Figure 3.13: Real and imaginary part of refractive index. The geometric parameters are taken from reference [34] for structure shown in Figure 3.10.

3.5 Optimized design

The role of the various geometrical parameters in the high frequency response of metamaterials helps to identify the dominant parameters for this response. These dominant parameters define optimization rules for high frequency metamaterials because metamaterials active at infrared and optical frequencies suffer very high loss which makes these structures non-functional. Structure optimization proved to be a very efficient way for the reduction of losses in metallic components of the metamaterials.

There are certain conditions for the achievement of optimized high frequency for instance optical magnetic material which are as follows

- a) The highest possible saturation value for the magnetic resonance frequency.
- b) The largest possible width of the negative permeability regime

c) The smallest possible loss factor which indicate losses in metamaterials.

The general requirement for meeting the above conditions can be concluded as follows

- Structures of small capacitance C .
- Structures of small kinetic inductance as compared to the magnetic inductance.
- Structures of low resistance R .
- High quality optical metamaterials demand metals of highest possible plasma frequency and lowest possible collision frequency.

It should be noted that low inductance facilitates the achievement of high magnetic resonance frequency but it results in the weaker resonances and higher losses [28].

3.6 Summary

The magnetic resonance frequency of the structures discussed in this chapter shows saturation behaviour at optical frequency rather than scaling linear to inverse lattice constant, as it occurs in the structures in the microwave region. The saturation value of this frequency depends upon the design, geometrical parameters, and properties of the constituent materials. The magnetic resonance frequency becomes weaker, the smaller the dimensions of the structure. The permeability ultimately ceases to reach negative values as the structures reach the nanoscale domain. The strength of the resonance depends upon the design, its geometrical parameters and properties of constituent materials. A strong resonance and wide negative permeability is obtained by using metals with high plasma frequency and low collision frequency. The ohmic losses are also lowest for high metal plasma frequency and lowest collision frequency.

3.7 References

- [1] V. G. Veselago, "The electrodynamics of substances with simulataneously negative values of ϵ and μ ," *Sov. Phys.Usp.* 10, 509-514 (1968).
- [2] J.B. Pendry, A. J. Holden , W.J. Stewart and I. Youngs, "Extremely low frequency Plasmons in metallic mesostructures," *Phys. Rev. Lett.*, 76, 4773 (1996).

- [3] D.R. Smith, S. Schultz, N. Kroll, M. Sigalas, K. M. Ho, and C. M. Soukoulis, “Experimental and theoretical results for a two dimensional metal photonic band gap cavity,” *Appl. Phys. Lett.* 65, 645 (1994).
- [4] J. B. Pendry, A. J. Holden, D. J. Robbins, and W. J. Stewart, “Magnetism from conductors and enhanced Non-Linear Phenomena,” *IEEE. Trans. Microwave. Theory. Tech.* 47 2075-2084 (1999).
- [5] D.R. Smith, W. J. Padilla, D. C. Vier, S. C. Nemat-Nasser and S. Schultz, “Composite medium with Simultaneously Negative Permeability and Permittivity,” *Phys. Rev. Lett.* 84 4184 (2000).
- [6] J. D. Baena, R. Marques, F. Medina, and J. Martel, “Artificial magnetic metamaterial design by spiral resonator,” *Phys. Rev. B* 69 014402 (2004).
- [7] B. Sauvignac, C. R. Simovski, and S. Tretyakov, “Double Split Ring Resonators: Analytical Modelling and Numerical Simulations,” *Electromagnetics* 24 317 (2004).
- [8] M. Shamonin, E. Shamonina, V. Kalinin, and L. Solymar, “Properties of a metamaterials element: Analytical Solutions and Numerical Simulations for a Singly Split Double Ring,” *J. Appl. Phys.* 95 3778 (2004).
- [9] R. B. Greengard, C. G. Parazolli, K. Li, and M. H. Tanielian, “Origin of dissipative losses in negative index of refraction materials,” *Appl. Phys. Lett.* 82 2356 (2003)
- [10] K. Aydin, K. Guven, M. Kafesaki, L. Zhang, C. M. Soukoulis, and E. Ozbay, “Experimental Observation of true left handed transmission peaks in metamaterials,” *Opt. Lett.* 29 2623 (2004).
- [11] T. J. Yen, W. J. Padilla, N. Fang, D.C. Vier, D. R. Smith, J. B. Pendry, D. N. Basov, and X. Zhang, “Terahertz Magnetic Response from Artificial Materials,” *Science*, 303, 1494 (2004).

- [12] N. Katsaraki, G. Konstantinidis, A. Kostopoulos, R. Penciu, T. Gundogdu, M. Kafesaki, E. Economou, Th. Koschny, and C. M. Soukoulis, *Opt. Lett.* 30 1348 (2005).
- [13] S. Linden, C. Enkrich, M. Wegener, J. Zhou, T. Koschny, and C. M. Soukoulis, "Magnetic Response of Metamaterials at 100 THz," *Science*, 306, 1353-1361 (2004).
- [14] S. Zhang, W. Fan, B. K. Minhas, A. Frauenglass, K. J. Malloy, and S. R. J. Breuck, "Midinfrared Resonant Magnetic Nanostructure exhibiting Negative Permeability," *Phys. Rev. Lett.* 94 037402 (2005).
- [15] N. Katsarakis, Th. Koschny, M. Kafesaki, E. N. Economou, and C. M. Soukoulis, "Electric coupling to the magnetic resonance of split ring resonators," *Appl. Phys. Lett.* 84 2943 (2004).
- [16] K. Aydin, I. Bulu, K. Guven, M. Kafesaki, C. M. Soukoulis, E. Ozbay, "Investigation of magnetic resonances for different split ring resonator parameters and designs," *New Journal of Physics*, 7 168 (2005).
- [17] R.S. Penciu, K. Aydin, M. Kafesaki, Th. Koschny, E. Ozbay, E. Economou, C. M. Soukoulis, "Multigap individual and coupled split ring resonator structures," *Optics Express*, 16, 18131 (2008).
- [18] J. Zhou, Th. Koschny, M. Kafesaki, E. Economou, J.B. Pendry, C.M. Soukoulis, "Saturation of Magnetic response of Split Ring Resonators at optical frequencies," *Phys. Rev. Lett.* 95, 223902 (2005).
- [19] S. Linden, C. Enkrich, G. Dolling, M. W. Klein, J. Zhou, T. Koschny, C. M. Soukoulis, S. Burger, F. Schmidt and M. Wegner, "Photonic Metamaterials: Magnetism at Optical Frequencies," *Journal of selected topics in Quantum Electronics*, 12, 6 1097-1103 (2006).
- [20] Lumerical solutions.

- [21] I.E. Kadly, M. M. Sigalas, R. Biswas, K. M. Ho, and C. M. Soukoulis, “Metallic photonic crystals at optical wavelengths,” *Phys. Rev. B*, 62, 299 (2000).
- [22] J. Zhou, Th. Koschny, M. Kafesaki, E. N. Economou, J. B. Pendry, and C. M. Soukoulis, “Saturation of the Magnetic Response of Split Ring Resonators at optical frequencies,” *Phys. Rev. Lett.* 95, 223902 (2005).
- [23] S. Tretyakov, “On geometric scaling of split ring and double bar resonators at optical frequencies,” *Metamaterials* 1, 40 (2007).
- [24] A. Ishikawa, T. Tanaka, and S. Kawata “Frequency dependence of magnetic response of metamaterials,” *J. Opt. Soc. Am. B* 24, 510 (2007).
- [25] A. K. Sarychev, G. Shvets, and V. M. Shalaev, “Magnetic plasmon resonance,” *Phys. Rev. E* 73, 036609, (2006).
- [26] E. N. Economou, C. M. Soukoulis, and M. Kafesaki, “The fourth quadrant in ϵ and μ plane: A New Frontier in Optics,” *J. Comput. Theor. Nanosci.* 6, 1827 (2009)
- [27] C. M. Soukoulis, T. Koschny, J. Zhou, M. Kafesaki, and E. N. Economou, “Magnetic response of split ring resonator at terahertz frequencies,” *Phys. Status Solidi B* 244, 1181 (2007).
- [28] R. S. Penciu, M. Kafesaki, Th. Koschny, E. N. Economou, and C. M. Soukoulis, “Magnetic response of nanoscale left-handed metamaterials”, *Phys. Rev. B* 81, 235111 (2010).
- [29] B. Lahri, S. G. McMeekin, A.Z. Khokhor, R. M. De La Rue and N. P. Johnson, “Magnetic response of split ring resonator at visible frequencies,” *Optics Express* 18 (3), 3210-3218, (2010).
- [30] N. P. Johnson, A. Z. Khokhar, H.M. H. Chong, R. M. De La Rue, S. G. McMeekin,

- “Characterization at infrared wavelengths of metamaterials formed by thin film metallic split ring resonator arrays on silicon,” *Electronics Letters* 42 (19), 1117-1119, (2006).
- [31] G. Dolling, C. Enkrich, M. Wegner, J. F. Zhou, C. M. Soukoulis and S. Linden, “Cut-wire pair and plate pair as magnetic atoms for optical metamaterials,” *Optics Lett.* 30, 3198 (2005).
- [32] V. A. Podlovsk, A. K. Sarychev, and V.M. Shalaev, “Plasmon modes and negative refraction in metal nanowire composites,” *Opt. Express*, 11, 735 (2003).
- [33] V. M. Shalaev, W. Cai, U. K. Chettiar, H. Yuan, A. K. Sarychev, V. P. Drachev, A. V. Kildishev, “Negative index of refraction in optical metamaterials”, *Optics Lett.*, 30 (24), 3356-3358 (2005).
- [34] J. Zhou, L. Zhang, G. Tuttle, Th. Koschny, C. M. Soukoulis, “Negative index materials using simple short wire pairs”, *Phys. Rev. B* 73 041101 (2006).

4. Metamaterials fishnet structures

4.1 Introduction

Since the inception of negative index metamaterials in the microwave region there has been sustained efforts to shorten the operating wavelength into optical regime. The most challenging implementation of metamaterial concept requires engineering both negative permittivity and permeability in the same spectral region and hence achieving metamaterials with a negative refractive index at optical frequencies.

The demonstrations of NIMs in the previous chapter do not provide negative permittivity and permeability simultaneously at optical frequencies. There have been both fundamental and engineering challenges in scaling such metamaterials to optical wavelengths. The fundamental challenge arises from the fact that at optical frequencies, one starts to approach the plasma frequency of metals causing saturation in the magnetic response of these structures. The optimization of these structures has led to the structure so called *fishnet* structure.

The fishnet structure can be considered as a combination of pair of short slabs with continuous wires which are physically connected. A thorough investigation of the structure has shown that the fishnet structure is an optimized way to obtain metamaterials behaviour. It provides negative permittivity and permeability simultaneously at optical frequency and hence negative refractive index over a wide range of frequency. The first component of the fishnet metamaterials is short slabs oriented along the direction of magnetic field. This provides a magnetic response or artificial permeability that can achieve negative values around resonance. The second component is thin metallic wires oriented in the direction of the electric field of the incoming light. These wires behave as diluted metal with the decreased plasma frequency providing a negative effective permittivity that can be engineered separately from the permeability. These two components are combined to form the fishnet metamaterial where both negative permittivity and permeability can be engineered at particular wavelength. This structure functions as an inductor and capacitor resonator wherein the antisymmetric currents are created in the short slabs, which give rise to an

induced magnetic polarization in this structure. This structure has also been successful at scaling the response into the visible regime.

In this chapter detailed simulations were performed to understand the behaviour of this structure. Simulations were performed by changing the different geometric parameters of the structure and a systematic study is presented in the infrared part of the spectrum. The knowledge of basic magnetostatic has been employed and results are analysed on the basis of *LC* circuit description of the structure. The polarisation dependence of the structure is discussed and simulation results are provided for both *TE* and *TM* polarisation. As the metallic component of the structure have a significant impact on determining the properties of metamaterials, accurate modelling of metals is essential to predict the properties of these structure. Detailed simulation results are shown for different material data sets by embedding the frequency dependent data in the simulation software. The Figure of Merit *FOM* is provided for the comparison purpose. This structure has a potential to provide negative refractive index at visible frequency. The influence of different metals to a fishnet structure is studied in the visible regime to show which metal will be the best choice to benefit metamaterials in the achievements of a negative index property. The structure is simulated with different metals for instance (silver Ag, gold Au, copper Cu and aluminium Al). Silver (Ag) is supposed to be the best option for metallic parts of the fishnet structure to achieve negative index in the visible regime. The *FOM* obtained for different metals is provided for comparison purpose. The effect of substrate and dielectric spacer is briefly discussed.

A monolayer of unit cells along the propagation direction does not allow the investigation of the interesting physics associated with negative phase propagation. For a monolayer it is simply not possible to form a thick object such as a lens to manipulate light. A three dimensional 3D optical negative index can be obtained by stacking up multiple fishnet layers along the direction of propagation. This chapter is concluded with the transmission results for a multilayer fishnet structures. The negative refractive index of multilayer fishnet structure is obtained and convergence of material parameters is briefly discussed.

4.2 Numerical modelling of the fishnet structure

The simulation tool available for the analysis of electromagnetic problems is Lumerical *FDTD* solutions. The designing and computation of complex electromagnetic fields have

been an active research field. The *FDTD* method is widely used to solve various types of electromagnetic problems. This method has been proven to be the one of the most effective numerical methods in the study of metamaterials. The *FDTD* method was first described by the Yee in 1966 [1]. It offers a simple and straight forward method to model complex periodic structures. This method is convenient to characterize metamaterials over a wide frequency band. The numerical dispersion effects can be reduced by keeping the unit cell size extremely small in comparison to the wavelength say on the order of $(\lambda/30)$ and $(\lambda/20)$. This method is still evolving as the development of *FDTD* schemes that are more accurate and computationally efficient are continuing. This method has enabled us to solve problems with large degrees of freedom, with many unknowns which are usually encountered while characterizing metamaterials.

The guidance from simulations is helpful and desirable because of the costly fabrication of metamaterials in the optical regime.

4.2.1 Simulation set up

The reflection and transmission characteristics are calculated from a single unit cell of fishnet structure. The single unit cell of fishnet structure is shown in Figure 4.1. A polarized plane wave source with its polarization defining electric field component E_x perpendicular to the long axis of the fishnet slab is applied. The fishnet structure is not stacked on any substrate. The structure is illuminated by a plane wave source over the wavelength range from 150 THz to 300 THz. The direction of propagation of source is in negative z -direction. The simulation area is a rectangular parallelepiped shape. The calculation region is 600 nm x 600 nm x 2000 nm³ with a conformal mesh region self-adapted to the structure. A perfectly matched layer is imposed on the edge planes of the simulation area perpendicular to the direction of propagation of source. This boundary condition is an absorbing boundary condition and ideally it should produce zero reflections but in practice there will always be small reflections. The reflections from this boundary can be reduced by increasing the number of perfectly matched layers. A very fine mesh size of 3 nm is used within the metal layers and is adequate for simulation convergence.

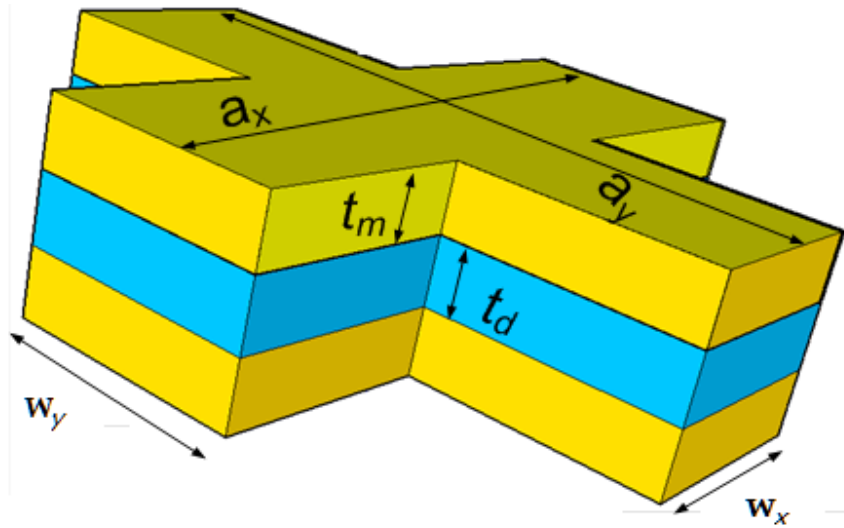


Figure 4.1: Unit cell of perforated fishnet structure with dielectric spacer MgF_2 embedded in between two metal Ag layers. The thickness of metal films $t_m = 30$ nm and dielectric spacer $t_d = 40$ nm are kept constant.

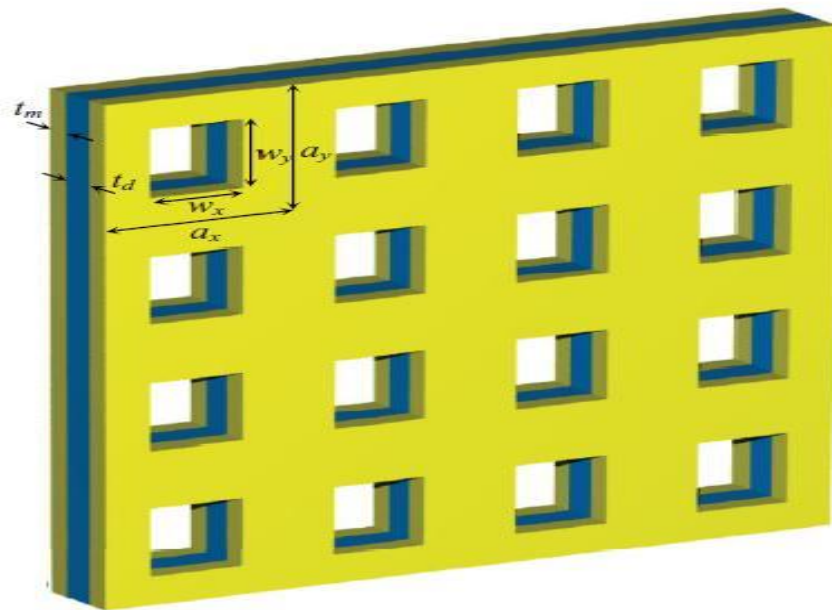


Figure 4.2: Sketch of the fishnet structure, a_x and a_y are the unit cell sizes along x and y directions respectively. w_x and w_y show the hole size. t_m and t_d are the thickness of metal films and dielectric spacer respectively. The dimensions of geometric parameters are given in Table 4.1.

The structure is periodic in both x and y directions. The periodic boundary conditions are used in both x and y directions. Depending upon the polarization of the source the periodic

boundaries in the x and y are replaced by imposing an antisymmetric/symmetric boundary condition. Antisymmetric/symmetric boundary conditions are used in the x and y directions respectively in case of TE polarisation. Symmetric/antisymmetric boundary conditions are used in x and y directions respectively in case of TM polarisation. The simulation volume and time can be reduced by factors of 2 or 4 by taking the advantage of symmetry of the structure. By choosing these boundary conditions it allows only quarter of the structure to be simulated thus running the simulation 4 times faster than the equivalent simulation without symmetry. The refractive index of a dielectric spacer material is set to 1.7.

4.3 Polarization dependence of the fishnet

It should be noted that there exists a difference in the spectral position as well as the magnitude of the resonance obtained from two different polarization configurations. For the transverse electric mode (TE) the electric field component of plane wave is parallel to the thin wires and perpendicular to the slab-pairs of the structure. These thin wires act as electric dipoles and their overall response can give rise to negative permittivity. The geometric parameters of the structure are given in Table 4.1. The thickness of metal films $t_m = 30$ nm and dielectric spacer $t_d = 40$ nm are kept constant.

| a_x | a_y | w_x | w_y |
|--------|--------|--------|--------|
| 500 nm | 600 nm | 300 nm | 250 nm |

Table 4.1: Table listing the geometric parameters for the unit cell of fishnet structure shown in Figure 4.1.

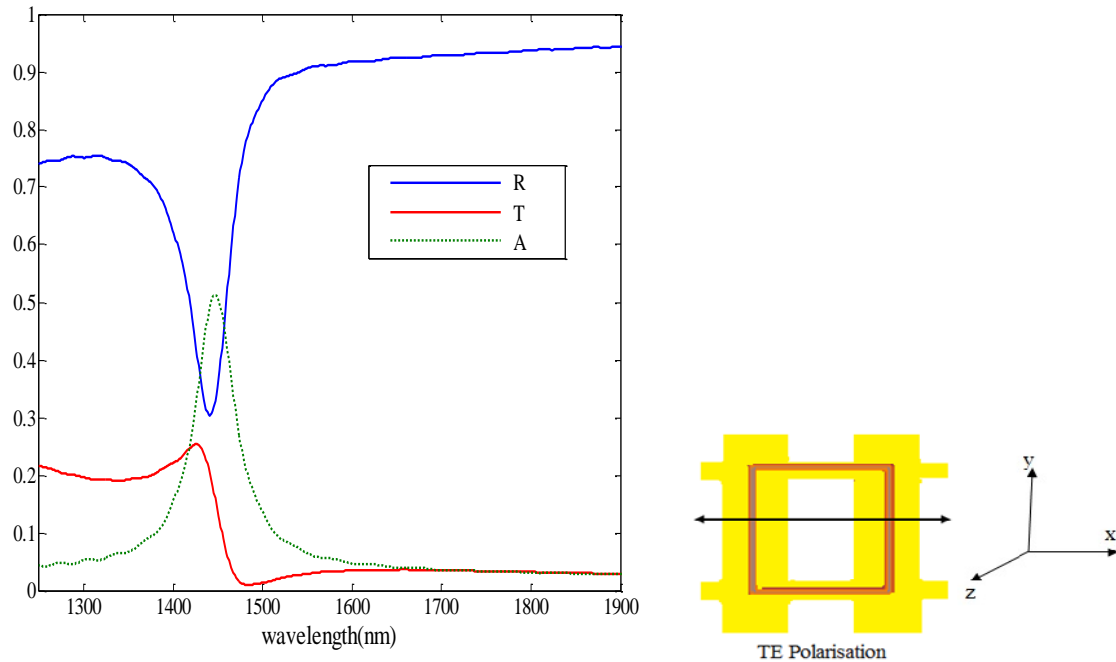


Figure 4.3: Simulated Reflection/Transmission/Absorption obtained from a fishnet structure. The polarisation configuration is also shown.

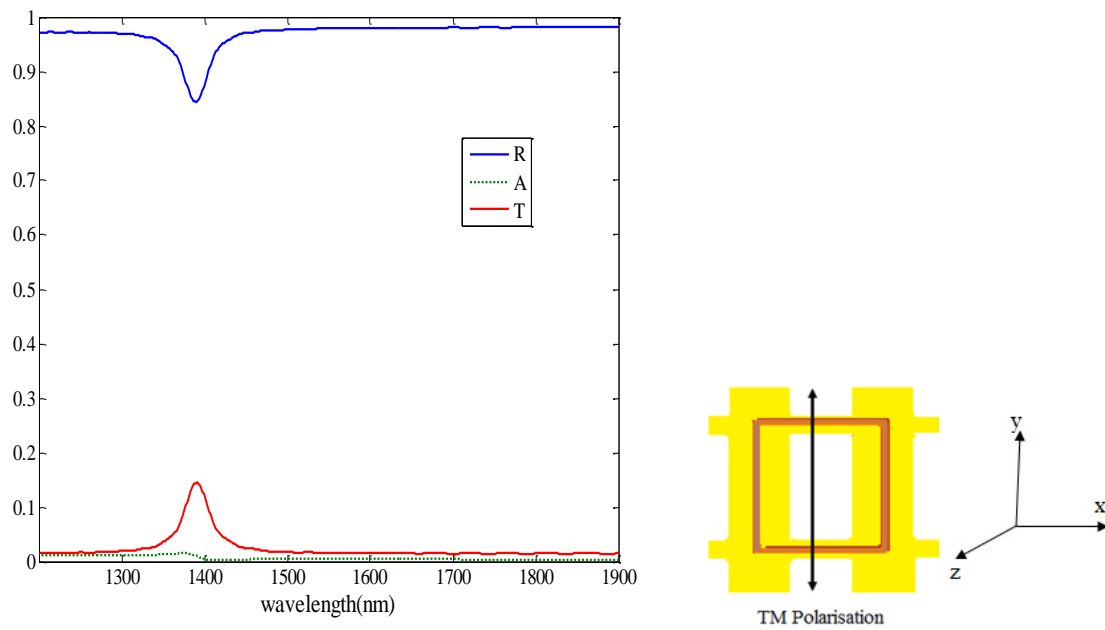


Figure 4.4: Simulated reflection/transmission/absorption coefficients obtained from TM Polarisation.

The electric field component of the plane wave is perpendicular to the *TM* mode and parallel to the slab pairs. It has been noted that fishnet structure does not show any response to electromagnetic wave for this polarization configuration. Hence there is a significant difference in the magnitude as well as the spectral position of the resonance as shown in Figure 4.4. A very small reflection/transmission dip at around 1400 nm is due to the fact that the aspect ratio of hole size in *x* and *y* direction is very small.

It is possible to obtain isotropic fishnet structure by making proper modifications in the conventional fishnet structure. It is essential to perform modifications of almost all structure parameters to achieve an isotropic fishnet structure. The isotropic fishnet metamaterials has the advantage of lower losses and higher transmission and holds the potential for further applications [2]. Planar fishnet metamaterials have been reported with optical properties independent of incident polarization configurations such as fishnet with equal width metallic stripes along two orthogonal directions which corresponds to structure with square holes [3-5]. However the square-hole fishnet structure displays more losses and inferior performance than the conventional fishnet structure [6].

4.4 Parametric investigation of fishnet structure

In this section, a systematic study of the fishnet design is presented in the infrared part of the spectrum, attempting to understand the behaviour of the design and the origin of its superior performance, mainly its ability to produce negative index behaviour over a wide range of structure parameters mainly length and width of the slab and width of the neck.

4.4.1 LC Circuit Model:

a) Magnetic response of the structure

The electromagnetic response of the structure can be studied by a simple *LC* circuit description of the structure. The fishnet structure can be treated as a physical combination of two different types of wires. The combination of short slab pairs is contiguous along magnetic field component *H* and continuous wires which are along *E* directions. The currents at the short slab pair are antiparallel forming a loop-current and the currents at the neck part forming another loop current opposite to one of the slabs which contributes to the magnetic response of the structure [7].

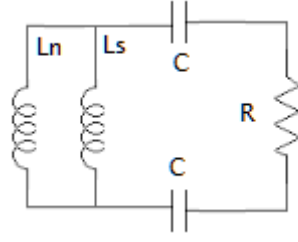


Figure 4.5: The equivalent RLC circuit used for the description of fishnet structure shown in Figure 4.1.

These contributions can be taken into account in an effective LC circuit model of the structure by considering the loop inductance of a neck L_n in parallel to the one of the slabs L_s .

$$\omega_m^2 = \frac{1}{LC} = \frac{1}{L_s C} + \frac{1}{L_n C} \quad (4.1)$$

C is the capacitance between the slabs of the pair. The inductance and capacitance of the isolated (which are not connected to wires) slab pairs are slightly different than those of the fishnet structure.

It is easy to obtain the geometrical dependence of magnetic resonance frequencies of the fishnet structure by using LC circuit analysis

The parallel plate capacitor formula for capacitance C of the slabs and solenoid inductor description for the loop inductances is given by

$$C \sim \frac{a_y w_x}{t_d}, \quad L_s \sim \frac{w_x t_d}{a_y}, \quad L_n \sim \frac{l_n t_d}{w_y} \quad (4.2)$$

Where a_y and w_y are the widths of the slabs and necks respectively, while w_x and l_n are the corresponding lengths. The qualitative behaviour of the magnetic resonance frequency is given by [7].

$$\omega_m \sim \sqrt{\frac{1}{w_x^2} + \frac{1}{a_y l_n} \frac{w_y}{w_x}} \quad (4.3)$$

b) Electric response of the structure

The electric response of the structure is also very important besides magnetic response of the structure. It plays an important role in determining the possibility of achieving left handed frequency band. The magnetic components such as *SRRs* and short slab pairs are introduced

in a thin wire system to obtain left handed frequency band [8]. This introduction severely modifies the plasma frequency of the thin continuous wires. The total plasma frequency of the left handed metamaterial (*LHM*) can be determined by the electric dipole-like resonance frequency of the magnetic structure which in most left handed metamaterials lies below the plasma frequency of thin wires. The effect of this dipole like resonance frequency is a strong downward shift of the plasma frequency which is an undesirable effect for the achievement of *LHM* [9, 10]. The effective inductance of the necks of the structure L'_n is parallel with the slab inductance L'_s , so

$$\omega_e^2 = \frac{1}{L'_s C'} = \frac{1}{L'_s C'} + \frac{1}{L'_n C'} \quad (4.4)$$

L'_s denotes the straight wire inductance of the slabs of the pair and L'_n denotes the inductance of one of the necks, C is the capacitance between neighbouring slabs.

The electric resonance frequency of the fishnet structure is higher than that of slabs only. This frequency is already higher than the magnetic resonance frequency. It is because of the large width of the slabs which leads to the small inductance L'_s and thus it has an insignificant effect of the plasma frequency of the fishnet structure. So the plasma frequency of the fishnet structure is only determined by the continuous wires.

The geometrical dependence of electric resonance frequency can be obtained by using *LC* circuit analysis [10]. The capacitance C' between neighbouring slabs is given by

$$C' \sim a_y \quad (4.5)$$

The inductances L'_s and L'_n can be given by the formulas for a straight wire inductances [20, 26]

$$L'_s \sim w_x \ln\left(\frac{w_x}{a_y}\right), L'_n \sim l_n \ln\left(\frac{w_x}{w_y}\right) \quad (4.6)$$

The electric resonance frequency takes the form [9]

$$\omega_e^2 = \frac{1}{a_y} \left[\frac{A}{w_x \ln(w_x/a_y)} + \frac{B}{l_n \ln(l_n/w_y)} \right] \quad (4.7)$$

Equations (4.3) and (4.7) show the dependence of the magnetic and electric resonance frequencies on the system parameters.

The geometric parameters of the structure are given in Table 4.1. Detailed simulations were performed by changing the different parameters of the structure to understand the behaviour of the structure. There is a qualitative agreement of the results with the reference [7] in which the parametric investigation is done for microwave frequency region.

4.4.2 The neck contribution in electromagnetic response of the fishnet

The neck width is an important parameter which determines the left handed and right handed regime in this structure. The dimensions of neck width has a significant effect on both electric and magnetic resonance of the structure and hence on the overall behaviour of the structure. Simulations were performed for three different neck widths w_y of the fishnet structure. The results are shown in Figure 4.6.

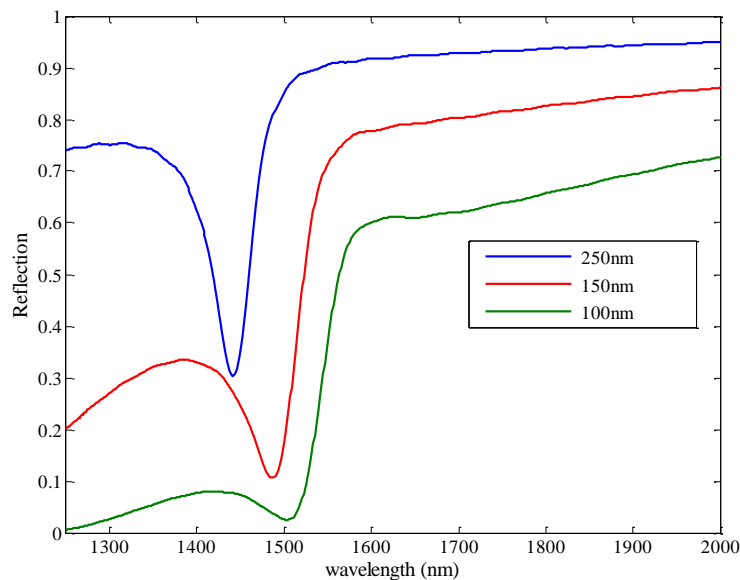


Figure 4.6: Simulated reflection spectra of fishnet structure for different widths of neck w_y . The geometric parameters are shown in Table 4.1 for the structure shown in Figure 4.1. The results are shown for three different neck widths of the fishnet structure i.e., 250 nm, 150 nm and 100 nm.

The decrease in the neck width leads to decrease of both electric and magnetic resonance of the structure which can be understood from equations 4.3 and 4.7. The decrease in the neck width is responsible for the downward shift in the plasma frequency which is due to the decrease of the continuous wires plasma frequency in the fishnet. Thinner wires in a continuous wire system lead to lower plasma frequency values due to the lower density of electrons and to larger magnetic field inductance [11]. The decrease in this parameter leads

to increase of loop inductance and hence decreasing neck's contribution to the magnetic resonance frequency [9]. The contribution of the neck's loop inductance results to an upward shift of the magnetic resonance frequency, compared to the slab-pairs only.

4.4.3 The slabs width contribution in electromagnetic response of the fishnet

The slab width has a significant effect on the overall plasma frequency of the system. This increase of the plasma frequency is a result of both the increased electric resonance frequency of the slabs due to increased slab straight-wire type inductance and decreased average width of the continuous-wire component of the structure. There is an increase in the magnetic resonance frequency by decreasing slab width which can be understood from equations 4.1 and 4.3. In isolated slab-pairs the width of the slabs does not affect their magnetic resonance frequency significantly as discussed in Chapter 3. Simulations were performed for three different slab widths a_y , the results are shown in Figure 4.7.

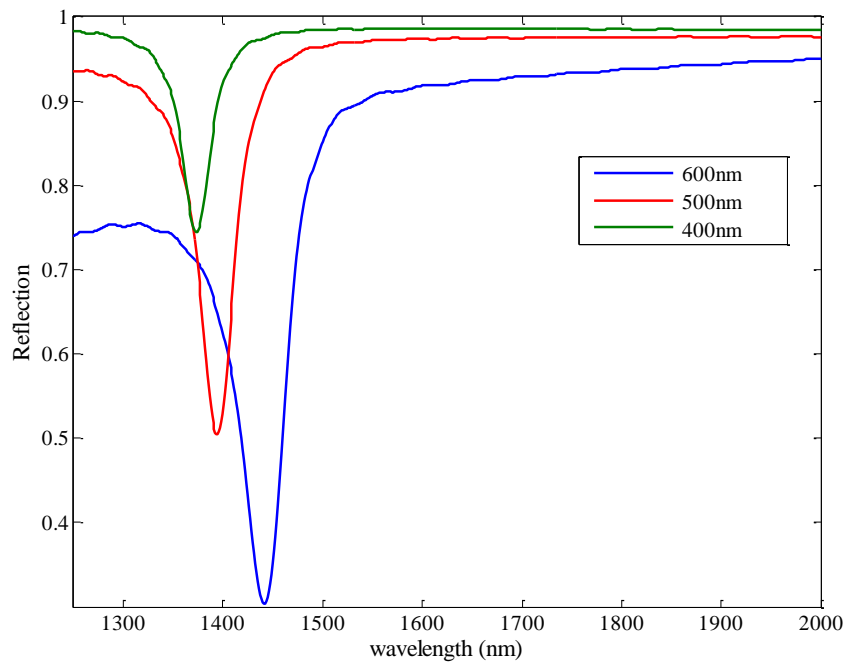


Figure 4.7: Simulated reflection spectra for fishnet structure for different widths of slab a_y . The geometric parameters are shown in Table 4.1 for the structure shown in Figure 4.1. The results are shown for three different slab widths of the fishnet structure i.e., 600 nm, 500 nm and 400 nm.

The reduction of width results in an increase of the slab inductance, which is compensated by an analogous decrease of the capacitance in an isolated slab pairs. But in the case of the fishnet the coupling between slabs and necks makes this parameter have a considerable influence. The ratio of slab inductance to the neck inductance has a significant effect on the electromagnetic response of the fishnet structure. The qualitative behaviour of the results shown in Figure 4.7 is in agreement with the results obtained at microwave frequencies [7]. There is a shift in the spectral position as well as the decrease in the magnitude of the resonance with the decrease in the slab width.

4.4.4 The slabs length contribution in electromagnetic response.

There is a slight upward shift of the system plasma frequency by increasing the slab length. This upward shift is due to the contribution of the straight-wire component of the structure which gets a larger average width and hence an increased plasma frequency. Simulations were performed by changing the length of the slab. The magnetic and electric resonance frequency increases with the decrease in the length of the slab as predicted from equations (4.3) and (4.7).

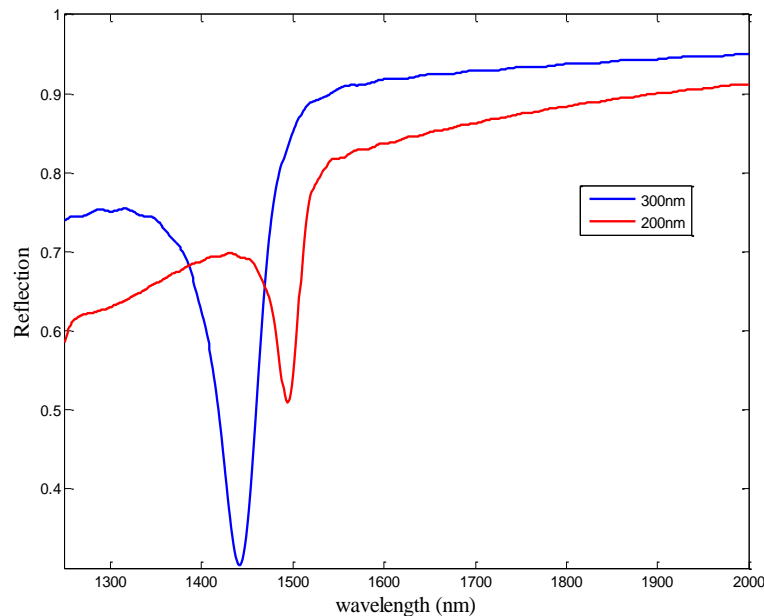


Figure 4.8: Simulated reflection spectra for fishnet structure for different lengths of slab w_x . The geometric parameters are shown in Table 4.1 for the structure shown in Figure 4.1. The results are shown for two different slab widths of the fishnet structure i.e., 300 nm, 200 nm.

The qualitative behaviour of the results obtained in this section is in agreement with the results obtained at microwave frequencies; more geometrical parameters or factors contribute to the performance of fishnet metamaterials at higher frequencies [7, 9].

4.4.5 Discussion.

Since the fishnet structure appears to be an optimized design for achievement LHM metamaterials, it is very important to investigate it in detail and to predict the electromagnetic response of this design. Since most of the conclusions on the fishnet design are based on the results of simulations in the microwave region is important to validate these conclusions in the infrared region. The following conclusions are made on the basis of analytical theory explained in section 4.4.1.

1. By changing the neck width w_y of the fishnet structure as shown in Figure 4.1, the resonance positions of the reflection properties are changing significantly as shown in Figure 4.6. By decreasing this parameter, both electric and magnetic resonance frequencies decrease which can be understood with the help of equations 4.3 and 4.7. The decrease in the electric and magnetic resonance frequency is responsible for the shift of resonance position towards the longer wavelength region.
2. By changing the slab width a_y of the fishnet structure as shown in Figure 4.1, there is a slight change in the resonance position of the reflection properties which can be understood with the help of equations 4.3 and 4.7. There is a significant decrease in the amplitude of reflection plot as shown in Figure 4.7 by reducing the slab width.
3. The slab length is an important parameter which changes the electric and magnetic resonance frequencies. There is a decrease of both electric and magnetic resonance frequencies with an increase in the slab's length. By decreasing the length of the slab, amplitude of the reflection properties decreases as well as the resonance position shifts towards the longer wavelength range.

This work can be treated as solid foundation for optimizing fishnet structure aiming at realizing more practical applications with in a wide range of frequency regimes.

4.5 Modelling of metallic constituent of the fishnet structure

It has been observed that the constituents of these metamaterials are not being accurately modelled. To accurately predict the behaviour of metamaterials it is required that all the related materials should be correctly modelled. The metallic components of structure have a significant impact on determining the properties of left handed metamaterials. Metamaterials involve the use of metal which leads to inherently large losses particularly at optical or visible frequencies. The discussion in this section covers how we should model metals accurately and which material model or experimentally measured material data provides best choice for modelling metals.

There are various sources providing different sets of frequency-dependent material data to describe noble metals for metamaterials. The thickness of metallic inclusions in metamaterials structure is only 25-50 nm. The material property of thin film metal is different from that of a bulk metal. It is because of the additional scattering for electrons resulting from the metal surfaces. The Drude model is widely used for the modelling of noble metals and to describe their properties [12, 13]. It is given by

$$\varepsilon(\omega) = \varepsilon_{\infty} - \frac{\omega_p^2}{\omega^2 + i\omega\omega_c} \quad (4.8)$$

Where ω is the frequency, ε_{∞} is the offset value of permittivity, ω_p and ω_c are the plasma and collision frequencies respectively. The real and imaginary parts of frequency dependant permittivity provided by Drude model are given by.

$$\varepsilon_r(\omega) = \varepsilon_{\infty} - \frac{\omega_p^2}{\omega^2 + \omega_c^2} \quad (4.9)$$

$$\varepsilon_i(\omega) = \frac{\omega_p^2\omega_c}{\omega(\omega^2 + \omega_c^2)} \quad (4.10)$$

The corresponding real and imaginary part of complex refractive index are given by

$$n = n_r + i\kappa \quad (4.11)$$

where n_r is the real part of refractive index and κ is the extinction coefficient or the imaginary part of refractive index. The relationship between complex dielectric constant and complex refractive index is as follows.

$$\varepsilon(\omega) = \varepsilon_r(\omega) + \varepsilon_i(\omega) \quad (4.12)$$

$$n_r = \left[\frac{1}{2} ((\varepsilon_r^2 + \varepsilon_i^2)^{1/2} + \varepsilon_r) \right]^{1/2} \quad (4.13)$$

$$\kappa = \left[\frac{1}{2} ((\varepsilon_r^2 + \varepsilon_i^2)^{1/2} - \varepsilon_r) \right]^{1/2} \quad (4.14)$$

The frequency dependent data for the desired metal is usually obtained before embedding in the electromagnetic solvers. However the Drude model does not may not be valid when the frequency range of interest goes in to the optical regime. Johnson and Christie (JC) data is specifically measured for thin film metals [14]. This data is proven to be independent of thickness in the range 25-50 nm. It is very appropriate for application in the modelling of metamaterials in the optical regime in which the thickness of metallic inclusions is usually tens of nanometers.

4.5.1 Numerical Example

A comparison of different sets of material data is provided for fishnet structure. The geometrical parameters are same as shown in Table 4.1. The reflection R , transmission T and retrieved effective electromagnetic parameters are obtained for infrared and visible frequency regimes. The Drude model for gold which is widely used in the field of metamaterials [15] has $\varepsilon_\infty = 1$, $\omega_p = 2175$ THz and $\omega_c = 10.725$ THz. This Drude model is labelled as Drude model A. The application of Drude model (A) for gold in the design of metamaterials fishnet in this instance may lead to an inaccurate and overly optimistic prediction of performance. Another improved Drude model (B) for gold which fits JC data better has $\varepsilon_\infty = 9.6$, $\omega_p = 2184$ THz and $\omega_c = 17$ THz [16]. The comparison of frequency dependent complex refractive index for Drude model (A) and (B) with JC data is shown in Figure 4.8.

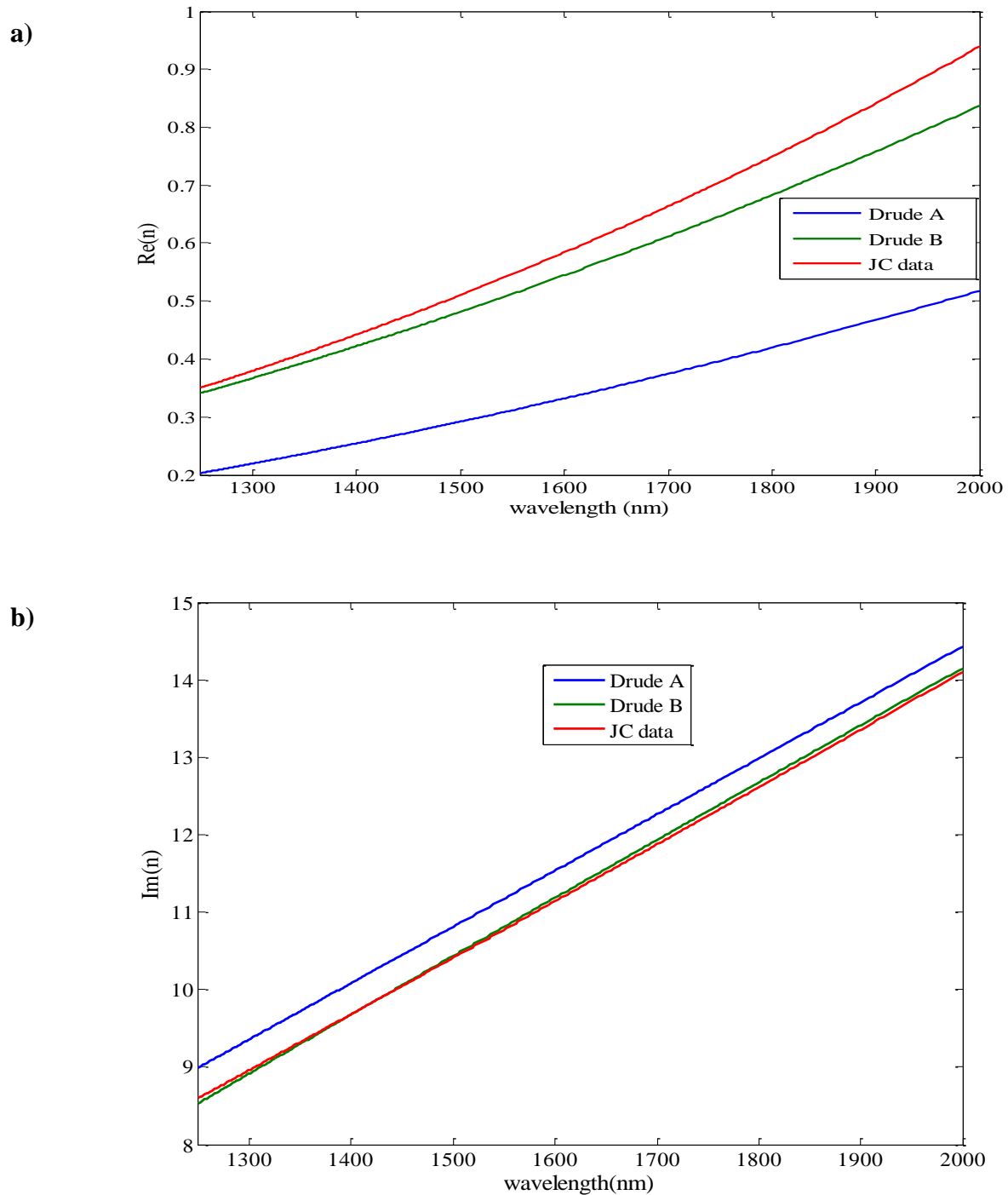


Figure 4.9: comparison of real and imaginary parts of refractive index for gold with Johnson-Christy data, Drude A, Drude B. a) Real part of refractive index $\text{Re}(n)$ b) Imaginary part of refractive index $\text{Im}(n)$.

Comparison of real and imaginary parts of complex refractive index for different material data sets are shown in Figure 4.9. It can be seen clearly that improved model Drude (B) fits experimentally measured data very well while widely used Drude model (A) has a significant variations with the JC data.

The electromagnetic material parameters are obtained from complex reflection/transmission coefficients for the fishnet structure in the infrared frequency range. Real and imaginary parts of dielectric permittivity, magnetic permeability and refractive index using Drude model (A) are shown in Figure 4.10. The negative refractive index has a magnitude of 4 and negative permeability has a magnitude of 1. This data provides a stronger magnetic resonance under the lower loss consideration. The results of this case are moderately superior over the other two cases of Drude model (B) and JC data. The results are in good agreement with the reference [16].

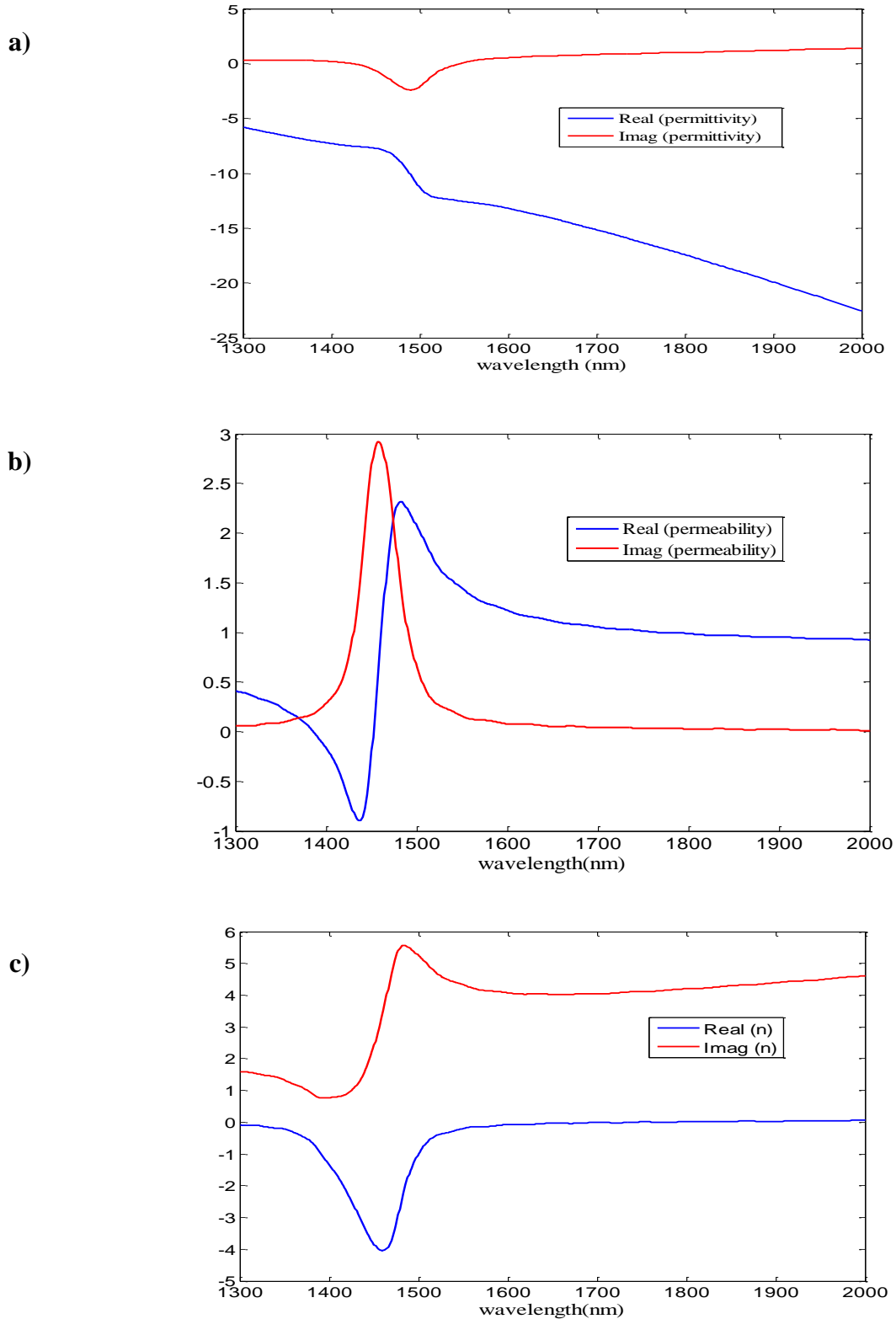


Figure 4.10: Retrieved electromagnetic parameters for the fishnet structure. The geometric parameters are shown in Table 4.1. a) Real and imaginary part of ϵ b) Real and imaginary part of μ c) Real and imaginary part of n .

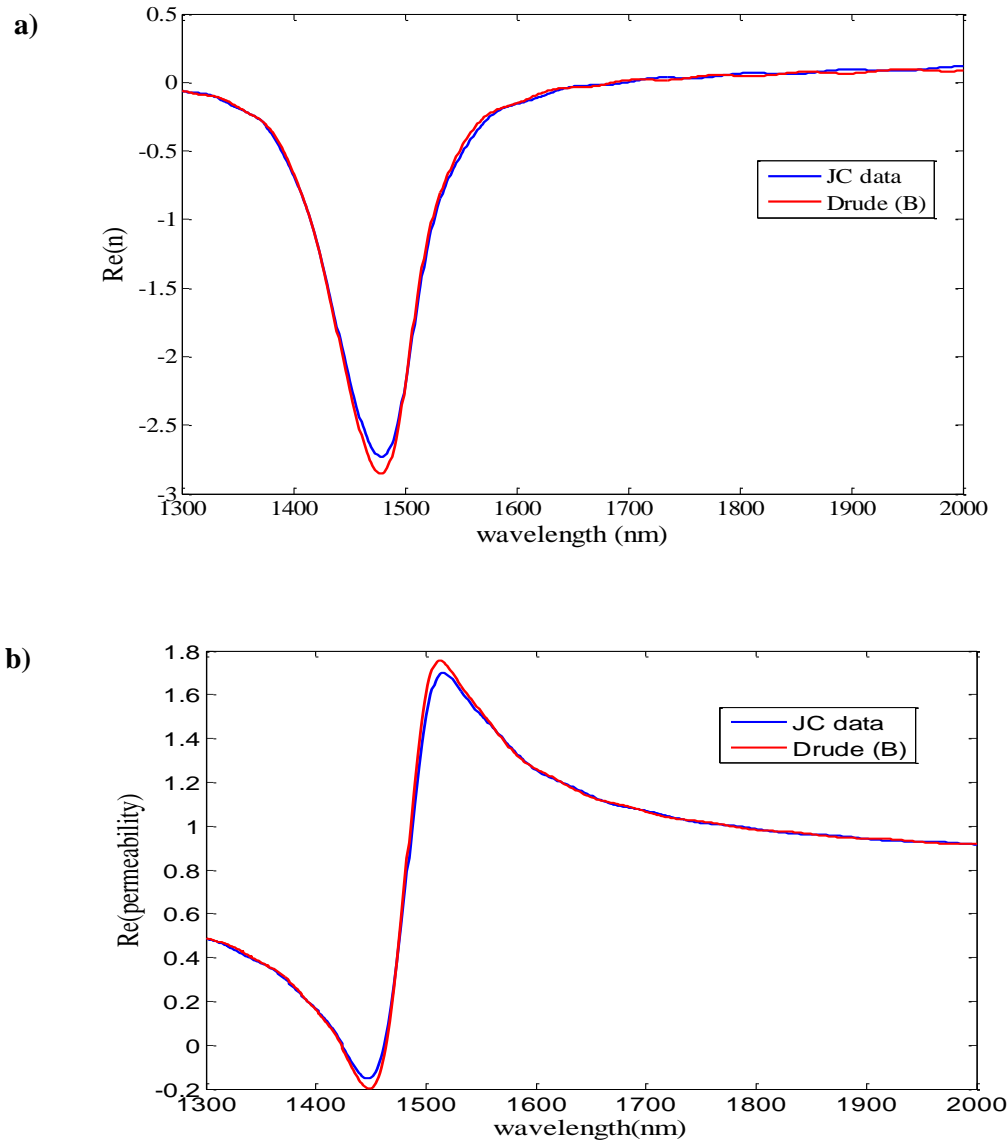


Figure 4.11: Comparison of Drude model (B) and Johnson & Christy data for the fishnet structure a) Real and imaginary part of n b) Real and imaginary part of μ .

The widely used Drude model (A) does not provide realistic properties of the metal for the infrared range. The results obtained from the comparison of Drude model (B) and Johnson & Christy data for the fishnet structure are shown in Figure 4.11. The results obtained are almost the same which are expected because of the perfect fit of the Drude model (B) to JC data for gold for this frequency region.

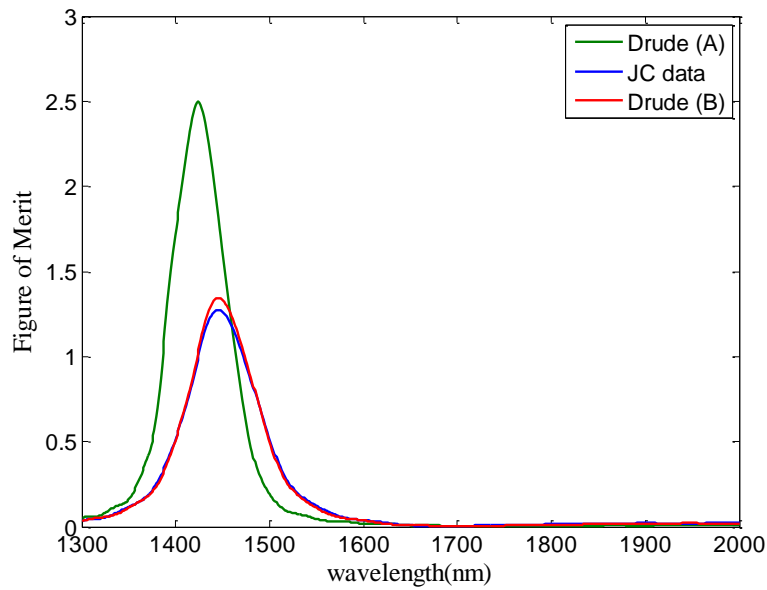


Figure 4.12: Comparison of the Figure of Merit for the fishnet structure for three different material data sets for gold.

4.6 Fishnet at Visible frequency

The fishnet has the potential to provide negative refractive index at visible frequency unlike its predecessors. Structure optimization has been proven to be a very effective way in obtaining desired properties of metamaterials. The fishnet has an advantage over the other commonly used structures that it can provide negative permittivity and negative permeability simultaneously occurring at visible frequency region and hence negative refractive index.

The simulated reflection/transmission/ absorption coefficients for the fishnet structure operating at visible frequency range are shown in Figure 4.12. The geometric parameters are obtained from [16] and are shown in Table 4.2. The simulation setup is almost the same as the fishnet operating at infrared range. It is explained in Section 4.2.1. The thickness of metal and dielectric spacer is also same. The metal properties are described by the Drude model (B) for gold because this model has proven to fit the experimental data very well at infrared range. The resonances in the reflection/transmission coefficients are occurring around 600 nm as shown in Figure 4.13.

| a_x | a_y | w_x | w_y |
|--------|--------|--------|--------|
| 200 nm | 220 nm | 100 nm | 120 nm |

Table 4.2: Table listing the geometric parameters for the unit cell of fishnet structure shown in Figure 4.1 for visible range.

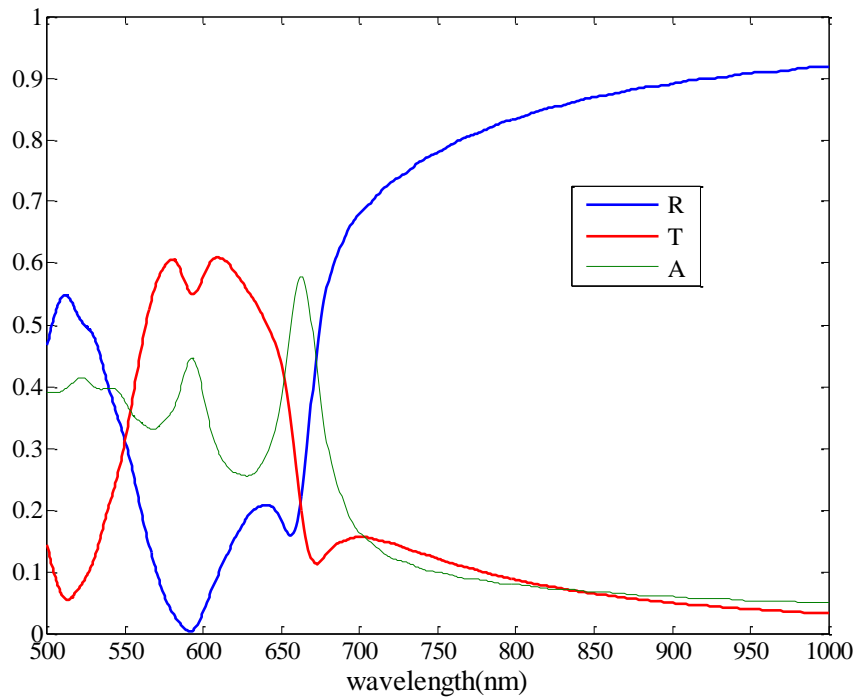


Figure 4.13: Reflection/transmission/absorption coefficient obtained from fishnet structure at visible frequency region. The geometric parameters are given in Table 4.2.

The electromagnetic material parameters are obtained from complex reflection/transmission coefficients for the fishnet structure at visible frequency. A magnetic resonance around 650 nm with positive values of permeability throughout the region. The negative refractive index does exist with quite low values. This negative refractive index is only due to negative permittivity and this provides very low values of figure of merit (FOM) indicating high losses. The choice of metal for fishnet structure is discussed in next section. Comparison of FOM for three material data sets is also shown in Figure 4.12.

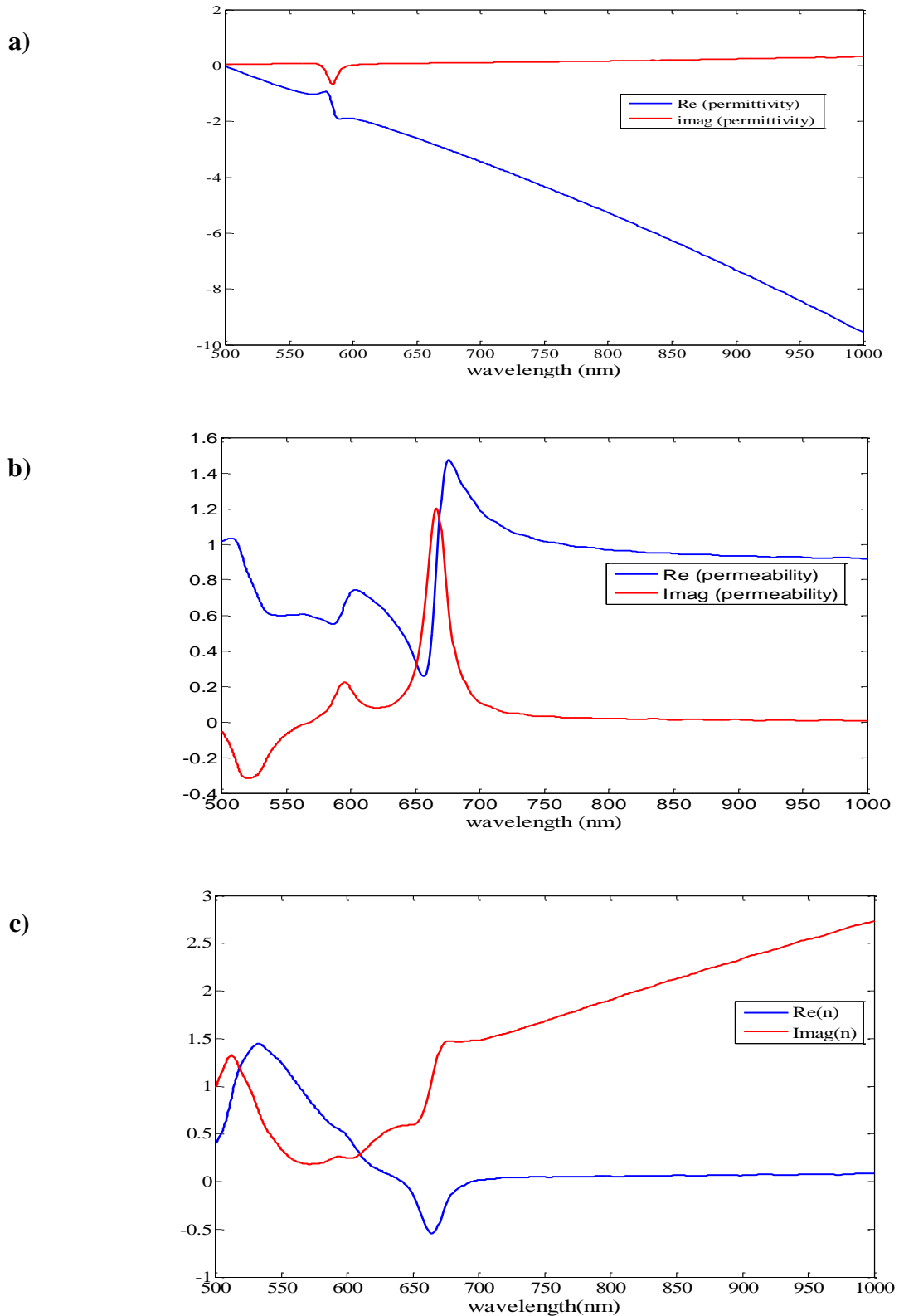


Figure 4.14: Retrieved electromagnetic material parameters for the fishnet structure at visible frequency range a) Real and imaginary part of ϵ b) Real and imaginary part of μ c) Real and imaginary part of n .

4.7 Choice of metal

In this section the influence of different metals to metallodielectric metamaterials is studied in the visible regime to show which metal will be the best choice to benefit metamaterials in the achievements of a negative index. Figure 4.15 shows the real and imaginary part of JC data from 500 nm to 1000 nm for thin film of gold, copper and silver. The JC data for aluminium is not available so Drude model is used to describe the properties of aluminium.

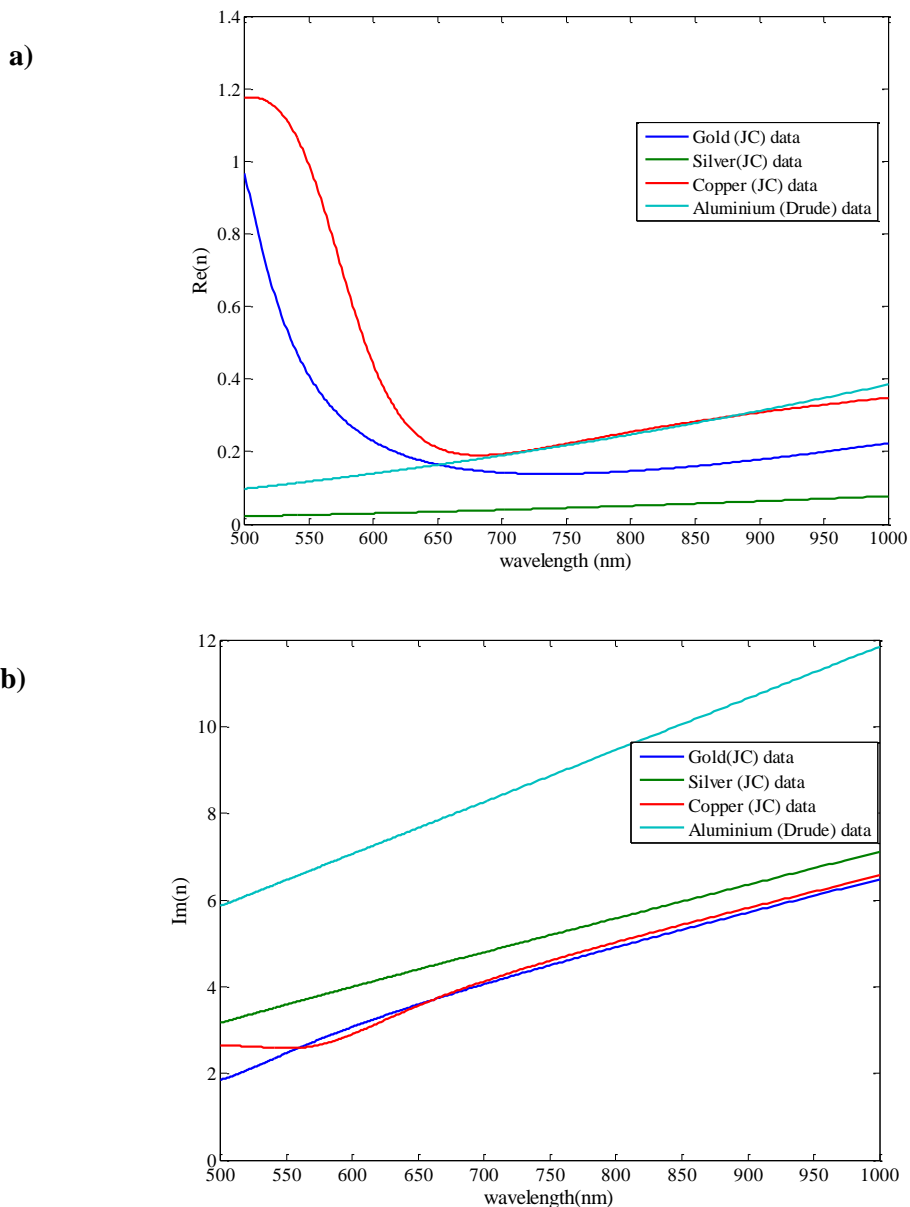


Figure 4.15: Comparison of real and imaginary part of refractive index for gold (Au), silver (Ag), copper (Cu), aluminium (Al).

To study the properties of metamaterials in the optical frequency region accurately, experimentally measured data is preferred to describe to the metal inclusions. These metallic inclusions begin to play a crucial role in determining the performance of metamaterials in the optical regime.

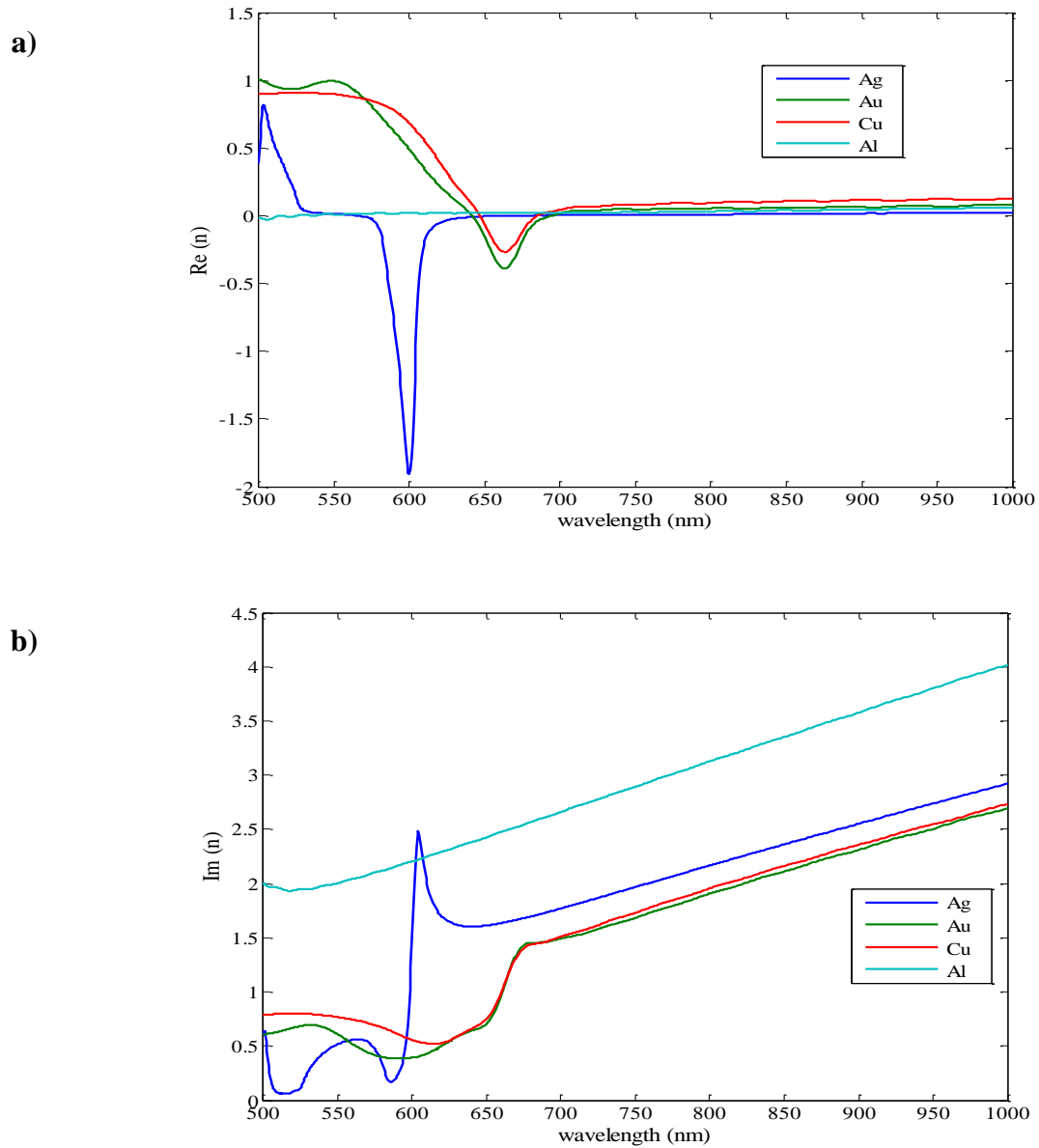


Figure 4.16: Comparison of a) real and b) imaginary part of refractive index n for fishnet structures in visible frequency range for gold (Au), silver (Ag), copper (Cu), and aluminium (Al).

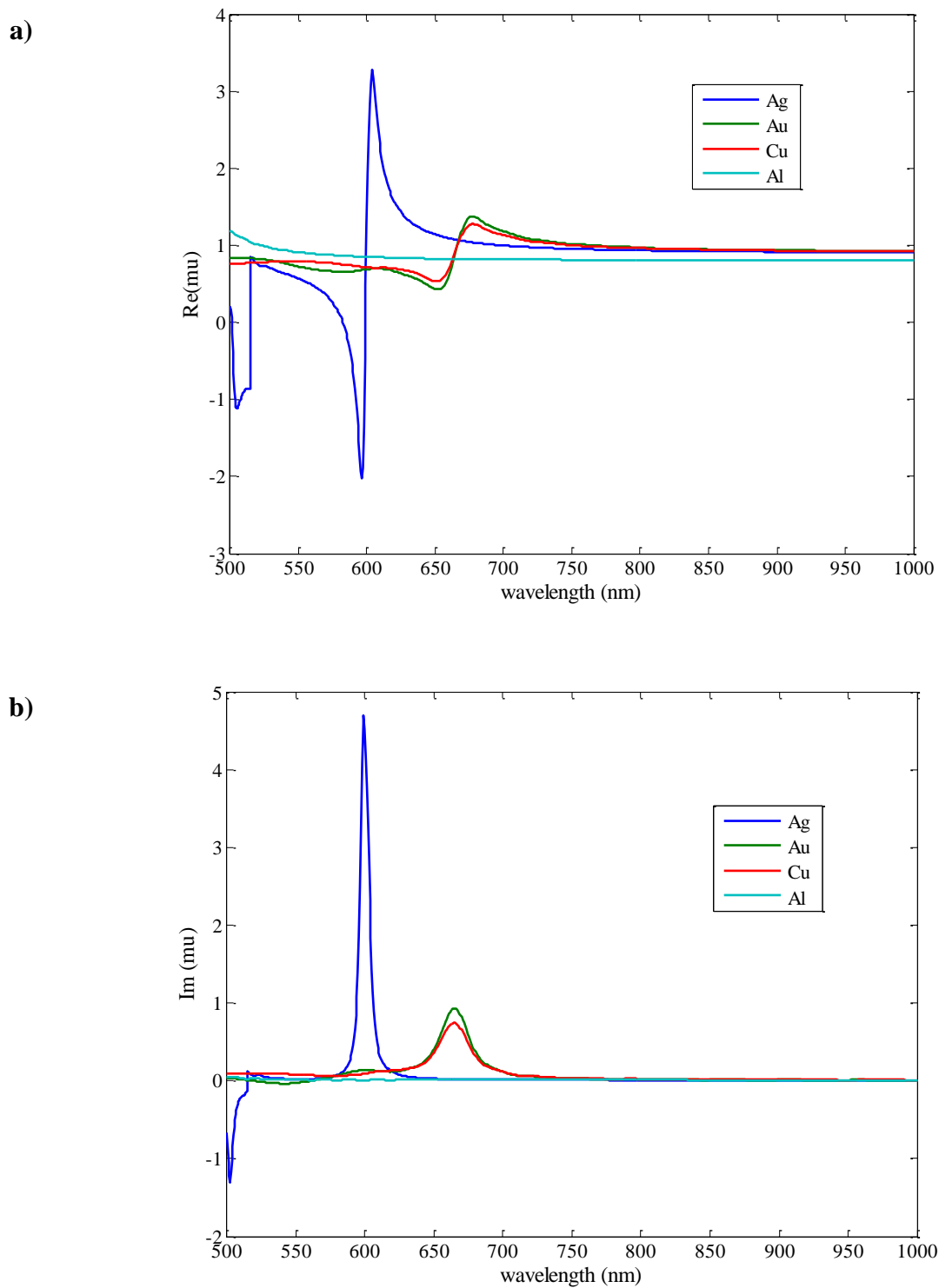


Figure 4.17: Comparison of a) real and b) imaginary part of μ for fishnet structure at visible frequency range for gold (Au), silver (Ag), copper (Cu) and aluminium (Al). The geometric parameters are given in Table 4.2.

The effective material parameters obtained from the fishnet structure for different metals are shown in Figure 4.16 and Figure 4.17. The negative n is achieved with gold with quite low values. In comparison, the cases for copper, silver and aluminium are shown. The

performance of fishnet is even worse for the aluminium than the case with the gold. The results obtained from aluminium are also not as good as for silver. It can be concluded from the above results that silver has the lowest loss throughout this frequency range. The silver made fishnet might be able to render the most promising property. This speculation needs to be confirmed through the comparison of real performances of metamaterials made with different metals [16].

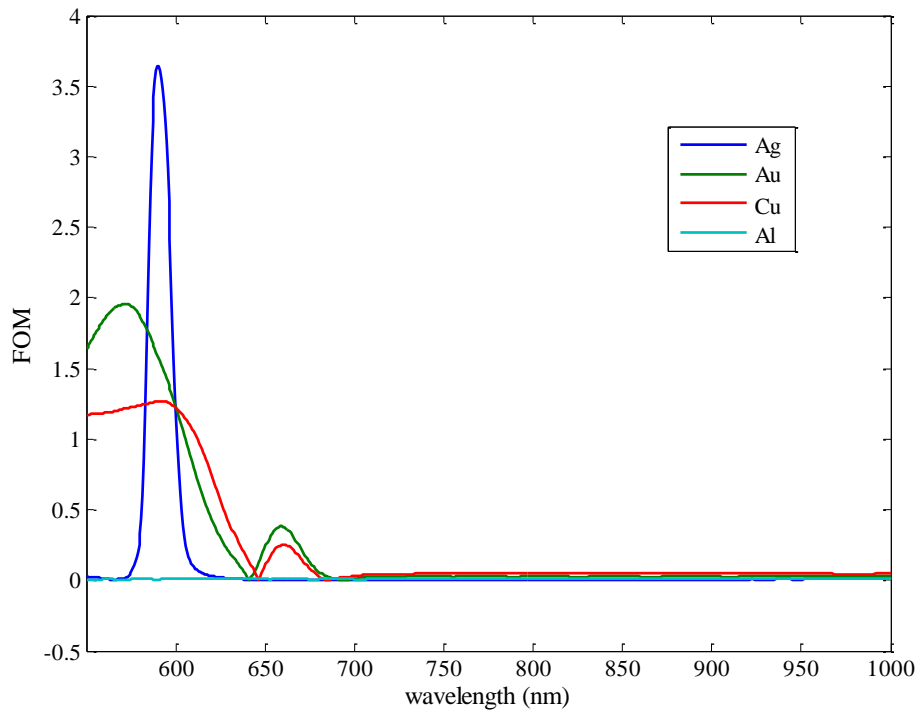


Figure 4.18: Comparison of FOM for fishnet structure at visible frequency range for different metals. The geometric parameters are given in Table 4.2.

The metallic inclusions in the metamaterials are usually composed of noble metals. But unfortunately the noble metals used in these photonic structures are not particularly good conductors at high frequencies. They result in a significant dissipative loss which is the most important challenge to their applicability in real world devices. It has been also proposed to reduce the loss problem by replacing noble metals by other materials.

4.8 Effect of substrate

Despite great advances in nanofabrication, the total thickness of all fabricated metamaterials, so far, remains of the order of wavelength. This immediately suggests that any additional media in close proximity to the metamaterials will influence its near field and therefore affect the metamaterials effective properties. Both simple and multi-layered fishnet metamaterials are fabricated on a substrate and this substrate is expected to have a strong influence on their properties. In many theoretical analyses of fishnet structures, the effect of substrate on material properties is not considered. The fishnet structure is embedded in an effective homogeneous medium with a refractive index $n = \sqrt{1.1}$ (i.e., no glass substrate) whereas the structures are usually located on a glass substrate in experiments [17, 18]. In many FDTD simulations, the back ground refractive index is simply increased instead of placing the metamaterials on the substrate. This effect avoids the Fabry- Perot effect, in which the impedance mismatch leads to reflectance at the metamaterials/air and metamaterials/glass interfaces [18]. This effect also moves the optical response to longer wavelength range compared with the case with air as the background medium [19]. This redshift is counteracted with the suitable choice of fishnet widths w_x and w_y or other geometrical parameters. The refractive index of a background medium $n = 1.2$ is used in the FDTD simulation to obtain transmission properties for eleven layer fishnet structure and to match experimental results [18].

It is already established that presence of substrate may substantially change the effective properties of the metamaterials at microwave frequency [20]. They can be effectively tuned by changing the substrate properties. The presence of the substrate deteriorates the performance of metamaterials especially its *FOM*. Moreover an interpretation of the results in terms of an effective material is highly questionable [21].

Because most metamaterials structures for the optical range are currently fabricated on a substrate, it is important to understand how the presence of a substrate modifies the effective properties of optical fishnet metamaterials. This issue is addressed in Chapter 5 where the complex refractive index is obtained from reflection/transmission coefficients of the fishnet structure formed from nanoimprint lithography (*NIL*). The effect of a glass substrate is accounted while retrieving complex refractive index from fishnet structure formed from *NIL*.

The presence of the substrate also changes the symmetry of the fishnet structure which is intended to be symmetric with respect to propagation direction. The presence of the substrate breaks the symmetry of the structure and induces bianisotropy [22].

4.9 Multilayer fishnet structure

There has been a sustained effort in the scientific community for the engineering and extension of the functionalities of metamaterials at terahertz and optical frequencies. The metal-dielectric-metal fishnet structure is the only structure which provides a negative refractive index. These structures consist of single functional layer along the direction of propagation making it equivalent to the atomic monolayer [18]. It is difficult to develop device applications and to explore phenomena of negative refraction in such a thin metamaterial. These structures suffer substantial loss at optical frequencies due to their resonant nature. It is therefore necessary to realize low-loss bulk optical metamaterials to demonstrate unambiguously the unique effects associated with negative refraction [18].

Thick materials are highly desirable so that the overall geometry of the material can be used to manipulate light such as in a lens or a prism [23]. But it is very difficult to fabricate thick metamaterials with the proper dimensionality at optical frequencies. At short wavelengths, nanoscale imperfections are at the scale of incident radiation, causing scattering loss and reduced material performance. It is difficult to fabricate thick metamaterials while maintaining the requisite nanoscale unit cell geometries.

4.9.1 Simulation set up.

The reflection and transmission characteristics are calculated from a single unit cell of multilayer fishnet structure. The simulation set up is similar to the single layer fishnet as explained in section 4.2.1 except calculation region which is larger than that due to thickness of the structure. A finer mesh is used with in the metal-dielectric-metal layers to simulate them accurately.

It has been suggested theoretically that stacking up multiple fishnet layers along the direction of propagation can provide us with the three *3D* optical negative index metamaterials [22]. This cascading leads to a strong magneto-inductive coupling between neighbouring functional layers. The tight coupling between adjacent *LC* resonators through mutual

inductance results in a broadband negative index of refraction. Reflection and transmission properties are obtained from three, seven, eleven and nineteen layer fishnet metamaterials. The geometric parameters are obtained from reference [24].

| a_x | a_y | w_x | w_y |
|--------|--------|--------|--------|
| 500 nm | 600 nm | 300 nm | 250 nm |

Table 4.3: Table listing the geometric parameters for the unit cell of multilayer fishnet structure shown in Figure 4.1.

It is important to establish a definition of bulk metamaterial. The definition of bulk properties has been well established in solid state physics. In case of metamaterials, the convergence of material properties is required for defining bulk as well as the requirement that the surface atomic layers do not affect the overall property of the system. It is only strictly meaningful to assign properties of a bulk metamaterials when the effective properties are not altered by the environment. A single or a few functional layers of fishnet metamaterials cannot be considered as bulk since their properties significantly changes.

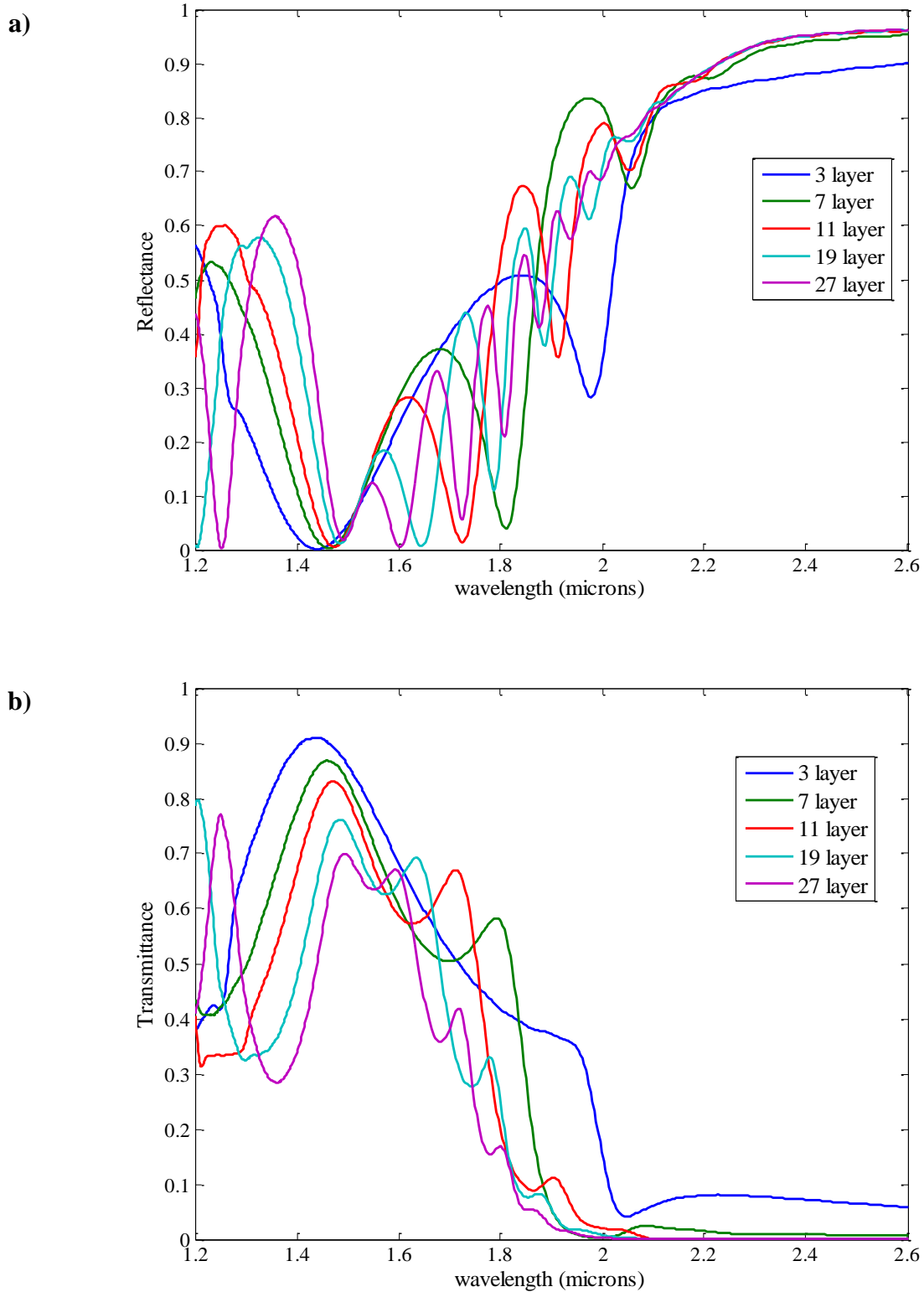


Figure 4.19: Simulated a) Reflection b)Transmission obtained from a multilayer fishnet structure. The results are in agreement with the reference [24]. The geometric parameters are given in Table 4.3.

4.10 Summary

A systematic study of the fishnet structure is presented in this chapter. This structure has been proven to be most promising candidate to obtain negative refractive index at optical frequencies. Numerical modelling of the structure was discussed in detail with different metallic constituents. Parametric investigation of the structure has been performed in the infrared frequency region. It has been established that qualitative behaviour of the results are in agreement with the results obtained at microwave frequency in the available literature. The effect of choice of different metal is discussed and silver is considered to be the most promising metal for the fishnet structure.

4.11 References

- [1] Allen Taflov, Computational Electromagnetics: The Finite Difference Time Domain Method: Artech House, (2005).
- [2] P. Ding, E. J. Liang, W. H. Hu, L. Zhang, Q. Zhou, Q. Z. Xue, "Numerical Simulation of terahertz double negative metamaterials with isotropic-like fishnet structure," *Photon. Nanostruct.: Fundam. Appl.* 7 92 (2009).
- [3] K.B. Alici, E. Ozbay, "A planar metamaterial: Polarization independent fishnet structure," *Photonics Nanostruct.: Fundam. Appl.* 6 102 (2008).
- [4] K.B. Alici, E. Ozbay, "Characterization and tilted response of a fishnet metamaterials operating at 100GHz" *J. Phys. D: Appl. Phys.* 41 135011 (2008).
- [5] K. Aydin, Z. Li, L. Sahin, E. Ozbay, "Negative phase advance in polarization independent, multilayer negative index metamaterials," *Opt. Express.* 16 8835 (2008).
- [6] G. Dolling, M. Wegener, C. M. Soukoulis and S. Linden, "Design related losses of double fishnet negative index photonic metamaterials," *Opt. Express.* 15 11536 (2007).

- [7] N. H. Shen, G. Kenanakis, M. Kefasaki, N. Katsarakis, E. N. Economou, C. M. Soukoulis, “Parametric investigation and analysis of fishnet metamaterials in the microwave regime,” *J. Opt. Soc. Am. B* 26, B61 (2009).
- [8] Th. Koschny, M. Kefasaki, E. N. Economou, and C. M. Soukoulis, “Effective medium theory of left handed metamaterials,” *Phys. Rev. Lett.*, 93, 107402 (2004).
- [9] M. Kafesaki, I. Tsiapa, N. Katsarakis, Th. Koschny, C. M. Soukoulis, and E. N. Economou, “Left handed metamaterials: the fishnet structure and its variations,” *Phys. Rev. B* 75, 235114 (2007).
- [10] J. Zhou, E. N. Economou, Th. Koschny, C. M. Soukoulis, “Unifying approach to left handed material design,” *Opt. Lett.* 31, 3620-3622 (2006).
- [11] J. B. Pendry, A.J. Holden, W. J. Stewart, and I. Youngs, “Extremely low plasmons in metallic nanostructures,” *Phys. Rev. Lett.* 76, 4773-4776 (1996).
- [12] A. David Olver, *Microwave and Optical Transmission* (John Wiley & sons).
- [13] John Gowar, *Optical Communication Systems* (Prentice Hall, 2nd Edition 1996).
- [14] P. B. Johnson, R. W Christy, “Optical properties of noble metals,” *Phys. Rev. B.*, 6, 4370 (1972).
- [15] S. Linden, C. Enkrich, M. Wegner, J. Zhou, Th. Koschny, and C. M. Soukoulis, “Magnetic Response of metamaterials at 100 THz,” *Science*, 306, 1351 (2004).
- [16] N. H. Shen, Th. Koschny, M. Kefasaki, and C. M. Soukoulis, “Optical metamaterials with different metals,” *Phys. Rev. B* 85, 075120 (2012).
- [17] G. Dolling, C. Enkrich, M. Wegener, C. M. Soukoulis, and S. Linden, “Low-loss negative-index metamaterial at telecommunication wavelengths,” *Opt. Lett.* **31**, 1800–1802 (2006).
- [18] D. Chanda, K. Shigeta, S. Gupta, T. Cain, A. Carlson, A. Mihi, A. J. Baca, G. R. Bogart, P. Braun and J. A. Rogers, “Large area 3D flexible optical negative index metamaterials formed by nanotransfer printing,” *Nat. Nanotechnology* 6 402–7 (2011).

- [19] S. Zhang, W. Fan, N. C. Panoiu, K. J. Malloy, R. M. Osgood, and S. R. J. Brueck, “Optical negative index bulk metamaterials consisting of 2D perforated metal dielectric stacks,” *Opt. Express* 14 6778 (2006).
- [20] Z. Shang, V.V. Varadan, “Tuning the effective properties of metamaterials by changing the substrate properties,” *J. Appl. Phys.* 101, 014909 (2007).
- [21] G. Dolling, C. Enkrich, M. Wegener, C. M. Soukoulis, and S. Linden, “Design related losses of double fishnet negative index photonic metamaterials, *Optics Express*, 18 11536 (2007).
- [22] D. A. Powell, Y.S. Kivshar, “Substrate induced bianisotropy in metamaterials,” arXiv: 1006.1159. URL <http://arxiv.org/abs/1006.1159>.
- [23] A. J. Hoffman, et al. “Negative refraction in semiconductor metamaterials,” *Nature Mater.* 6, 946–950 (2007).
- [24] J. Zhou, Th. Koschny, M. Kafesaki, and C. M. Soukoulis, “Negative refractive index of weakly and strongly coupled optical metamaterials,” *Phys. Rev. B.* 80 035109 (2009).

5. Metamaterial fishnets formed from nanoimprint lithography

5.1 Introduction

Electromagnetic metamaterials have come a long way from microwave to visible frequencies. They have also become truly three dimensional *3D* materials at optical frequencies only for certain propagation directions or for certain polarizations of light. However none of these intricate *3D* structures are yet available in quantities approaching the gram level. It is therefore a challenge to develop techniques for fabricating large scale *3D* isotropic metamaterials. Some nanofabrication technologies have been developed significantly for this purpose or have been modified from existing technologies.

In the previous chapter a detailed study has been performed for different aspects of the fishnet design. The *LC* circuit description of the structure, polarisation dependence and numerical modelling of the structure is explained with the help of simulations. The effect of choice of metal on determining the properties of structure and retrieval of effective material parameters was shown. The influence of presence of substrate to the fishnet structure is also discussed. The results obtained and conclusions made in the previous chapter have been utilized to model a fishnet structure formed from nanoimprint lithography.

This chapter describes fabrication and characterisation of fishnet structures of various dimensions on a polymer layer with metal-dielectric-metal pillars suppressed beneath. The metamaterials structures are fabricated using nanoimprint lithography by Dr. Graham Sharp at the University of Glasgow, allowing large areas to be patterned quickly and with good reproducibility through multiple use of a nanoimprint stamp. A tri-layer comprising of silver (Ag) and magnesium fluoride (MgF_2) is deposited on thick polymer layer before being directly imprinted by a stamp. In this instance, the polymer used is polymethyl-meth-acrylate (*PMMA*). When the metal dielectric layered pillars are imprinted to a sufficient depth in the (*PMMA*) below the fishnet, distinct resonance peaks can be measured at infrared frequencies. The precise wavelength of the resonant peaks at near infrared and its *Q* factor can be changed

by altering the physical dimensions and number of metal dielectric layers of the fishnet respectively.

Silver and magnesium fluoride layers that comprise the suppressed pillars that are crushed during the imprinting process but still allow for the light to be transmitted. Despite imprinting directly into multiple metal and dielectric layers, high quality structures are observed with a minimum feature size as small as 200 nm. Resonance peaks are measured experimentally in reflectance using an FTIR spectrometer with a calcium fluoride (CaF_2) beam splitter and a visible wavelength range spectrometer with a silicon (Si) detector.

Two different fishnet structures have been designed and fabricated of varying dimensions using this method and their resonant wavelengths measured in the near infrared at 1.45 μm and 1.88 μm . The experimental results are supported by simulations using Finite Difference Time Domain (*FDTD*) solutions. Simulations suggest that a negative refractive index real part with a magnitude as large as 5, with the figure of merit (*FOM*) of 2.74 can be obtained.

5.2 Fabrication challenges

The fabrication of negative refractive index metamaterials (*NIM*) at optical frequency is quite challenging due to requirements for 100 nm and sub-100 nm feature sizes in the unit cells of the metamaterials. It also requires small periodicities on the order of 300 nm or less. The fabrication techniques to fabricate high quality *NIM* are electron beam lithography (*EBL*), focussed ion beam (*FIB*) milling, interference lithography (*IL*), nanoimprint lithography (*NIL*) and direct laser writing. The future of this research area depends upon the possibility of creating three-dimensional *3D* metamaterials. The scientific community is facing challenges in creating truly *3D* metamaterials for real life applications and future manufacturing of optical metamaterials. The boom in *NIM* related research comes from recent advances in nanofabrication techniques that allow different materials to be structured on the nanometre scale.

The challenging task is to move from planar structures to a *3D* slab of layered metamaterials and to develop new isotropic designs. The fabricated materials so far do not really enter the material regime where the unit cell size is of the orders of magnitude smaller than the wavelength due to the limitations of current nanolithography tools. The feature size is

typically small enough compared to the wavelength of operation so that these materials could be described as a medium with effective permittivity ϵ , and effective permeability μ . It is also required to choose material carefully for *NIM* fabrication in addition to sub wavelength resolution.

5.2.1 Electron-beam lithography

2D metamaterial layers are normally fabricated using electron beam lithography (EBL) due to expense of difficulty of using photolithography at the required feature sizes; EBL also offers fast turn-around. In this process, a beam of electrons is used to generate patterns on a surface. The beam width is of the order of 5 nm but the resolution is determined by the resist and back scattered electrons. It is a serial process where in the electron beam must be scanned across the surface to be patterned. It offers tens of nm resolution and almost complete pattern flexibility. Different *NIM* structures have been successfully fabricated by *EBL* and experimentally investigated by several groups [1, 2]. The fabrication of *NIM* requires small periodicities below 300 nm and tiny feature sizes down to several tens of nanometre. The metamaterials are still fabricated by *EBL* despite low throughput of the serial writing and high fabrication cost. Only small areas can normally be structured within reasonable time and reasonable cost. This method does not offer a solution for the large scale *NIM* fabrication which is the essential requirement of many application and devices.

5.2.2 FIB milling

The focussed ion beam milling technique is used for rapid prototyping of metamaterials. In this method a focussed beam of gallium ions is used to sputter atoms from the surface making the surface amorphous. The *FIB* is used as a micromachining tool because of the sputtering capability. This technique has been used for fabricating magnetic materials based on the split ring resonators [3]. *EBL* based fabrication requires time consuming tests and careful optimization of writing parameters and processing steps leading to overall long fabrication times. Whereas as the rapid prototyping of complete structures can be fabricated by *FIB* writing in times as short as 20 minutes [3]. The structure is ready and no further post processing steps are required after *FIB* writing. *FIB* is the first choice for rapid prototyping for different structures but it has certain design and material limitations combined with low throughput.

Interference lithography *IL* can be considered as an approach for making 3D optical *NIMs*. *IL* offers high structural uniformity combined with pattern flexibility while its resolution is now approaching to 20 nm scale [4]. The fabrication of square centimetre area structure has been demonstrated by using this technique [5, 6, and 7]. A negative refractive index is obtained over a wavelength range 1.56 μm -2 μm , 1.64 μm -2.2 μm , and 1.64 μm -1.98 μm for *NIMs* with circles, ellipses and fishnet respectively [8]. This is a large area patterning technique and does not require expensive cleanroom equipment.

5.2.3 Nanoimprint lithography

Nanoimprint lithography offers another promising approach for the fabrication of production-compatible, large area high quality optical *NIMs* at low processing cost and fast processing time [9]. *NIL*, a next generation lithography candidate, accomplishes pattern transfer by the mechanical deformation of a resist via a stamp rather than a photo or electro- induced reaction in the resist as in most lithographic methods. The smallest attainable features are given solely by stamp fabrication and the resolution of this technique is not limited by the wavelength of light source. *NIL* provides parallel processing with high throughput. The fabrication of *NIMs* requires high patterning resolution; *NIL* is well suited for large scale production of optical *NIMs*. It provides wafer-scale processing using standard clean room procedures combined with simplicity and low cost. Two types of *NIMs* operating at near and mid-infrared frequencies have been fabricated by *NIL*. The first structure was composed of fishnet that demonstrated negative permittivity and permeability in the same frequency region with the negative refractive index of $n = -1.6$ at a wavelength near 1.7 μm [10]. In the mid *IR* range *L*-shaped resonators have been shown to exhibit negative permittivity and negative permeability near wavelengths of 3.7 μm and 5.25 μm respectively. *NIL* was successfully applied for the fabrication of planar, chiral, and photonic metamaterials to study novel polarization effects where both dielectric and metamaterials with feature sizes from micrometre scale down to sub-100 nm are fabricated [11].

Nanoimprint lithography has achieved sub-10 nm resolution patterning in its early development almost a decade ago. It has a resolution and cost advantage over photolithography and it does not suffer from proximity effect as electron beam lithography in high resolution patterning. The International Technology roadmap for semiconductors officially listed *NIL* as one of the next generation lithography candidates.

NIL can be used in multilayer processes for creating 3D structures. It is an ultrahigh resolution patterning technique and it offers sub 50 nm resolution and sub 10 nm layer alignment capabilities simultaneously. *NIL* has the potential for very large scale and inexpensive manufacture of structures. Some process requires multilayer lithography and plating techniques [12]. There is a newly developed nanofabrication technique namely reverse-contact *UV* nanoimprint lithography. This is a combination of *NIL* and contact printing lithography [13]. Three dimensional polymer structures can be fabricated by this technique. This method has also provided encouraging results for fabricating 3D woodpile like structures for polymer photonic devices [13].

Besides the requirements of nanometre scale resolution and high throughput, highly controllable thin film deposition methods are needed for the realization of good performance *NIMs*. The possibility of creating thin metal films and dielectric films with reduced surface roughness is very important, whatever approach is chosen as a manufacturing method for the next generation of optical *NIMs*. The main limit to obtain lower loss metamaterials is high roughness of the metal film since it leads to increase scattering losses in the system and can annihilate the negative index effect [14]. The conventional way to improve the quality of the metal film is to use a lower deposition rate and a dielectric material with stronger adhesion and better surface quality. Silver is the most used metal for optical *NIMs* [14, 15-17] due to its optical properties. Silver oxidizes at ambient temperature in air. The silver deterioration can be prevented by the deposition of a dielectric layer on the top of the structure [17].

5.3 Fabrication of fishnet using NIL

In this section the detailed procedure of the fabrication is explained. The steps of metamaterial fabrication from nanoimprint lithography can be summarized as follows.

5.3.1 Stamp fabrication

The fabrication was performed by Dr. Graham Sharp and a brief description will be given here. Fabrication of the stamp is the most important and crucial step of the imprint lithography. The desired size and shape of the stamp directly affects the patterning of the sample. Therefore each step in the stamp fabrication is done with great care. Prior to the start of fabrication cleaning is very important to prevent serious wafer contamination and process

failures. Purity of the initial material is very important. The main contamination types can be listed as particles, organic, native oxide, micro roughness and inorganic contamination [18]. Methanol, ethanol, isopropyle *IPA* and acetone are commonly used solvents to remove organic impurities [19]. In addition; particle removal with ultrasonic shockwave (20-40 kHz) is advantageous.

The SiC nanoimprint stamp was fabricated using hydrogen silesquioxane (HSQ) as the resist and post development as a mask for inductively coupled plasma etching. The cleaved SiC substrate used was 500 μm thick and measured 1 cm^2 in area with square patterned area of 3 mm^2 . After etching to a depth of 1 μm the HSQ is removed by hydroflouric acid (HF), after which the sample is treated in a solution of heptane and a silane compound (F_{13} -OTCS) ((tridecafluoro-1,1,2,2-tetrahydrooctyl)-trichlorosilane), a common hydrophobic non-stick coating for silicon substrates. This treatment prevents the stamp adhering to the target sample during imprinting and eases separation after patterning. It is important to achieve vertical sidewalls following the etch process, in order to avoid distortion of the pattern dimensions in the fabricated structure during the imprinting process [20].

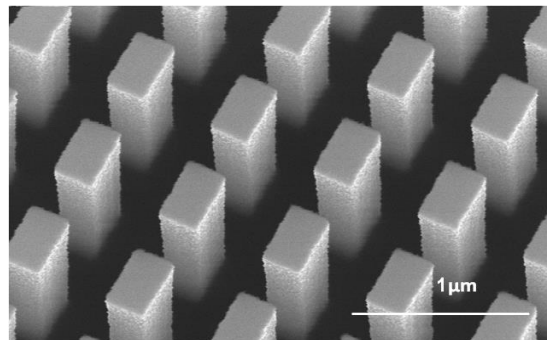


Figure 5.1: An angled micrograph of a SiC stamp used for imprinting showing etched pillars 1 μm in height [21].

5.3.2 Sample fabrication

The target sample consists of a polished fused silica substrate that is spin-coated with a 1 μm thick layer of polymethyl-methacrylate *PMMA*. A metal–dielectric–metal tri-layer of Ag (30 nm), MgF_2 (50 nm) and Ag (30 nm) is then electron-beam evaporated on to the *PMMA*. Silver has been selected in preference to gold because of the lower associated optical losses [15]. The *SiC* stamp is imprinted directly into the tri-layer using a modified Specac hydraulic press applying a half tonne force (4.9 kPa pressures) at room temperature [20]. The etched *SiC*

pillars define the structure when imprinted and displace part of the metal–dielectric–metal tri-layer into the *PMMA* beneath, forming rectangular pillars in the apertures of the fishnet. The *PMMA* beneath the metal–dielectric stack is compressed when the nanopillars are displaced from the fishnet. The compression of *PMMA* has been shown to change the associated refractive index [22]. The behaviour of *PMMA* during the imprinting process has also been reported [23]. It is estimated that with the imprint force used the refractive index real part of the compressed *PMMA* may increase by approximately 0.05, although it should be noted that the values stated in [22] are given for shorter wavelengths than measured here. This change is noted but the variation of index with pressure is not modelled. The imprinting process itself typically takes only two minutes and the stamp can be cleaned in acetone afterwards for re-use. It is found in these experiments that the stamps can be used at least ten times without damage occurring. While the etched pillars remained intact throughout, continued use of a stamp for more than ten imprints resulted in the gradual formation of small cracks in the SiC. These cracks eventually resulted in fragments breaking from the substrate, usually near the cleaved edges. The depth of the pillars can be varied with the imprint force used, but it has been found that a half-tonne force (4.9 kPa pressure) results in a depth in the *PMMA* of approximately 300 nm from the fishnet on top. The *NIL* process is often enhanced by reducing the viscosity of the polymer that is to be patterned by heating the substrate [23]. However, heating the *PMMA* to improve its flow causes the metal and dielectric layers on top of the *PMMA* to crack and break up, making lithography at room temperature desirable. The fabricated fishnet and nano-pillar structure exhibits good uniformity across the patterned 3mm² area, with only small, localized regions at the four corners of the imprinted area showing breaks in the metal–dielectric–metal tracks. Close inspection of the imprinted pattern, shown in Figure 5.2, shows uniform, continuous silver wires.

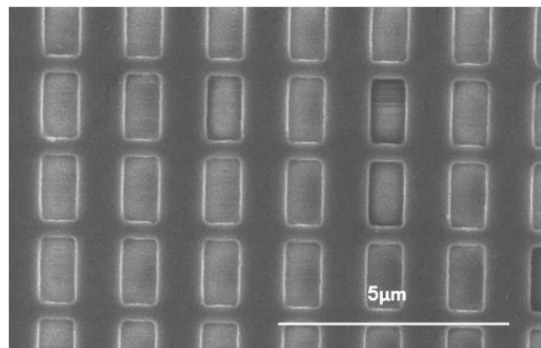


Figure 5.2: Angled *SEM* micrograph of structure B showing, in detail, the interlocking Ag–MgF₂–Ag wires, and imprinted nano-pillars pushed into *PMMA*. The dark region located between the fishnet and imprinted nano-pillar is *PMMA* [20].

The apertures defined by the imprint process are consistent in dimension and show rounding at the corners. The edges of the wires exhibit roughness resulting from the cutting of the metal and dielectric by the *SiC* pillars. Nano-sized cracks are also visible on the imprinted nano-pillars, the regions that are in direct contact with the nanoimprint stamp. Unlike other techniques that utilize *NIL* to pattern a resist or polymer mask, imprinting directly into the metal–dielectric–metal stack removes the need for etching [24, 10].

5.4 Numerical modelling of fishnets formed from NIL

5.4.1 Simulation setup

The reflection and transmission characteristics are calculated from a single unit cell of fishnet formed from nanoimprint lithography. A single unit cell of fishnet formed from nanoimprint lithography is shown in Figure 5.4. A tri-layer comprising of Ag-MgF₂-Ag is stacked on thick polymer, in this instance is *PMMA*. Ag-MgF₂-Ag comprising the suppressed pillars that are crushed during the imprinting process is also carefully designed. The structure including tri-layer Ag-MgF₂-Ag along with the suppressed nanopillars and *PMMA* are all stacked on the substrate. The semi-infinite silica SiO₂ is used as a substrate for this structure.

The structure is illuminated by a plane wave source over the wavelength range from 1000 nm to 4000 nm. The direction of propagation of source is in negative *z* direction. The simulation area is a rectangular parallelepiped shape. The calculation region is 660 nm x 660 nm x 2000 nm³ with a conformal mesh region self-adapted to the structure. A perfectly matched layer is imposed on the edge planes of the simulation area perpendicular to the direction of propagation of source. This boundary condition is an absorbing boundary condition and ideally it should produce zero reflections but in practice there will always be small reflections. The reflections from this boundary can be reduced by increasing the number of perfectly matched layers. A very fine inner mesh size of 3nm in the *z*-direction is used within the top Ag-MgF₂-Ag metal layers and extended to the crushed nanopillars comprising Ag-MgF₂-Ag and is adequate for simulation convergence. Since this structure has variation within the structure in the *x* and *y* directions, a very fine inner mesh of at least 5nm is used in the *x* and *y* directions.

The structures unit cell is periodic in both *x* and *y* directions. Periodic boundary conditions are used in both *x* and *y* directions. Depending upon the polarization of the source the

periodic boundaries in the x and y are replaced by imposing an antisymmetric/symmetric boundary condition. Antisymmetric/symmetric boundary conditions are used in the x and y directions respectively in case of TE polarization.

The refractive index of dielectric spacer material MgF_2 is set to 1.38. It has no losses over the entire wavelength range of interest. The refractive index of fused silica SiO_2 is also embedded using dielectric material properties only. Its refractive index is set to 1.48. It also has no losses over this wavelength range and hence there is no imaginary part of refractive index. The refractive index of $PMMA$ is also set using dielectric properties of material database. Its refractive index (real part) is set out to 1.49 with no imaginary part as it has no losses over this wavelength range. A Drude model is used for the dielectric function of Ag, with a plasma frequency of 9.0 eV and damping frequency of 0.054 eV [25]. The damping frequency is increased by a factor of three compared with that of bulk silver to account for the additional scattering losses in real films [26]. For simulations of just the fishnet portion of the structure, the calculation region is set with the background index of air ($n=1$).

If the dielectric is too thick, the interaction between the metal layers will be weak, resulting in limited enhancement of material properties. However if the capacitive gap between each metal layer is optimised and sufficiently thin, coupling will be much stronger and produce lower losses, an increase in the magnitude of negative refractive index and figure of merit. The dimensions used in the simulation are given in Table 5.1 for the structure shown in Figure 5.3.

The reflection and transmission data is obtained with the help of monitors placed on above and beneath the structure. The time monitor is used to provide information for field components over the course of the simulation.

5.4.3 Unit Cell

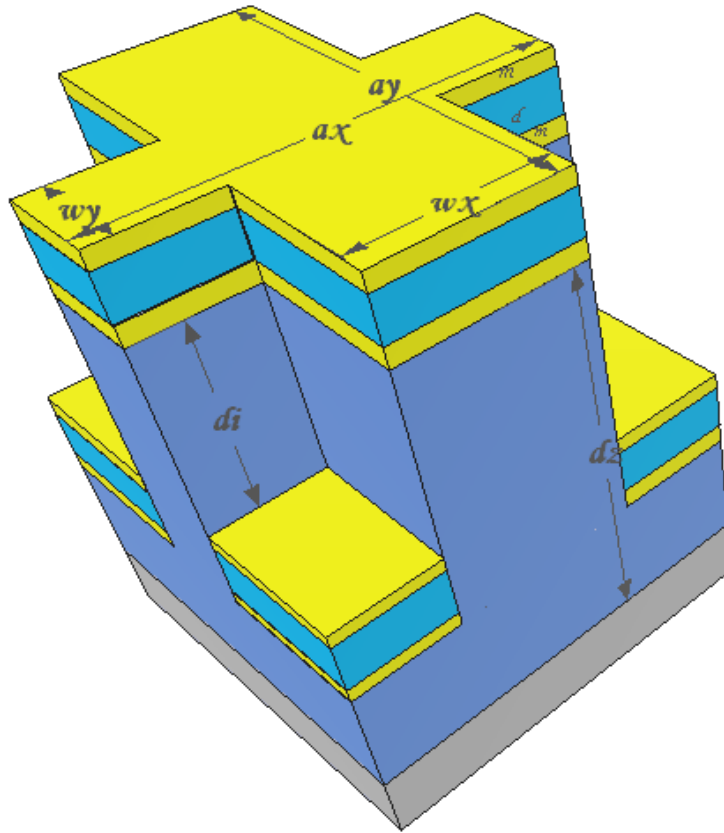


Figure 5.3: 3D model of an ideal single unit cell of the fishnet with pillars, detailing dimensions and material thickness (not to scale). The depth of the PMMA layer at its thickest d_z is 1000 nm. This is the thickness of the PMMA when it is spun on to the SiO_2 substrate and same thickness is used for modelling. The thickness of SiO_2 substrate is kept as semi-infinite in the simulations. The fishnet sits on the top of the sample with the pillars pressed down into the PMMA layer. The imprinted depth of the pillars in the PMMA is denoted by d_i , which equals 300 nm for both designs. The metal-dielectric-metal tri-layer of silver-magnesium fluoride-silver (Ag-MgF₂-Ag) is denoted by $m-d-m$ and has a total thickness of 110 nm (30 nm Ag, 50 nm MgF₂, 30 nm Ag). Light incident normally on the top of the fishnet is polarized as shown. The electric field component is parallel to thin wire tracks of the structure and perpendicular to the wide tracks.

| Structure | a_x | a_y | w_x | w_y |
|-----------|--------|--------|--------|--------|
| A | 640 nm | 640 nm | 410 nm | 220 nm |
| B | 860 nm | 870 nm | 590 nm | 280 nm |

Table 5.1: Table listing measured dimensions of the two fabricated structures. The same dimensions are used for modelling.

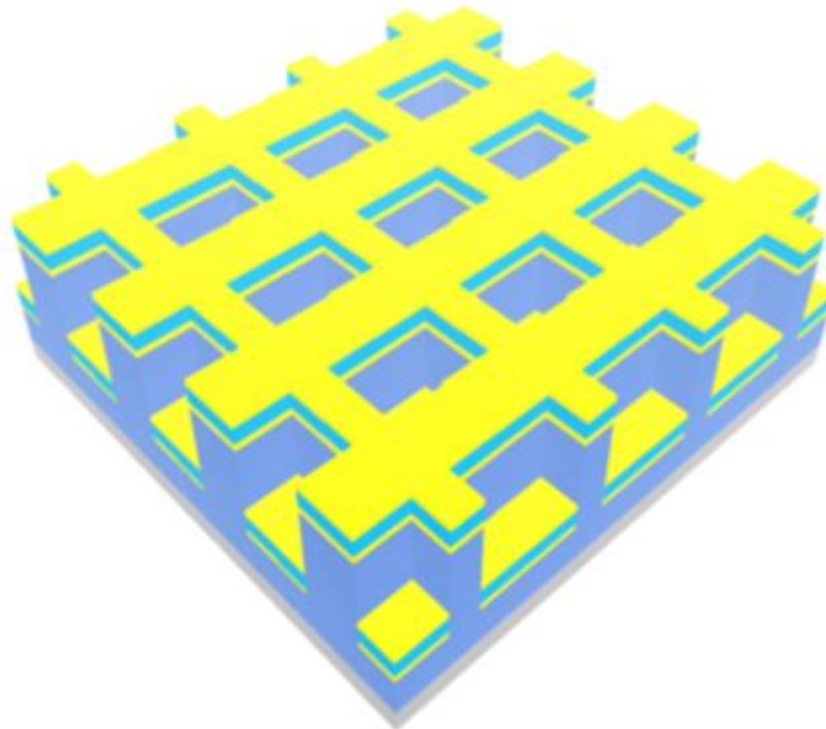


Figure 5.4 Sketch of the NIL fishnet metamaterials slab used for the retrieval of negative refractive index.

5.5 Reflection and transmission

Simulated reflection and transmission spectra are obtained using the dimension and constituent material properties of two different fabricated structures.

| Data | a_x | a_y | w_x | w_y |
|-------------|--------|--------|--------|--------|
| A | 640 nm | 640 nm | 410 nm | 220 nm |
| B | 650 nm | 640 nm | 420 nm | 220 nm |
| C | 645 nm | 645 nm | 415 nm | 225 nm |
| D | 640 nm | 650 nm | 410 nm | 230 nm |

Table 5.2: Table listing measured dimensions of the fabricated structures. These dimensions are used for understanding the behaviour of the structure shown in Figure 5.3.

The reflection and transmission spectra obtained with data A as shown in the Table 5.2 is used for the comparison with the experimental results. The results obtained with this data shows a close agreement between the experimental and simulated results.

To further understand the behaviour of the structure the dimensions of the structure w_x and w_y are slightly changed which changes the lattice constant a_x and a_y of the structure. These dimensions are also responsible for the change in hole size and nanopillars of the fishnet structure. It has been noticed that change in hole size changes the position of the resonance as well as the amplitude of reflection and transmission spectra. This can be understood with the help of data B and data D in which one of the lattice constants a_x , a_y is changed by 10 nm which increases length or width of the hole size respectively. The reflection spectrum obtained with this data shows a significant change in the amplitude as well as the position of the resonance as shown in Figure 5.5.

It has been noticed that if both the lattice constants a_x and a_y are changed simultaneously, there is a significant change in the amplitude of the reflectance and transmittance spectra. The

results obtained with the help of data C in which both the lattice constants are changed simultaneously by at least 5 nm shows significant change in the amplitude of the results.

5.5.1 Depth parameter

| Data | d_i | $(d_z - d_i)$ |
|------|--------|---------------|
| A | 300 nm | 700 nm |
| B | 200 nm | 600 nm |
| C | 350 nm | 650 nm |
| D | 400 nm | 600 nm |

Table 5.3: Table listing depth parameter of the simulated structures. These dimensions are used for understanding the behaviour of the structure shown in Figure 5.3.

It should be remembered that metal-dielectric-metal pillars that are displaced during the imprinting process still fill the area of the fishnet apertures, only they are situated below the fishnet in the PMMA. Therefore from the perspective normal to the fishnet the Ag-MgF₂-Ag stack still covers the area of the structure in its entirety. The thickness of the PMMA d_z is kept as 1000 nm. A close agreement has been obtained between the experimental and simulated results when the depth parameter is kept as 300 nm. Detailed simulations were performed to understand the effect of depth parameter on reflection and transmission properties of the structure.

It has been noticed that this parameter is responsible for the amount of light transmitted through the hole and does not change the position of the resonance of reflection and transmission. As we increase the vertical distance between the top of the pillar and the bottom layer of the fishnet, a significant amount of light is able to be transmitted. This can be seen with the results obtained with the data D in which the depth is kept as 400 nm. When the depth parameter is reduced to 200 nm, the amount of light transmitted through the hole is reduced which can be seen in Figure 5.6.

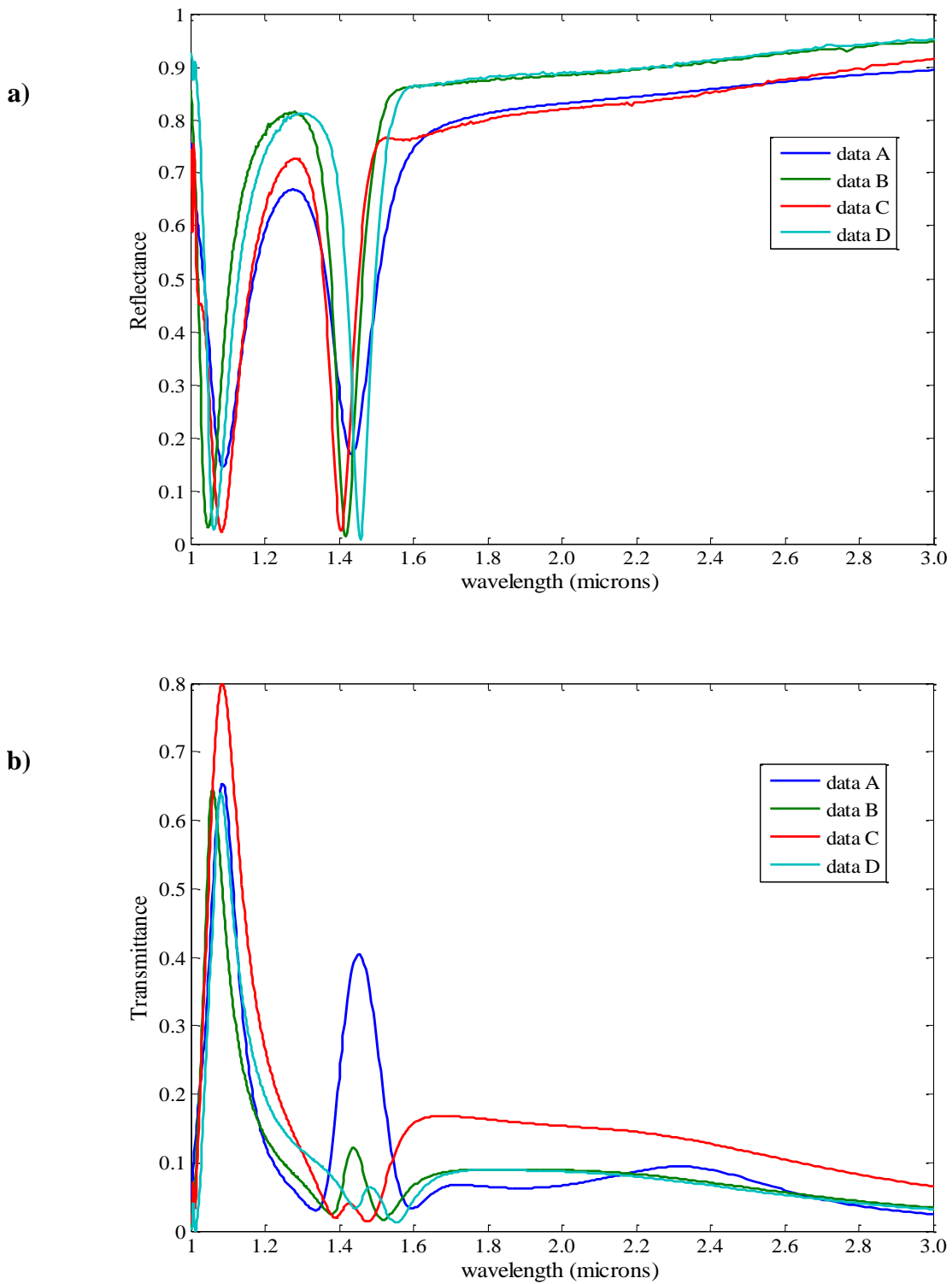


Figure 5.5: Simulated transmission and reflectance spectra of fishnets and nanopillars of varying dimensions. The spectra are obtained from structures patterned to the specifications detailed in Figure 5.4. The data used to obtain these results is shown in Table 5.2.

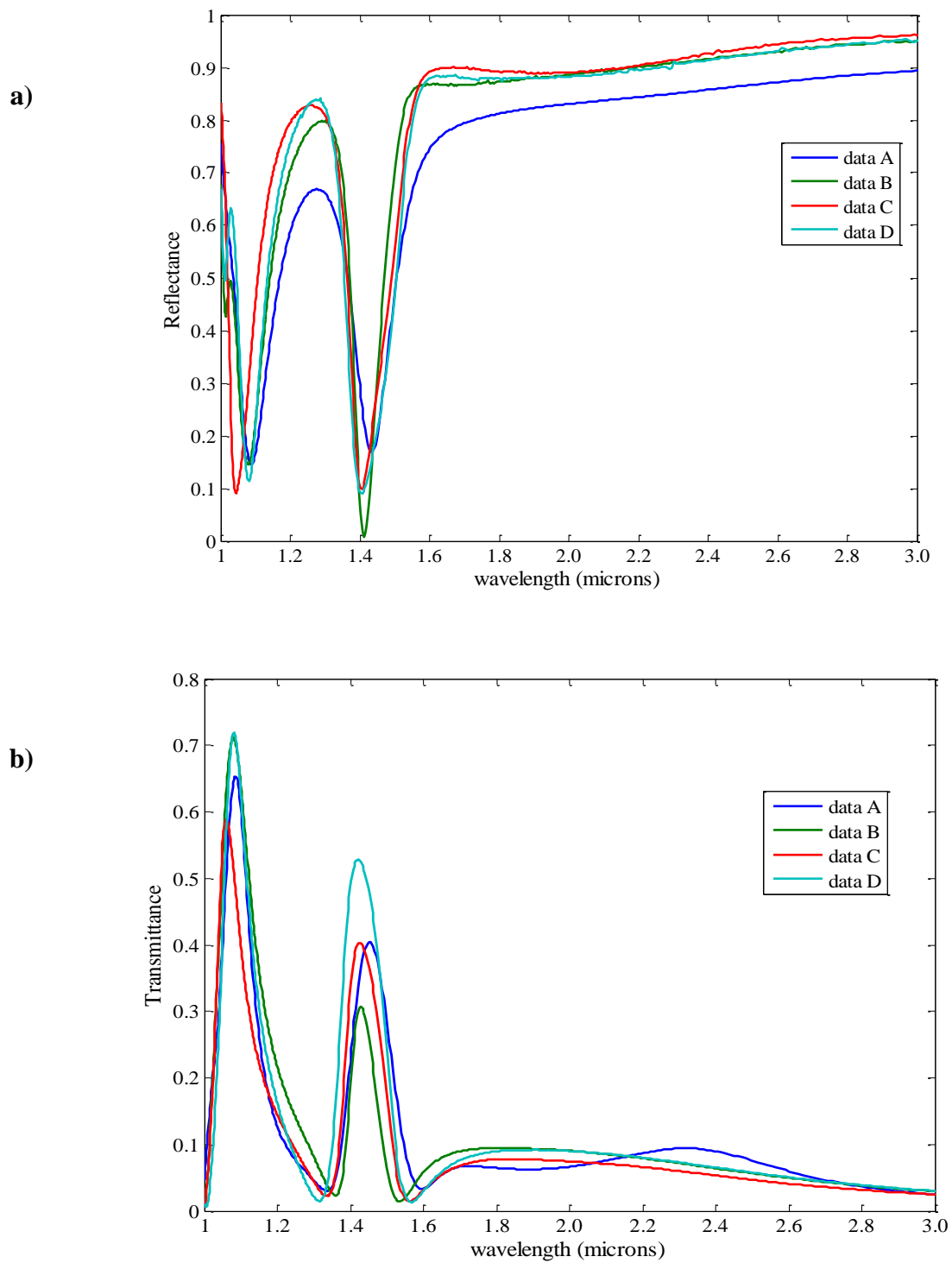


Figure 5.6: Simulated transmission and reflectance spectra of fishnets and nanopillars of varying dimensions. The spectra are obtained from structures patterned to the specifications detailed in Figure 5.4. The data used to obtain these results is shown in Table 5.3.

5.5.2 Measurements at infrared wavelength

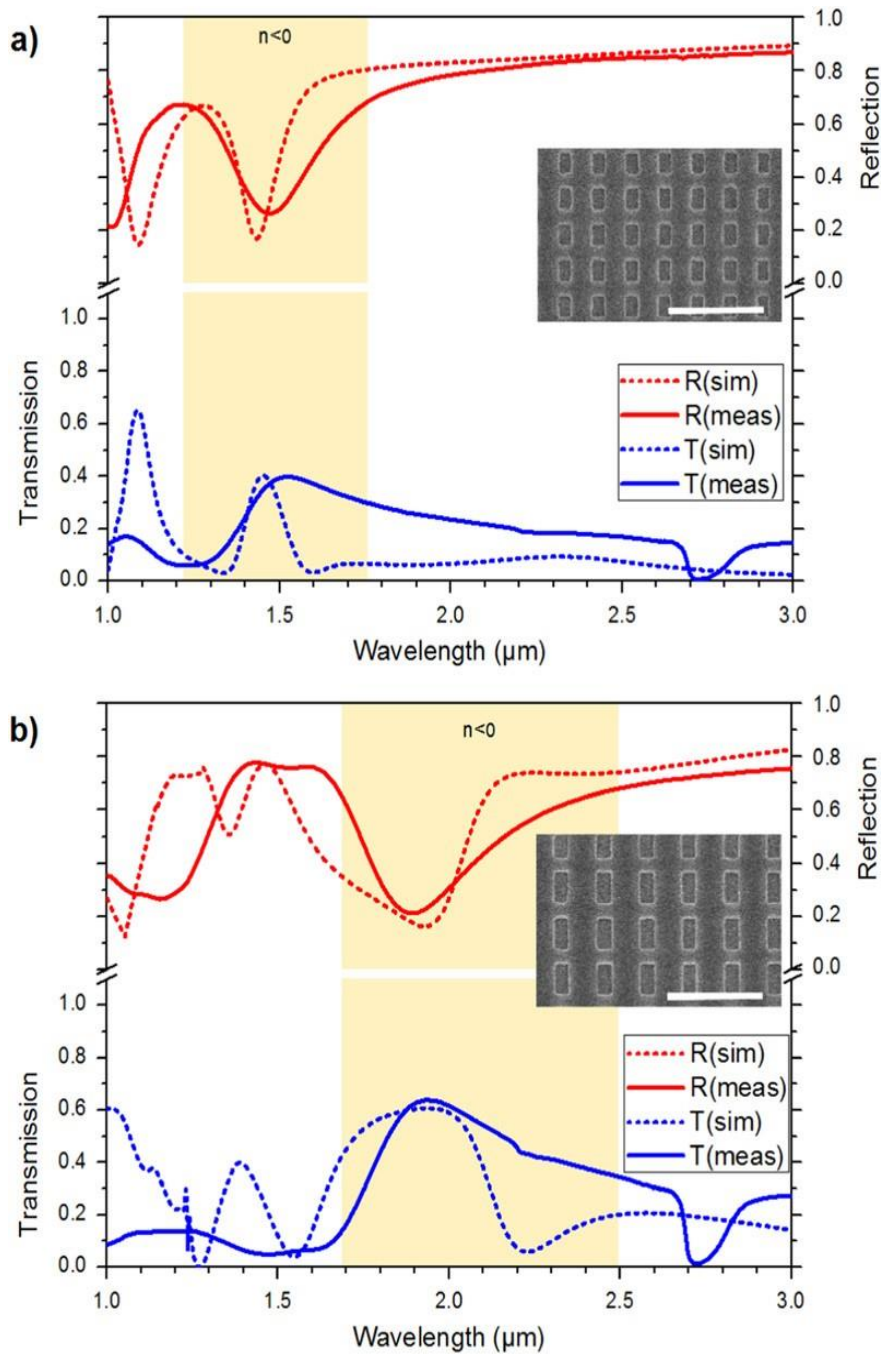


Figure 5.7: Measured and simulated transmission and reflectance spectra of fishnets and nanopillars of varying dimensions, with a micrograph of each structure inset. The scale bar is $2\ \mu\text{m}$ in both instances. The spectra are obtained from structures patterned to the specifications detailed in Figure 5.4. The shaded regions on both plots indicate the wavelengths at which n is negative [27].

There is a close agreement between the experimental and simulated reflection and transmission spectra as shown in Figure 5.7. Reflectance and transmittance measurements were obtained using a Bruker FTIR spectrometer with a CaF₂ beam splitter. A polariser was also positioned between the light source and the sample to polarize light as shown in Figure 5.3. The reflection measurements were normalized using an unpatterned 30 nm thick sheet of silver on a fused silica substrate as background and transmission measurements were normalized against a fused silica substrate with 1 μm of PMMA spun on the top. Measurements were done on an imprinted area of 400 μm². The area of one unit cell is around 4.1 x 10⁻¹³ m². The number of unit cells illuminated is around 9.8 x10⁸. In measurements the sample is illuminated by a focussed spot and not a plane wave, this also explains differences between measured and simulated results.

Resonances are observed experimentally at 1.45 μm and 1.88 μm respectively as the critical dimension of the structure are increased in scale. The experimental transmission spectra show a trough at approximately 2.7 μm with near-zero transmission for both structures. This trough can reasonably be attributed to the excitation of the O–H ion stretch vibration at 2.7 μm in the fused silica substrate, not the fishnet and pillar structures or the PMMA that supports them. This trough cannot be seen in simulated reflection and transmission spectra. Figure 5.8 shows the measured transmission spectra of a bare unpatterned of fused silica substrate of type used to support fishnet and nano-pillar structures. A prominent trough is present at the same wavelength range observed in the experimental transmission measurements of the fabricated structures.

The magnitude of the experimental transmission at negative index wavelengths is, at maximum, approximately 40% and 65%, for structures A and B respectively. It is observed from the reflection spectra of both structures that at longer wavelengths the fishnets act increasingly similar to mirror, with reflectance tending towards 100 % and transmission decreasing. Both the experimental and simulated transmission and reflection spectra are absolute and not arbitrary units. It should be noted that the metal–dielectric–metal pillars that are depressed into the PMMA fill the areas beneath the apertures of the fishnet, meaning that transmitted light must pass through the sidewall of the rectangular PMMA holes. Therefore from a perspective normal to the fishnet the Ag-MgF₂ stack still covers the area of the structure in its entirety. Therefore light can feasibly be transmitted through the structure by two means. Firstly the light can pass through the sidewall of the PMMA between the fishnet and nano-pillars, i.e. the vertical distance between the top of the pillar

zand bottom layer of the fishnet, will have a significant effect on the proportion of light that is able to be transmitted. Light can also be transmitted by “extraordinary optical transmission”. This concept was first described by Ebbesen’s 1998 paper [28-29], which studied the transmission of light, through periodic sub-wavelength hole arrays in silver, a structure not unlike the metamaterials fishnet. EOT can exhibit an enhancement in transmitted light due to the incident wave coupling to and exciting the surface plasmons present at the interface between the metal and insulator.

The divergence between experimental and simulated results below $1.5\ \mu\text{m}$ can be attributed to Fabry–Perot resonances between the fishnet, nanopillars and substrate which are accentuated in the simulations due to impedance mismatch between metamaterials/air and metamaterials/substrate boundary and seen in other reported work concerning fishnets [30]. This not uncommon occurrence is largely the result of imperfections present in the structure, such as potential cracks in the silver wires, tracks and rounded corners and non-uniform edges of the aperture.

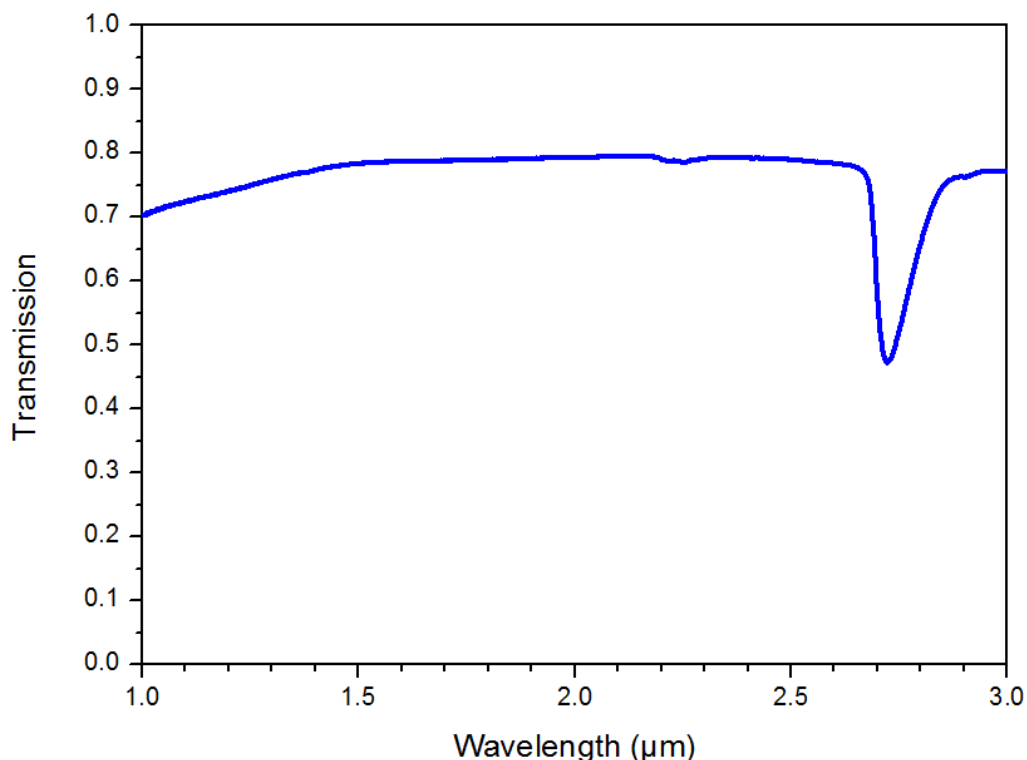


Figure 5.8: Experimental transmission spectra of an unpatterned, 1mm thick fused quartz substrate without PMMA. It is the same type as used for measurements of the fabricated structures. This data is taken from reference [27].

While attention is given to modelling the fabricated structures as closely as possible it is not possible for all defects to be included in the simulations. There are number of components that can contribute to optical losses in the fabricated structures. Firstly the fused silica substrate is a source of optical loss. The wavelength dependent refractive index of quartz means that while the material is transparent at visible frequencies, it becomes increasingly opaque towards the infra-red. The fabricated structure use a 1 mm thick fused silica substrate as it was found that thinner silica substrate could not withstand the high imprint forces required for patterning, thus adding to the optical losses. As shown in the Figure 5.8 even when the bare unpatterned substrate is measured transmission never rises above a maximum value of 80%. It is not possible to keep 1mm thick fused silica substrate in modelling. The semi-infinite silica is used as a substrate for this structure by extending the structure through the PML boundary. Ideally there should be no reflection from the PML boundary but in practice there are always some reflections from the PML boundary which can interfere with the other properties of the structure thus creating differences between experimental and simulated results.

The 1 μm thick PMMA layer is another source for introducing losses to the fabricated structures, introducing physical discontinuities and a refractive index change between the substrate and metamaterials. The dimensions of the fabricated structures are taken from SEM micrographs but it was not possible to get a full cross section of the fishnet structure as the metal was flaking off the substrate during cleaving. The cross sectional dimensions of the fishnet structure are not properly measured and are assumed for modelling which is also responsible for differences between simulated and experimental result.

5.6 Refractive index calculations

The wavelength dependent refractive index of the fabricated structure can be obtained by using simulated reflection and transmission spectra as shown in Figure 5.9. The modified retrieval method for asymmetric structure has been used to retrieve the complex effective index of the structure [31-34]. It should be noted that retrieval process is not trivial in especially when the metamaterials of interest are anisotropic or bianisotropic [35, 36]. If the optical path length across the unit cell is not small then the effective medium limit fails to provide unique answer for n [34].

To calculate the generalized scattering parameters; we consider the two values of the reflection coefficient when illuminating from free space (S_{11}) or through the substrate (S_{22}). The differences between the magnitudes of S_{11} and S_{22} are modest. However there is a large contrast in the phases of S_{11} and S_{22} , implying very different properties for the structure and depending on which side of the unit cell is first impacted by the incoming wave (both the phases and magnitudes of S_{12} and S_{21} are identical) [37]. Depending on the direction of propagation of incident wave with respect to the unit cell, the refractive index is defined by either

$$\cos(nkd) = \frac{1}{2S_{21}} (1 - S_{11}^2 + S_{21}^2) \quad (5.1)$$

$$n = \frac{1}{kd} \cos^{-1} \left[\frac{1}{2S_{21}} (1 - S_{11}^2 + S_{21}^2) \right] \quad (5.2)$$

Or

$$\cos(nkd) = \frac{1}{2S_{21}} (1 - S_{22}^2 + S_{21}^2) \quad (5.3)$$

$$n = \frac{1}{kd} \cos^{-1} \left[\frac{1}{2S_{21}} (1 - S_{22}^2 + S_{21}^2) \right] \quad (5.4)$$

where k is the wavenumber of the free space and d is the thickness of the metamaterials slab. The inverse cosine is a multivalued function and mathematical solution of the inverse cosine is given by

$$n = \frac{1}{kd} \cos^{-1}(x) \quad (5.5)$$

where,

$$x = \left[\frac{1}{2S_{21}} (1 - S_{22}^2 + S_{21}^2) \right] \quad (5.6)$$

$$n = \frac{1}{kd} [-1i \log(x + \sqrt{1 - x^2})] \quad (5.7)$$

Or

$$n = \frac{1}{kd} [-1i \log(x - \sqrt{1 - x^2})] \quad (5.8)$$

The logarithmic function is also a multivalued function and it has multiple branches. The problem with the different branches of $\text{Re}(n)$ can be solved by considering different lengths of the structure in the direction of propagation. Especially if there are many layers of the structure then many branches exist and one has to be very careful to select the correct ones [39]. The structure under discussion has only one active layer of the fishnet and only meaningful results are presented in Figure 5.9.

The fishnet and nanopillars of structures A and B on a 1 μm thick layer of *PMMA* and silica substrate were simulated to show the real and imaginary part of the refractive index near the respective resonant wavelength and are shown in Figure 5.9. For structure A, a refractive index real part of -0.24 was found at 1.53 μm . This decreased to a maximum magnitude of -0.57 at 1.9 μm . With structure B a refractive index of -0.7 was observed at 2.35 μm and was shown to decrease to -1.5 at 3.35 μm . The *PMMA* and suppressed pillars are here responsible for the increasing material losses and for limiting the magnitude of n . The broad response of $\text{Re}(n)$ in Figure 5.9 is consistent with previously reported periodicity effects in metamaterials with reduced symmetry [34]. Discontinuities observed in real part of refractive index displays physical asymmetry and numerous material refractive indices. It should be remembered that any optimization of the pillar dimensions [38] using the NIL technique that we have described will also alter the dimensions of the fishnet, since both are defined by the same nanoimprint stamp. These discontinuities however are not precedent and are clearly visible in work concerning asymmetric fishnets previously reported by Kochny et al [34] and Zhou et al [39]. The volatility of the reflection and transmission coefficients is further increased by increased asymmetry and impedance mismatches [39]. The FOM for the fabricated structure is not presented because discontinuities due to multiple refractive changes in the material make the calculation unreliable. The effects of periodicity on these unphysical spectral anomalies and their prominence in metamaterials with the reduced translational symmetry in the direction of propagation are discussed in detail in reference [34].

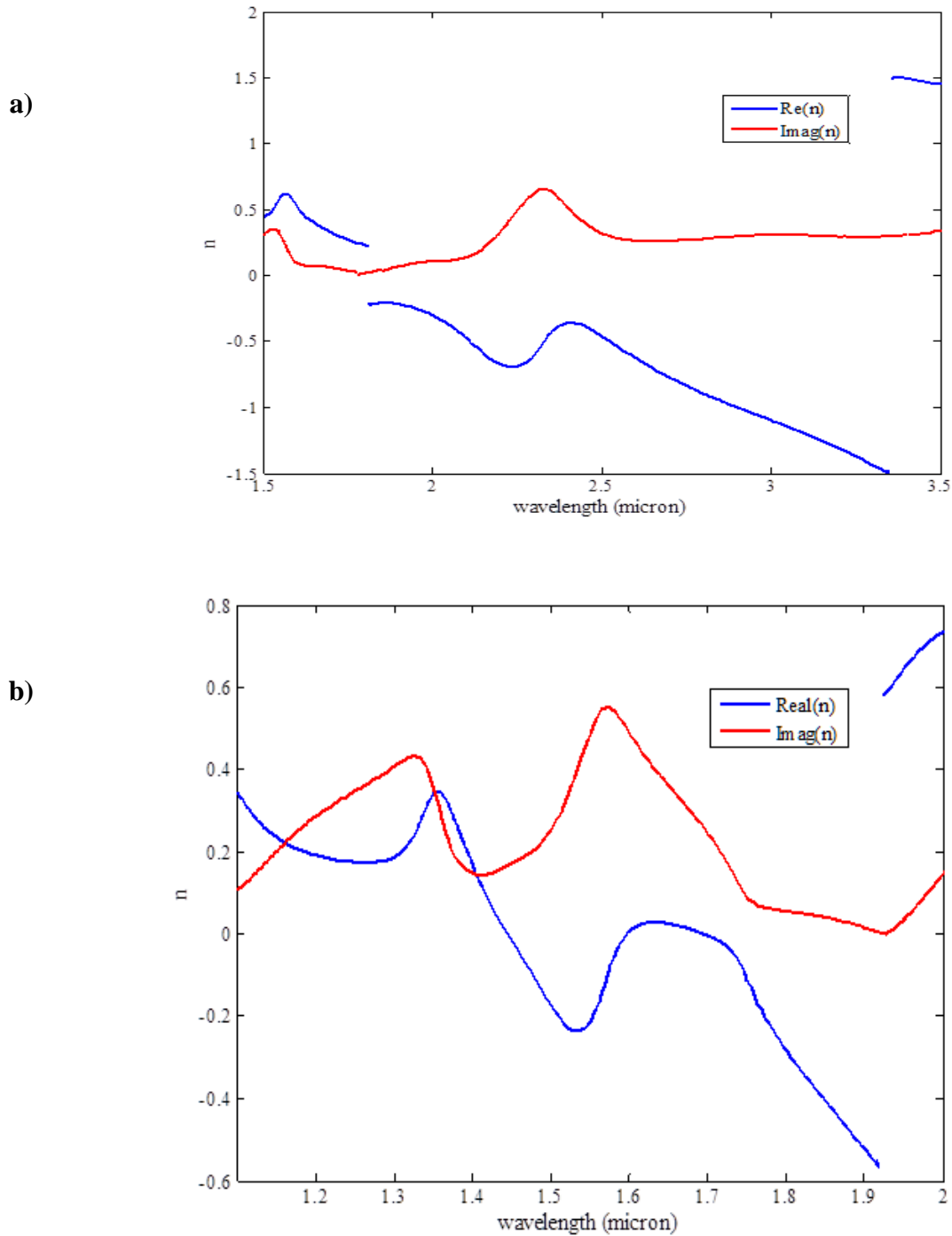


Figure 5.9: Real and imaginary values of refractive index n obtained from simulations modelling the fishnet and pillars structure supported on PMMA for the dimensions of (a) structure A (b) structure B. The discontinuities observed are taking scaling of dimensions into consideration, consistent with those previously reported by Koschny et al [34] and Zhou et al [39].

The simulation that modelled solely the fishnet for structure A (and not the nanopillars on PMMA and SiO₂ substrate) shows a refractive index of -4 , while the equivalent values for structure B, is -5 respectively. The results are shown in Figure 5.10. These values are comparable with those quoted for single active layer fishnets that have been reported previously [30, 40, and 41].

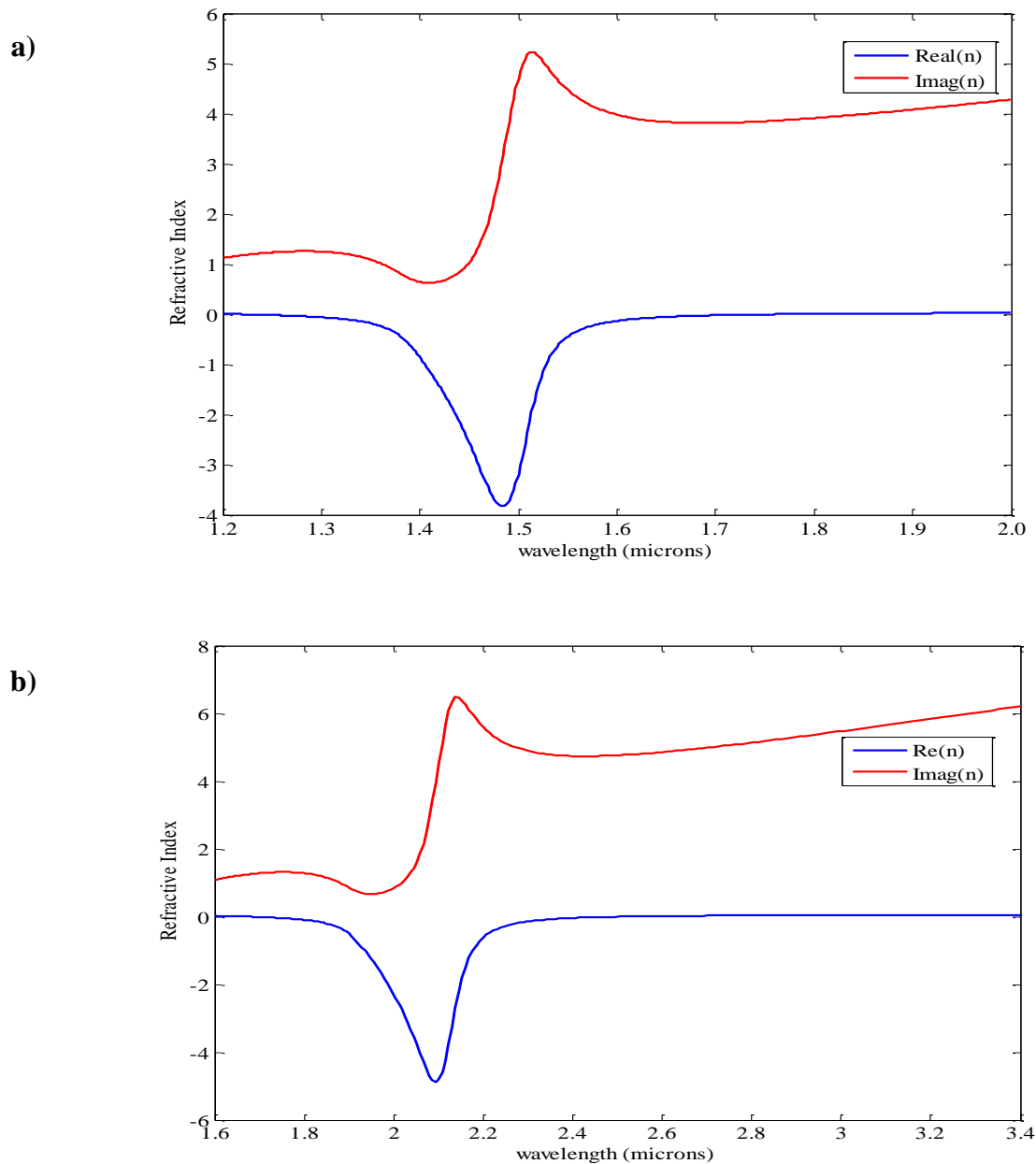


Figure 5.10: Real and imaginary values of refractive index n obtained from simulations modelling fishnets only without the PMMA, metal-dielectric-metal pillars and SiO₂ substrate. Values are obtained using dimensions measured from the fabricated fishnets and with the structure suspended in air. (a) Real and imaginary part of refractive index obtained from structure A. (b) Real and imaginary part of refractive index obtained from structure B.

5.7 Figure of merit calculations

The losses in the metamaterials can be quantified by a dimensionless quantity Figure of Merit (*FOM*). It is defined as

$$FOM = |\operatorname{Re}(n) / \operatorname{Im}(n)|$$

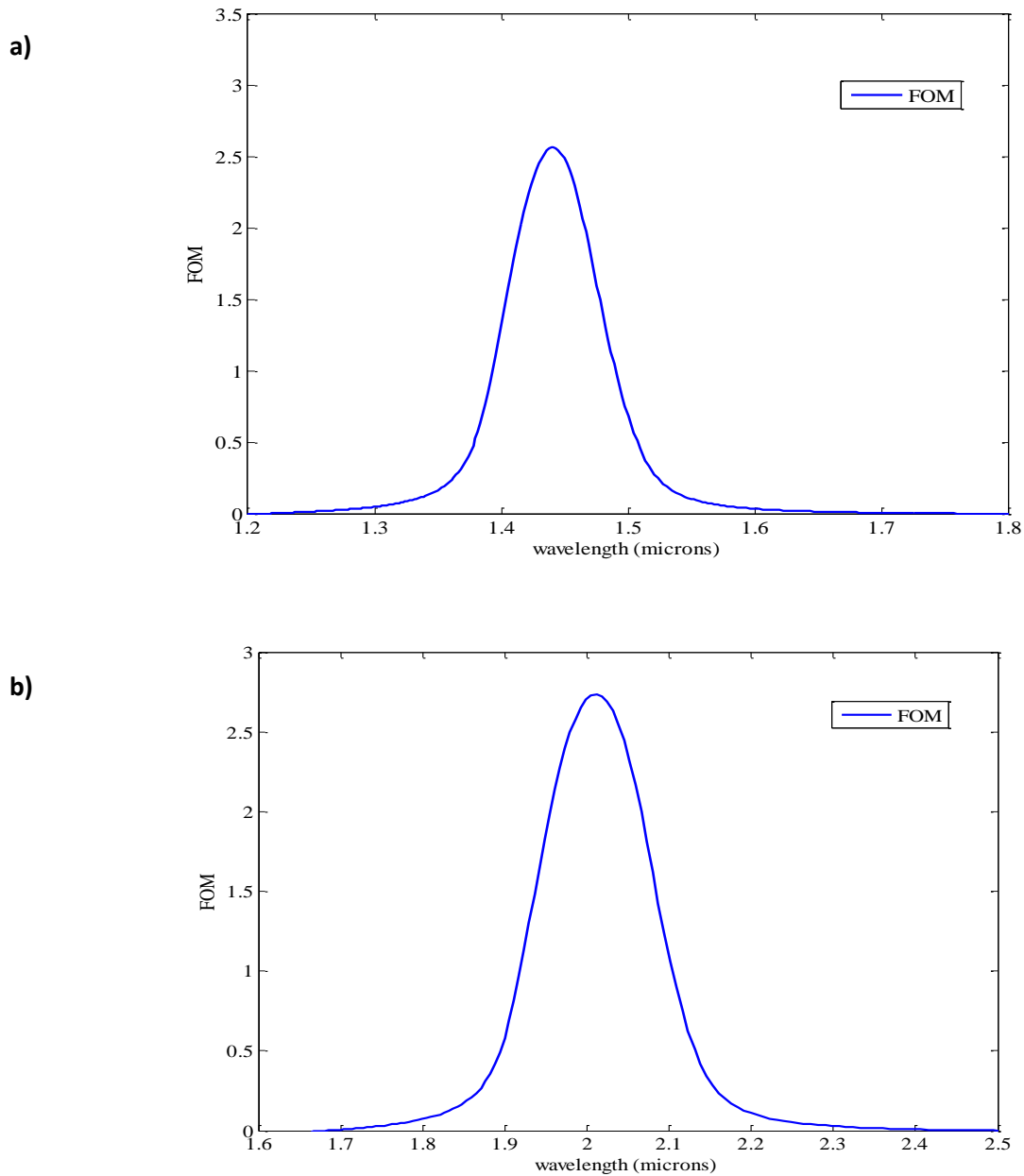


Figure 5.11: (a) The FOM calculated for the structure A (b) The FOM calculated for the structure B.

The results shown in Figure 5.11 suggest that if the fishnet were to be detached from the supporting PMMA and substrate, the negative real part of the refractive index would increase in magnitude, making a more effective metamaterial. The maximum FOM is calculated as 2.49 and 2.74 for the fishnets of structure A and structure B respectively. The FOM for the as fabricated structure is not presented because discontinuities due to multiple refractive changes in the material make the calculation unreliable. Koschny et al [33] notes the effect of periodicity on these “unphysical” spectral anomalies and their prominence in metamaterials with a reduced translational symmetry in the direction of propagation.

5.8 Field plots

The electric field intensity exiting the top of the structure can be plotted using a frequency domain field and power monitor placed just above the structure. The electric field intensity profile shown in Figure 5.12 is obtained when the source is x polarised. The monitors placed just above the structure records the data for the electric field distribution of the structure.

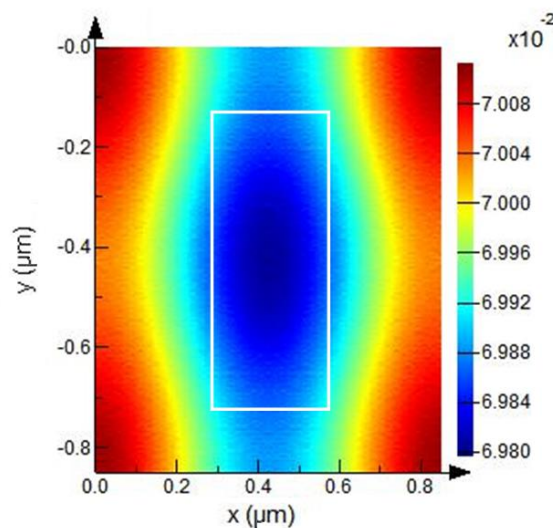


Figure 5.12: Field plot showing a unit cell of the fishnet and nanopillar on the x - y plane from normal incidence. The electric field distribution of a single unit cell of structure B at resonant wavelength $1.88 \mu\text{m}$ has shown the top silver layer of the fishnet and aperture on the x - y plane. The wide metal tracks exhibit a strong electric field induced by the magnetic field of the incident wave.

This data is obtained at resonant wavelength $1.88 \mu\text{m}$ and shows the resonant fields in the structure. The scale bar is also shown with the electric field profile. The distribution pattern shows a strong electromagnetic field along the wide tracks parallel to the long edge of the fishnet aperture, although it is noted that the variation between the weakest and strongest field strength is low. An outline of the structure is added for clarity and it shows the rectangular aperture of the fishnet structure. The field inside the rectangular aperture is not very strong as indicated. The wide metal track exhibit a strong electric field induced by the magnetic field component of the incident plane electromagnetic wave obtained at resonant wavelength of the structure.

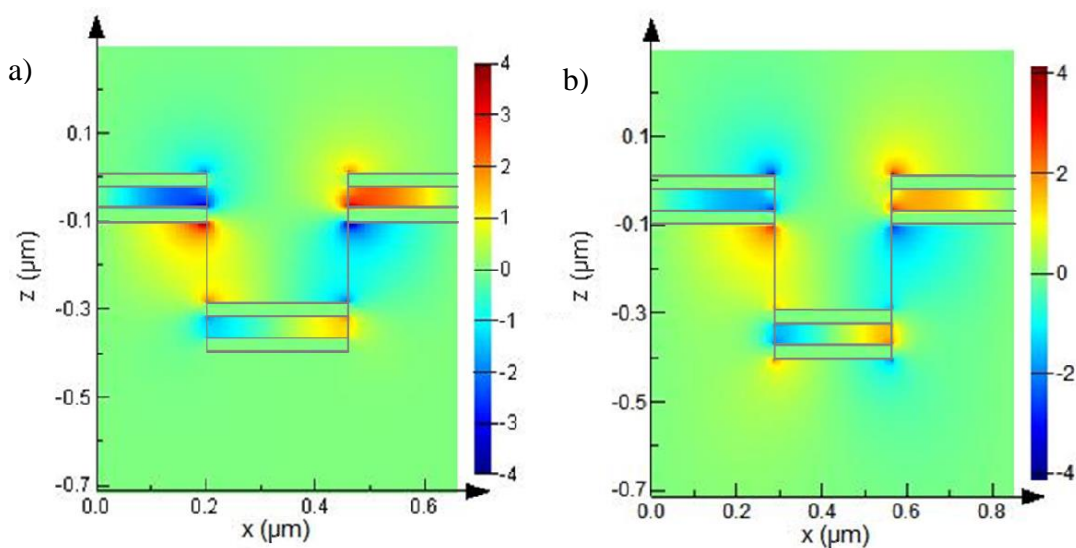


Figure 5.13: Field plots showing the electric field across two different planes of structures, with incident light as polarized in Figure 5.3. An outline of the structure has been added for clarity. Axis values are in microns and indicate the dimension of each structure. (a) A cross section of the structure A (x - z) plane showing the electric field distribution of the Ag-MgF₂-Ag in the fishnet, pillars and supporting PMMA at a wavelength of $1.44 \mu\text{m}$. (b) The x - z plane cross section field plot of structure B at a wavelength of $1.88 \mu\text{m}$. The field plots in Figures 5.10 (a) and (b) show electromagnetic coupling between the fishnets and pillars, through the PMMA.

A cross section of the two different structures is also obtained with the help of a 2D monitor placed in the (x - z) direction. The field profiles for two structures of different dimensions are shown in Figure 5.13. The source is x polarised and propagating in negative z -direction. The axes values are in microns and indicate the dimensions of the two structures. An outline is drawn which shows the top tri-layer (Ag-MgF₂-Ag) fishnet and (Ag-MgF₂-Ag) nanopillars at the bottom. The scale bar is also shown which indicates the strength of the electric field

between the top and bottom metal films of the fishnet and nanopillars. These field plots show the electromagnetic coupling between the fishnet and pillars through the PMMA. It is observed that the electric field strength at the material interfaces at the aperture of the fishnet is stronger for structure A than they are for structure B. It is noted from the cross sectional field plots that the electric field strength is strongest at the aperture edges of the MgF₂ layer of the fishnet. The field plots also show that current flow on top and bottom silver layers of the fishnet are out of the phase.

It has been shown that adding more metal-dielectric layers to a fishnet, thus increasing the number of functional layers, reduce the effect of substrate. This is explained as an increase in the number of functional layers results in the currents in the metal tracks being prevalent further away from the interface with the substrate. As the fishnet structures studied in this chapter contain only one functional layer, the presence of PMMA and nano-pillars significantly inhibits the plasmonic coupling and the effectiveness of the structure operating as a NIM.

5.9 Summary:

A rapid and effective method for fabricating negative index fishnet has been demonstrated. The reflection and transmission coefficients obtained from the fishnet structure formed from NIL. There is a good agreement between simulated and experimental results which further confirm effectiveness of this fabricating technique. The imprinting technique used for the fabrication of fishnet structure could be adapted for use in pattern transfer by lifting the imprinted fishnet from a sacrificial layer and moving into a new substrate or membrane.

Detailed simulations were performed to obtain effective properties of the structure. The complex refractive index of the structure has been obtained by using modified retrieval method for an asymmetric structure. In the available literature, the metamaterial is embedded in the effective medium to avoid any discontinuity arising in the real part of refractive index. So the effect of substrate upon complex refractive index is also taken into account here. Simulations have shown that the refractive index and FOM values of NIL based fishnet are comparable with those previously reported from single active layer fishnets.

Acknowledgement

The author would like to acknowledge Dr. Graham Sharp at the University of Glasgow for experimental work (fabrication and measurements) detailed in this chapter. She is also grateful for many discussions in relating to the fishnet structure.

5.10 References

- [1] V.M. Shalaev, W. Cai, U.K. Chettiar, H.K. Yuan, A.K. Sarychev, V.P. Drachev, A.V. Kildishev, “Negative index of refraction in optical metamaterials,” *Opt. Lett.* 30 3356 (2006).
- [2] S. Zhang, W. Fan, N.C. Panoiu, K.J. Malloy, R.M. Osgood, S.R.J. Brueck, “Experimental demonstration of near-infrared negative index metamaterials,” *Phys. Rev. Lett.* 95 137404 (2005)
- [3] C. Enkrich, F. Perez-Williard, D. Gerthsen, J. Zhou, T. Koschny, C.M. Soukoulis, M. Wegener, S. Linden, “Focused-ion-beam nanofabrication of near-infrared magnetic metamaterials,” *Adv.Mater.* 17 2547 (2005).
- [4] S. R. J. Brueck, “Optical and interferometric lithography nanotechnology enablers,” *Proc. IEEE* 93 1704 (2005).
- [5] S. Zhang, W. Fan, B.K. Minhas, A. Frauenglass, K.J. Malloy, S.R.J. Brueck, “Midinfrared resonant magnetic nanostructures exhibiting a negative permeability,” *Phys. Rev. Lett.* 94 037402–37404 (2005).
- [6] N. Feth, C. Enkrich, M. Wegener, and S. Linden, “Large-area magnetic metamaterials via compact interference lithography,” *Opt. Express.* 15 501 (2006).
- [7] S. Fan, S. Zhang, K.J. Malloy, S.R.J. Brueck, “Large-area, infrared nanophotonic materials fabricated using interferometric lithography,” *J. Vac. Sci. Technol. B* 23 2700 (2005).

- [8] Z. Ku, S.R.J. Brueck, “Comparison of negative refractive index materials with circular, elliptical and rectangular holes,” *Opt.Express* 15 4515 (2007).
- [9] S.Y. Chou, P.R. Krauss, P.J. Renstrom, “Nanoimprint lithography,” *J. Vac. Sci. Technol. B* 14 4129 (1996).
- [10] W. Wu, E. Kim, E. Ponizovskaya, Z. Liu, Z. Yu, N. Fang, Y.R. Shen, A.M. Bratkovsky, W. Tong, C. Sun, X. Zhang, S.-Y. Wang, R.S. Williams, “Optical metamaterials at near and mid-IR range fabricated by nanoimprint lithography,” *Appl. Phys. A*. 87 147 (2007).
- [11] Y. Chen, J. Tao, X. Zhao, Z. Cui, A.S. Schwanecke, N.I. Zheludev, “Nanoimprint lithography for planar chiral photonic meta-materials,” *Microelectron. Eng.* 78–79 612 (2005).
- [12] F.B. McCormick, J.C. Verley, A.R. Ellis, I. El-kady, D.W. Peters, M.Watts, W.C. Sweatt, J.J. Hudgens, J.G. Fleming, S. Mani, M.R. Tuck, J.D. Williams, C.L. Arrington, S.H. Kravitz, C. Schmidt, G. Subramania, “Fabrication and characterization of large-area 3D photonic crystals,” *Aerospace Conf. IEEE* 1 (2006).
- [13] N. Kehagias, V. Reboud, G. Chansin, M. Zelsmann, C. Jeppesen, C. Schuster, M. Kubenz, F. Reuther, G. Gruetzner, C.M. Sotomayor Torres, “Reverse-contact UV nanoimprint lithography for multilayered structure fabrication,” *Nanotechnology* 18 175303–175304 (2007).
- [14] H.K. Yuan, U.K. Chettiar, W. Cai, A.V. Kildishev, A. Boltasseva, V.P. Drachev, V.M. Shalaev, “A negative permeability material at red light,” *Opt. Express* 15 1076 (2007).
- [15] G. Dolling, C. Enkrich, M. Wegener and C.M. Soukoulis, S. Linden, “Low-loss negative-index metamaterial at telecommunication wavelengths,” *Opt. Lett.* 31 1800 (2006).

- [16] G. Dolling, M. Wegener, C.M. Soukoulis and S. Linden, “Negative index metamaterial at 780 nm wavelength,” *Opt. Lett.* 32 53 (2007).
- [17] U.K. Chettiar, A.V. Kildishev, H.K. Yuan, W. Cai, S. Xiao, V.P. Drachev, V.M. Shalaev, “Dual-band negative index metamaterial: double negative at 813 nm and single negative at 772 nm,” *Opt. Lett.* 32 1671 (2007).
- [18] S. Franssila, *Introduction to Microfabrication*, 2nd edition, John Wiley & Sons, 2010.
- [19] A. K. Reinhardt, K. Werner, *Handbook of Silicon Wafer Technology*, 2nd edition 2008.
- [20] G. J. Sharp, S. I. Khan, A. Z. Khokhar, R. M. De La Rue and N. P. Johnson, “Negative index fishnet with nanopillars formed by direct nanoimprint lithography,” *Mat. Res. Express.* 1 045802 (2014).
- [21] G. J. Sharp, S. I. Khan, A. Z. Khokhar, R. M. De La Rue, and N. P. Johnson, “Negative index fishnet structures with nanopillars formed by nanoimprint lithography,” SPIE Photonics Europe, Brussels, Belgium, 14-17 Apr 2014.
- [22] S.S. Anan’ev, I. D. Bernal, B. A. Demidov, Y.G. Kalinin, and V. A. Petrov, “Measurement of the refractive index of polymethylmethacrylate behind the current of a shock wave excited by a high current electron beam,” *Tech. Phys.* 55 703–8 (2010).
- [23] L. J. Heyderman, H. Schiff, C. David, J. Gobrecht and T. Schweizer, “Flow behaviour of thin polymer films used for hot embossing lithography,” *Microelectron. Eng.* 54 229–45 (2000).
- [24] I. Bergmair, B. Dastmalchi, M. Bergmair, A. Saeed, W. Hilber, G. Hesser, C. Helgert, E. Pshenay-Severin, T. Pertsch, E. B. Kley, U. Hübner, N. H. Shen, R. Penciu, M. Kafesaki, C M Soukoulis, K. Hingerl, M. Muehlberger and R. Schoeftner, “Single and Multilayer metamaterials fabricated by nanoimprint lithography,” *Nanotechnology* 22 325301 (2011).

- [25] M. A. Ordal, R.J. Bell, W. A. Alexander, L. L. Long, and M. R. Querry, “Optical properties of Au, Ni and Pb at submillimeter wavelengths,” *Appl. Opt.* 26 744 (1987).
- [26] P.B. Johnson and W. R. Christy, “Optical constants of noble metals,” *Phys. Rev.B* 6 4370 (1972).
- [27] G. J. Sharp, “*Metamaterials and optical sensing at visible and near infra-red wavelengths*” University of Glasgow, (2015).
- [28] E.T. Ebbesen, H.J. Lezec, H.F. Ghaemi, T. Thio, and P.A. Wolff, “Extraordinary optical transmission through subwavelength hole arrays,” *Nature* 391 667–9 (1998).
- [29] C. Garcia-Meca, R. Ortuno, F.J. Rodriguez-Fortuno, J. Marti, and A.Martinez, “Negative refractive index metamaterials aided by extraordinary optical transmission,” *Opt. Express* 17 6026–31 (2009).
- [30] J. Valentine, S. Zhang, T. Zentgraf, E. Ulin-Avila, D.A. Genov, G. Bartal, and X. Zhang, “Three dimensional optical metamaterial with negative refractive index,” *Nature* 455 376–9 (2008).
- [31] D.R.Smith, S. Schultz, P. Markos, and C.M. Soukoulis, “Determination of effective permittivity and permeability from reflection and transmission coefficients,” *Phy. Rev. B* 65 195104 (2002)
- [32] X. Chen, T. M. Grzegorzcyk, B. I. Wu, J. Pacheo and J. A. Kong, “Robust method to retrieve the constitutive effective parameters of metamaterials,” *Phys. Rev. E* 70 016608 (2004).
- [33] X. Chen, B. I. Wu, J. A. Kong and T. M. Grzegorzcyk, “Retrieval of the effective constitutive parameters of bianisotropic metamaterials,” *Phys. Rev. E* 71 046610 (2005).
- [34] T. Koschny, P. Markos, E. N. Economou, D. R. Smith, D. C. Vier, and C. M. Soukoulis, “Impact of inherent periodic structure on effective medium

- description of left handed and related metamaterials,” *Phys. Rev. B* 71245105 (2005).
- [35] Z. Ku, J. Zhang, and S.R.J. Brueck, “Bianisotropy of multiple layer fishnet negative index metamaterials due to angled sidewalls,” *Opt. Express* 17 6782–9 (2009).
- [36] C. Menzel, T. Paul, C. Rockstuhl, T. Pertsch, S. Tretyakov, and F. Lederer, “Validity of effective material parameters for optical fishnet metamaterials,” *Phys. Rev. B* 81 035320 (2010).
- [37] D. R. Smith, D. C. Vier, T. Koschny, and C.M. Soukoulis, “Electromagnetic parameter retrieval from inhomogeneous metamaterials,” *Phys. Rev. E* 71 036617 (2005).
- [38] V. M. Shalaev, W. Cai, U. K. Chettiar, H. Yuan, A. K. Sarychev, V. P. Drachev, and A. K. Kildishev, “Negative index of refraction in optical metamaterials,” *Opt. Lett.* 30 3356–8 (2005).
- [39] J. Zhou, T. Koschny, M. Kafesaki, and C. M. Soukoulis, “Negative refractive index response of weakly and strongly coupled optical metamaterials,” *Phys. Rev. B* 80 035109 (2009).
- [40] C. Garcia-Meca, J. Hurtado, J. Marti, A. Martinez, W. Dickson, and A. V. Zayats, “Low loss Multi-layered Metamaterial Exhibiting a Negative Index of Refraction at Visible Wavelengths,” *Phys. Rev. Lett.* 106 067402 (2011).
- [41] D. Chanda, K. Shigeta, S. Gupta, T. Cain, A. Carlson, A. Mihi, A. J. Baca, G. R. Bogart, P. Braun and J. A. Rogers, “Large area 3D flexible optical negative index metamaterials formed by nanotransfer printing,” *Nat. Nanotechnology* 6 402–7 (2011).

6. Angle Resolved Reflection and Transmission Coefficients

6.1 Introduction

Much of the present interest in the field of metamaterials has been inspired by the fascinating and possibly far reaching advances of the perfect lens. It is an idea based on the realization of lossless isotropic negative index metamaterials. This new field offers the possibility of several novel applications which may revolutionize optics.

It is difficult to characterize all but the simplest artificial materials. Many metamaterials of current interest are extended heterogeneous structures comprising a large number of interactive constitutive elements may be required to operate at oblique incidence. The methods and techniques of electromagnetic characterization of metamaterials are not fully developed. Instead designers must rely on full numerical solution tools, even for relatively straight forward designs. Accurate numerical methods are often slow, and do not necessarily provide the degree of insight into the operating principles that a well understood analytical model can provide. Furthermore, it is difficult to design a larger system that relies in part on metamaterials, if the metamaterial cannot be described at a macroscopic level. It is therefore desirable to develop further and extend existing approaches for calculating and describing the electromagnetic parameters of a structure.

There is a variety of methods dedicated to the calculation of material parameters but particular attention has been paid to the so called The Nicholson-Ross-Weir (NRW) method. This method is based on the determination of effective material parameters from the complex reflection and transmission coefficients R and T of a slab with finite thickness. The basic idea is quite simple. Analytical expressions for the complex reflection and transmission coefficients are calculated for a slab of a medium obeying certain constitutive relations. Then these expressions are inverted to determine the material parameters. Depending on the assumed constitutive relations several pairs of R and T are in general necessary to obtain the complete set of material parameters. In the initial proposal by Nicholson, Ross and Weir [1,2] and later on by D. R. Smith et al [3] the retrieval was established for normal incidence with scalar values of effective permittivity and permeability.

The NRW method has the potential to be extended towards the case of oblique incidence. The extension to oblique incidence was first reported by C. Menzel et al [4] for a fishnet structure. They have used the standard numerical technique Fourier Modal Method (FMM) [5] to calculate reflection and transmission coefficients for a fishnet structure. The details of this method are beyond the scope of this thesis. However this approach certainly requires a huge central processing unit (CPU) and memory resources and also it is not suitable for every geometry. Therefore the aim of this chapter is to set out an approach for obtaining these angle and the polarization-dependent complex reflection and transmission coefficients for metamaterials. Analysis of the oblique incidence propagation in metamaterial can reveal the effects of spatial dispersion which is not visible from the study of normal propagation. It is the name of an effect based on non-locality of electromagnetic response in materials. If all the material parameters depend only on the frequency and also possibly on the spatial coordinates, but they are invariant for the direction into which the applied field is changing in space (i-e. the direction of the wave propagation, in the case of plane wave excitation), only then is the medium local.

Spectroscopic ellipsometry has become a standard method among the polarization dependent optical techniques to explore the optical properties of solids and liquids [6]. Most of the results obtained with conventional ellipsometry are reported from isotropic materials. Investigations on arbitrarily anisotropic layered systems or samples with geometrical structures of high complexity are mainly restricted to data collection and qualitative analysis. This is because of

- (1) the complex formulas associated with highly anisotropic systems, and
- (2) Conventional ellipsometry is restricted to isotropic surfaces.

A convenient mathematical formalism is necessary for calculation of the optical response of anisotropic layered structures. Likewise, appropriate experimental setups are required which determine non-redundant optical parameters from a general anisotropic sample [6]. The polarization of the incident and emerging plane waves represents the fundamental properties that allow for optical characterization of samples by generalized ellipsometry. The Jones Calculus described in chapter 2 section 2.7.1 effectively describes such device interaction. Jones vector components are complex scalars that represent the phase and amplitude of the electromagnetic field components within their reference plane. Diagonal Jones matrices are

related to structures that reflect or transmit p and s polarized light into p and s polarized light only, respectively. In the general case Jones matrix has non-vanishing off diagonal elements. These elements provide the cross-polarization properties of the sample i.e., the ability to progress incident p or s polarized light into emerging s and p polarized light, respectively. Conventional ellipsometry is restricted to surfaces that do not cause cross polarization effects.

The experimental set up used in conventional ellipsometry is usually restricted to single wavelength and few angles whereas the experimental set up used in VASE measures reflection and transmission coefficients over a large wavelength range and variable angles. A general rule for the treatment of anisotropic materials does not exist, and the experimenter needs to find best conditions for any new situations. A further task is to find solutions for treatment of general bianisotropic materials.

This chapter describes work that is still in progress and the results have not yet been fully and comprehensively analysed and explained. The main factor that restricts the determination of material parameters at oblique incidence is that to the best of author's knowledge, no algorithm is available to obtain the complex reflection and transmission coefficients for a metamaterial slab, over a range of angles of incidence. In the present work an algorithm is proposed for obtaining complex reflection and transmission coefficients for a metamaterial slab, over range of angles and for both polarizations.

It is possible to calculate complex reflection and transmission coefficients for a complicated geometry like metamaterial structure using Lumerical software but it requires excessively large computational resources. It is discussed in section 6.4.1.

6.2 Reflection and Transmission Coefficients at normal incidence

A method has been proposed by Smith et al [5] to retrieve the constitutive parameters by using scattering parameters which is suitable for both numerical simulations and comparison with experimental measurements. Several reports have been published that discuss the applications of the retrieval method under various situations [7-10]. It has been proposed that these materials respond to electromagnetic radiation as continuous materials when the wavelength is much larger than the spacing between inclusions and the size of these inclusions to such materials.

6. Angle Resolved Reflection and Transmission Coefficients

The essence of the NRW method is that, in a real composite structure, an equivalent continuous material is substituted with respect to the reflection and transmission of a normally incidence plane wave. In the simplest cases, the electromagnetic properties of the materials are described plainly using permittivity and permeability. The normalized characteristic impedance and refractive index can be found from the Fresnel-Airy formulas for known reflection and transmission coefficients. The inversion of scattering parameters is an established method for the experimental characterization of unknown materials and structures. The scattering parameters are related to the refractive index n and wave impedance z by

$$r = \frac{r_{12} + r_{23} e^{2i\beta}}{1 + r_{12} r_{23} e^{2i\beta}} \quad (6.1)$$

$$t = \frac{t_{12} + t_{23} e^{2i\beta}}{1 + r_{12} r_{23} e^{2i\beta}} \quad (6.2)$$

Where,

$$\beta = knh$$

$$k = \frac{2\pi}{\lambda_0}$$

$$r_{12} = \frac{z - 1}{z + 1}$$

$$r_{23} = -r_{12}$$

Where k is the wavenumber of the incident wave in free space, h is the thickness of the slab, n is the refractive index and z is the impedance.

The refractive index n and impedance z in terms of reflection and transmission coefficients are as follows

$$z = \sqrt{\frac{(1+r^2)-t^2}{(1-r^2)-t^2}} \quad (6.3)$$

$$n = \frac{1}{kh} \cos^{-1} \left[\frac{1}{2t} (1 - r^2 + t^2) \right] \quad (6.4)$$

6. Angle Resolved Reflection and Transmission Coefficients

The refractive index n and wave impedance z are related to permittivity and permeability by using the following relationships

$$\varepsilon = \frac{n}{z} \quad (6.5)$$

$$\mu = nz \quad (6.6)$$

This formulation provides a complete material description for a slab that is composed of homogeneous material but is only valid for inhomogeneous material under the illumination conditions for which the scattering parameters are calculated. For an isotropic material, scattering parameters data from a single angle of incidence is sufficient, but for an anisotropic material, scattering parameters are required for incidence at more than one angle. Most metamaterials of present interest are intrinsically anisotropic because of the orientations of their inclusions, leading to limitations in the application of this standard retrieval method [11]. Most techniques reported for the extraction of material parameters can only be applied to isotropic metamaterials. It is known that artificial materials are intrinsically anisotropic because of the orientations of their inclusions. Such materials are also anisotropic due to the asymmetry of the composite components. Moreover, there are some special metamaterial designs that take advantage of the bianisotropy property [11]. When calculating the effective parameters of bianisotropic materials, one has to take the magnetoelectric coupling into consideration, which plays an important role in the propagation of electromagnetic waves. Only then can the true electromagnetic parameters be obtained. The constitutive relations of bianisotropic materials are as follows.

$$\vec{D} = \vec{\varepsilon} \cdot \vec{E} + \vec{\xi} \cdot \vec{H}$$

$$\vec{B} = \vec{\mu} \cdot \vec{H} + \vec{\zeta} \cdot \vec{E}$$

$$\vec{\varepsilon} = \varepsilon_0 \begin{pmatrix} \varepsilon_x & 0 & 0 \\ 0 & \varepsilon_y & 0 \\ 0 & 0 & \varepsilon_z \end{pmatrix}, \quad \vec{\mu} = \mu_0 \begin{pmatrix} \mu_x & 0 & 0 \\ 0 & \mu_y & 0 \\ 0 & 0 & \mu_z \end{pmatrix}$$

$$\vec{\xi} = \frac{1}{c} \begin{pmatrix} 0 & 0 & 0 \\ 0 & 0 & 0 \\ 0 & -i\xi_0 & 0 \end{pmatrix} \text{ and } \vec{\zeta} = \frac{1}{c} \begin{pmatrix} 0 & 0 & 0 \\ 0 & 0 & i\xi_0 \\ 0 & 0 & 0 \end{pmatrix}$$

In the above equations μ_0 and ε_0 are the permittivity and permeability of the vacuum respectively. The seven unknowns are quantities without dimensions. In order to obtain a true picture of a metamaterial, it is important to present all the components of permittivity and permeability, along with the magneto-electric coefficients.

Most metamaterials are sensitive to polarisation, even at normal incidence. It is necessary to consider the polarisation of light with respect to the plane of incidence and also the orientation of the structure under investigation. In order to obtain complete description of a metamaterial, it is essential to obtain material parameters for the electric field vector perpendicular or parallel to the plane of incidence and as a function of the angle of incidence.

6.2.1 The NRW method at Oblique incidence

The NRW method has the potential to be extended towards the case of oblique incidence. In order to obtain all the components of permittivity and permeability, angle-resolved reflection and transmission coefficients are required for a metamaterial under consideration as shown schematically in Figure 6.1

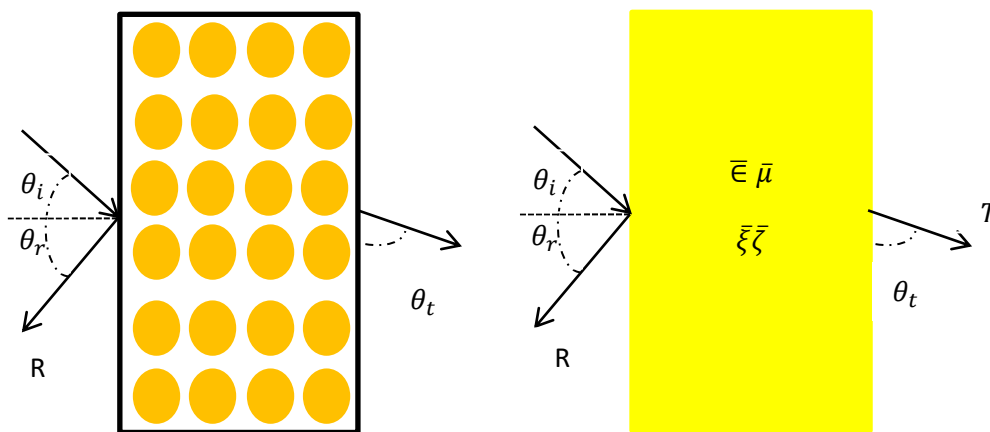


Figure 6.1: An illustration of The NRW retrieval procedure applied to a finite thickness lattice of small particles at oblique incidence.

The determination of the angularly-resolved reflection and transmission coefficients for a metamaterial is complicated: it implies huge CPU and memory requirements. Although the processing power of modern computers has increased steadily. These advances in computer technology have directly affected scientific research. Multicore processing units allow multi-

6. *Angle Resolved Reflection and Transmission Coefficients*

tasking and vast amounts of memory are now accessible. Even so, the CPU time for simulating these artificial materials is very high and some properties of these artificial structures are still unknown due to these reasons.

The traditional procedure for obtaining material parameters from complex reflection and transmission coefficients, as demonstrated by D.R. Smith et al [3], utilizes analytical expressions for the dielectric media. It is proposed in the present chapter that this method can be extended to obtain angle-resolved reflection and transmission coefficients for artificial structures by utilizing analytical expressions for the complex reflection and transmission coefficients of an absorbing medium [12, 13]. The basic equations relating to the propagation of a plane time-harmonic wave in a conducting medium differ from those relating to the properties of a non-absorbing transparent dielectric medium only in that the real dielectric constant ϵ is replaced by complex dielectric constant. The analytical expressions for an absorbing media allow us to input real and imaginary parts of dielectric constant for the real situations. It is possible to obtain the complex reflection and transmission coefficients of a material if its material constants for instance dielectric permittivity, magnetic permeability, and refractive index are known and vice versa. In the ideal case, the complex reflection and transmission coefficients for a particular illumination source distribution for instance (if the plane wave is incident normally) and for a particular polarization (either TE or TM) are known. It is then possible to obtain the complex reflection and transmission coefficients for a range of angles, for the particular polarization by utilizing the data obtained at normal incidence. This approach can be utilized to obtain the complex reflection and transmission coefficients for metamaterials over a range of angles and for both polarizations.

The NRW method has been the most widely used method for the characterization of metamaterials. The material properties obtained by this method have limited region of validity but compromises often have to be made, since in many instances, there is no better way to describe the metamaterial response other than by using these material properties. One of the main reasons that these material parameters have limited validity is that material parameters obtained at one angle of incidence are not applicable for all the other angles. Therefore an attempt has been made to obtain the reflection and transmission coefficients at oblique incidence.

It is possible to obtain the reflection and transmission coefficients at oblique incidence by embedding the complex refractive index data obtained at normal incidence in the analytical expressions for an absorbing film.

6.2.2 Reflection and transmission coefficients for an absorbing film

In this section the complex reflection and transmission coefficients of an absorbing film are obtained by substituting an alternative definition $\hat{n} = n + i\kappa$ of complex refractive index in the analytical expressions [14] that apply for a finite thickness metal film. The definition of refractive index in [14] is $\hat{n} = n(1 + i\kappa)$ where n is the real part and κ is the extinction coefficient. This modification has been made because the fact that in most commercial electromagnetic solvers this alternative definition of refractive index is being used. The agreement of the results obtained is provided in section 6.4. The qualitative behaviour of the results obtained by these analytical expressions is in agreement with the reference [14].

Absorbing film on a transparent substrate

Consider a plane parallel absorbing film of thickness h situated between two dielectric media as shown in Figure 6.2. The refractive indices of dielectric media are n_1 and n_3 . The refractive index of an absorbing film is given by

$$\hat{n}_2 = n_2 + i\kappa_2 \quad (6.6)$$

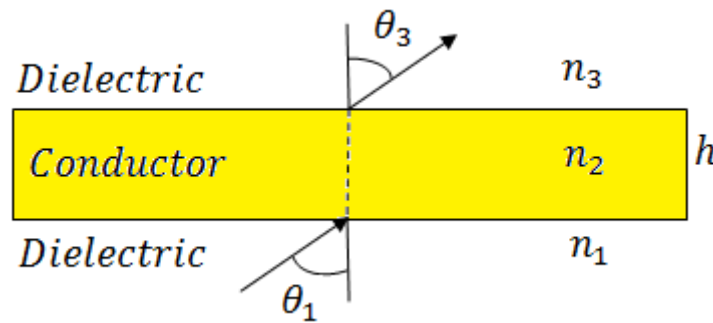


Figure 6.2: An absorbing film situated between two dielectric media. The thickness of the absorbing film is h and refractive index is n_2 . The refractive indices of dielectric media are n_1 and n_3 .

When a plane wave is incident on a plane parallel film obliquely, the behaviour of the reflected and transmitted wave depends on the polarization of the incident wave. In order to be specific about the direction of the electric field, the plane of incidence is defined as the plane containing the vector indicating the direction of propagation of the incident wave and

6. Angle Resolved Reflection and Transmission Coefficients

the normal to the boundary surface. The angle of incidence θ_1 is measured from the normal to the boundary surface.

Since according to the law of refraction

$$\widehat{n}_2 \sin \theta_2 = n_1 \sin \theta_1, \text{ that}$$

$$\widehat{n}_2 \sin \theta_2 = n_3 \sin \theta_3,$$

angle θ_3 is determined from θ_1 by means of the formula

$$n_3 \sin \theta_3 = n_1 \sin \theta_1$$

$$\theta_2 = \text{asin}\left(\frac{n_1}{(n_2 + i\kappa_2)} \sin \theta_1\right)$$

$$\theta_3 = \text{asin}\left(\frac{(n_2 + i\kappa_2)}{n_3} \sin \theta_2\right)$$

The formulae relating to the reflection and transmission of a plane monochromatic wave by the film are obtained by setting

$$\widehat{n}_2 = n_2 + i\kappa_2$$

$$\widehat{n}_2 \cos \theta_2 = a_2 + ib_2,$$

Where a_2 and b_2 are real. They can be expressed in terms of the angle of incidence and the constants which characterize the optical properties of the first and the second medium. It follows, on squaring (6.6) and using the law of refraction

$$\widehat{n}_2 \sin \theta_2 = n_1 \sin \theta_1, \text{ that}$$

$$(a_2 + ib_2)^2 = \widehat{n}_2^2 - n_1^2 \sin^2 \theta_1 \tag{6.7}$$

On equating real and imaginary part this gives

$$a_2^2 - b_2^2 = (n_2^2 - \kappa_2^2) - n_1^2 \sin^2 \theta_1 \tag{6.8}$$

$$a_2 b_2 = n_2^2 \kappa_2$$

From equation (6.8) we find that

6. Angle Resolved Reflection and Transmission Coefficients

$$2a_2^2 = (n_2^2 - \kappa_2^2) - n_1^2 \sin^2 \theta_1 + \sqrt{((n_2^2 - \kappa_2^2) - n_1^2 \sin^2 \theta_1)^2 + 4n_2^2 \kappa_2^2} \quad (6.9)$$

$$2b_2^2 = -[(n_2^2 - \kappa_2^2) - n_1^2 \sin^2 \theta_1] + \sqrt{((n_2^2 - \kappa_2^2) - n_1^2 \sin^2 \theta_1)^2 + 4n_2^2 \kappa_2^2}$$

It is necessary to evaluate the reflection and transmission co-efficients for the interfaces 1-2 and 2-3 respectively, to allow enter these co-efficients into the formulae for the reflection and transmission coefficients of the film. The two cases are separately considered when the electric vector of the incident wave is perpendicular or parallel.

Electric vector perpendicular to the plane of incidence (TE wave)

The reflection and transmission coefficients for an electric field vector perpendicular to the plane of incidence can be obtained by using Fresnel formulae for the same polarization. The reflection and transmission coefficients at each interface can be obtained by replacing $n_2 \cos \theta_2$ by $\widehat{n}_2 \cos \theta_2 = a_2 + ib_2$ in Fresnel formulae.

The reflection coefficient at the first interface is given by

$$r_{12} = \rho_{12} e^{i\varphi_{12}} = \frac{n_1 \cos \theta_1 - (a_2 + ib_2)}{n_1 \cos \theta_1 + (a_2 + ib_2)} \quad (6.10)$$

The explicit expressions for the amplitude ρ_{12} and phase φ_{12} are obtained by separating real and imaginary parts as follows

$$\rho_{12}^2 = \frac{(n_1 \cos \theta_1 - a_2)^2 + b_2^2}{(n_1 \cos \theta_1 + a_2)^2 + b_2^2} \quad (6.11)$$

$$\tan \varphi_{12} = \frac{2b_2 n_1 \cos \theta_1}{a_2^2 + b_2^2 - n_1^2 \cos^2 \theta_1} \quad (6.12)$$

The transmission coefficient at the first interface is given by

$$t_{12} = \tau_{12} e^{i\psi_{12}} = \frac{2n_1 \cos \theta_1}{n_1 \cos \theta_1 + a_2 + ib_2} \quad (6.13)$$

The expressions for the amplitude τ_{12} and phase ψ_{12} are given as follows

$$\tau_{12}^2 = \frac{(2n_1 \cos \theta_1)^2}{(n_1 \cos \theta_1 + a_2)^2 + b_2^2} \quad (6.14)$$

$$\tan \psi_{12} = -\frac{b_2}{n_1 \cos \theta_1 + a_2} \quad (6.15)$$

6. Angle Resolved Reflection and Transmission Coefficients

In a strictly analogous way we obtain the following expressions relating to reflection and transmission at the second interface.

$$\rho_{23}^2 = \frac{(n_3 \cos \theta_3 - a_2)^2 + b_2^2}{(n_3 \cos \theta_3 + a_2)^2 + b_2^2} \quad (6.16)$$

$$\tan \varphi_{23} = \frac{2n_3 b_2 \cos \theta_3}{a_2^2 + b_2^2 - n_3^2 \cos^2 \theta_3} \quad (6.17)$$

$$\tau_{23}^2 = \frac{4(a_2^2 + b_2^2)}{(n_3 \cos \theta_3 + a_2)^2 + b_2^2} \quad (6.18)$$

$$\tan \Psi_{23} = \frac{b_2 n_3 \cos \theta_3}{a_2^2 + a_2^2 - a_2 n_3 \cos \theta_3} \quad (6.19)$$

These expressions are utilized to obtain the analytical expressions for complex reflection and transmission coefficient, reflectance and transmittance of an absorbing film for the electric field vector perpendicular to the plane of incidence.

Electric vector parallel to the plane of incidence (TM wave)

The formulae for the reflection and transmission coefficients for an electric vector parallel to the plane of incidence can be obtained from those for an electric field vector perpendicular to the plane of incidence simply by replacing the quantities for instance, $p_j = n_j \cos \theta_j$, by $q_j = \cos \theta_j / n_j$, it being assumed that media are non-magnetic.

The reflection coefficient at the first interface is given by

$$r_{12} = \rho_{12} e^{i\varphi_{12}} = \frac{\frac{1}{n_1} \cos \theta_1 - \frac{1}{n_2} \cos \theta_2}{\frac{1}{n_1} \cos \theta_1 + \frac{1}{n_2} \cos \theta_2}$$

$$r_{12} = \frac{n_2^2 \cos \theta_1 - n_1 n_2 \cos \theta_2}{n_2^2 \cos \theta_1 + n_1 n_2 \cos \theta_2}$$

$$r_{12} = \frac{([n_2^2 - \kappa_2^2] + 2in_2 \kappa_2) \cos \theta_1 - n_1(a_2 + ib_2)}{([n_2^2 - \kappa_2^2] + 2in_2 \kappa_2) \cos \theta_1 + n_1(a_2 + ib_2)} \quad (6.20)$$

From above equation we find after a straightforward calculation

$$\rho_{12}^2 = \frac{[(n_2^2 - \kappa_2^2) \cos \theta_1 - n_1 a_2]^2 + [2n_2 \kappa_2 \cos \theta_1 - n_1 b_2]^2}{[(n_2^2 - \kappa_2^2) \cos \theta_1 + n_1 a_2]^2 + [2n_2 \kappa_2 \cos \theta_1 + n_1 b_2]^2} \quad (6.21)$$

6. Angle Resolved Reflection and Transmission Coefficients

$$\tan\varphi_{12} = 2n_1 \cos\theta_1 \frac{[2n_2\kappa_2 u_2 - (n_2^2 - \kappa_2^2)]b_2}{(n_2^2 + \kappa_2^2)^2 \cos^2\theta_1 - (a_2^2 + b_2^2)n_1^2} \quad (6.22)$$

The transmission coefficient at the first interface is given by

$$\begin{aligned} t_{12} = \tau_{12} e^{i\psi_{12}} &= \frac{\frac{2}{n_1} \cos\theta_1}{\frac{1}{n_1} \cos\theta_1 - \frac{1}{n_2} \cos\theta_2} \\ &= \frac{2[(n_2^2 - \kappa_2^2) + 2i\kappa_2 n_2] \cos\theta_1}{[(n_2^2 - \kappa_2^2) + 2i\kappa_2 n_2] \cos\theta_1 + n_1(a_2 + ib_2)} \end{aligned} \quad (6.23)$$

The amplitude and phase of the transmission coefficient is given by

$$\tau_{12}^2 = \frac{4(n_2^2 - \kappa_2^2)^2 \cos^2\theta_1 + 16n_2^2 \kappa_2^2 \cos^2\theta_1}{[(n_2^2 - \kappa_2^2) \cos\theta_1 + n_1 a_2]^2 + [2n_2^2 \kappa_2 \cos\theta_1 + n_1 b_2]^2} \quad (6.24)$$

$$\tan\Psi_{12} = \frac{n_1[2n_2\kappa_2 a_2 - (n_2^2 - \kappa_2^2)b_2]}{\cos\theta_1(n_2^2 + \kappa_2^2) + n_1[(n_2^2 - \kappa_2^2)a_2 + 2\kappa_2 n_2 b_2]} \quad (6.25)$$

In a similar way we obtain the following formulae for the reflection and transmission coefficients relating to the second interface

$$\rho_{23}^2 = \frac{[(n_2^2 - \kappa_2^2) \cos\theta_3 - n_3 a_2]^2 + [2n_2\kappa_2 \cos\theta_3 - n_3 b_2]^2}{[(n_2^2 - \kappa_2^2) \cos\theta_3 + n_3 a_2]^2 + [2n_2\kappa_2 \cos\theta_3 + n_3 b_2]^2} \quad (6.26)$$

$$\tan\varphi_{23} = 2n_3 \cos\theta_3 \frac{2n_2\kappa_2 a_2 - (n_2^2 - \kappa_2^2)b_2}{n_2^4(1 + \kappa_2^2)^2 \cos^2\theta_3 - n_3^2(u_2^2 + a_2^2)} \quad (6.27)$$

and

$$\tau_{23}^2 = \frac{4n_3^2(a_2^2 + b_2^2)}{[n_3 a_2 + (n_2^2 - \kappa_2^2) \cos\theta_3]^2 + [n_3 b_2 + 2\kappa_2 n_2 \cos\theta_3]^2} \quad (6.28)$$

$$\tan\Psi_{23} = \frac{[(n_2^2 - \kappa_2^2)b_2 - 2\kappa_2 n_2 a_2] \cos\theta_3}{n_3(a_2^2 + b_2^2) + (n_2^2 - \kappa_2^2)a_2 + 2\kappa_2 n_2 b_2} \cos\theta_3 \quad (6.29)$$

6. Angle Resolved Reflection and Transmission Coefficients

The complex reflection and transmission co-efficients of the film may immediately be evaluated from the knowledge of the quantities for instance amplitude and phase of the reflection and transmission coefficients for the interfaces 1-2 and 2-3 for a particular wavelength.

It will be useful to set.

$$\eta = (2\pi/\lambda) h$$

$$\beta = \frac{2\pi}{\lambda} * \widehat{n}_2 h \cos\theta_2 = (a_2 + ib_2) * \eta$$

The complex reflection r and transmission t coefficient for an absorbing film is given by

$$r = \rho e^{i\delta_r} = \frac{\rho_{12} e^{i\varphi_{12}} + \rho_{23} e^{-2b_2\eta} e^{i(\varphi_{12} + 2a_2\eta)}}{1 + \rho_{12}\rho_{23} e^{-2b_2\eta} e^{i(\varphi_{12} + \varphi_{23} + 2a_2\eta)}} \quad (6.30)$$

$$t = \tau e^{i\delta_t} = \frac{\tau_{12}\tau_{23} e^{-2b_2\eta} e^{i(\psi_{12} + \psi_{23} + a_2\eta)}}{1 + \rho_{12}\rho_{23} e^{-2a_2\eta} e^{i(\varphi_{12} + \varphi_{23} + 2a_2\eta)}} \quad (6.31)$$

From above equation we obtain, after straight forward calculation, the reflectance R of an absorbing film

$$R = \frac{\rho_{12}^2 e^{2b_2\eta} + \rho_{23}^2 e^{-2b_2\eta} + 2\rho_{12}\rho_{23} \cos(\varphi_{23} - \varphi_{12} + 2a_2\eta)}{e^{2b_2\eta} + \rho_{12}^2 \rho_{23}^2 e^{-2b_2\eta} 2\rho_{12}\rho_{23} \cos(\varphi_{12} + \varphi_{23} + 2a_2\eta)} \quad (6.32)$$

In the similar way the following expressions for the transmittance T can be obtained

$$T = \frac{n_3 \cos\theta_3}{n_1 \cos\theta_1} * \frac{\tau_{12}^2 \tau_{23}^2}{e^{2b_2\eta} + \rho_{12}^2 \rho_{23}^2 e^{-2b_2\eta} 2\rho_{12}\rho_{23} \cos(\varphi_{12} + \varphi_{23} + 2a_2\eta)} \quad (6.33)$$

These formulae are valid for a TE wave as well as for a TM wave. In the former case one must substitute for ρ and φ the values given by equations (6.10) to (6.19), in the latter case those given by (6.20) to (6.29). For a TM wave the factor $n_3 \cos\theta_3 / n_1 \cos\theta_1$ must be replaced by $(\cos\theta_3 / n_3) / (\cos\theta_1 / n_1)$.

The equations (6.30) to (6.33) allow the computations of four basic quantities that characterize reflection and transmission by an absorbing film of known optical properties and of prescribed thickness. These analytical expressions can be utilised to obtain amplitude and phase as well as reflectance and transmittance of a metal film for the range of angles.

6.3 Numerical Examples

The validity of the analytical expressions for an absorbing film has been verified by substituting numerical data. Results are obtained for finite thickness dielectric slab and metal film.

6.3.1 Dielectric slab

The dielectric slab is assumed to have finite thickness and a known refractive index. The reflectance and transmittance of a dielectric slab at oblique incidence has been obtained for a slab thickness of 1.875 microns. The refractive index of the dielectric slab is 3.5. The results are obtained by substituting $\kappa_2 = 0$ in the expressions 6.30 and 6.31, which simplifies them for the dielectric case. The results are shown in Figure 6.3 and 6.4 for TE and TM polarization.

6. Angle Resolved Reflection and Transmission Coefficients

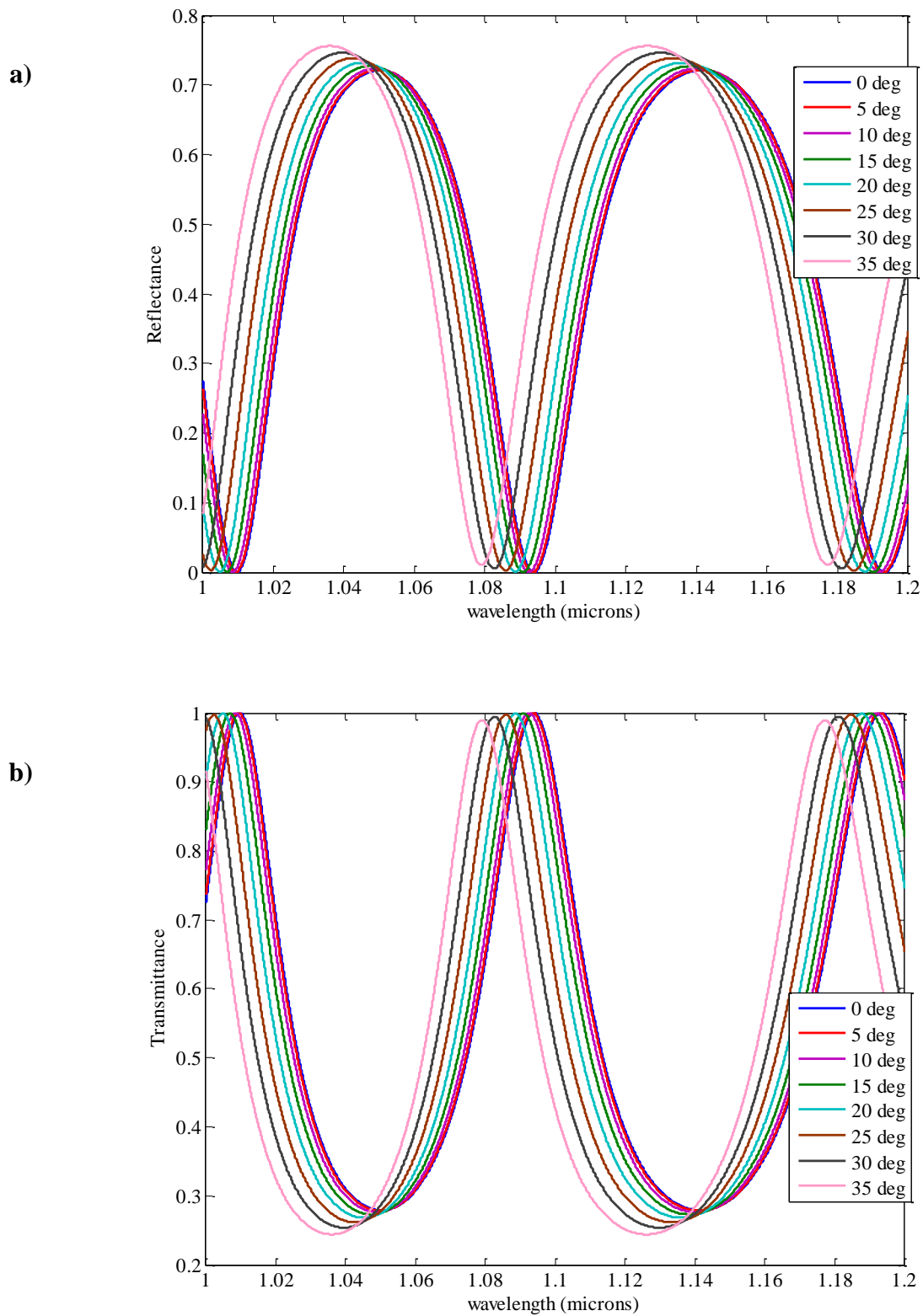


Figure 6.3: a) Reflectance b) Transmittance of a dielectric slab for TE polarization.

6. Angle Resolved Reflection and Transmission Coefficients

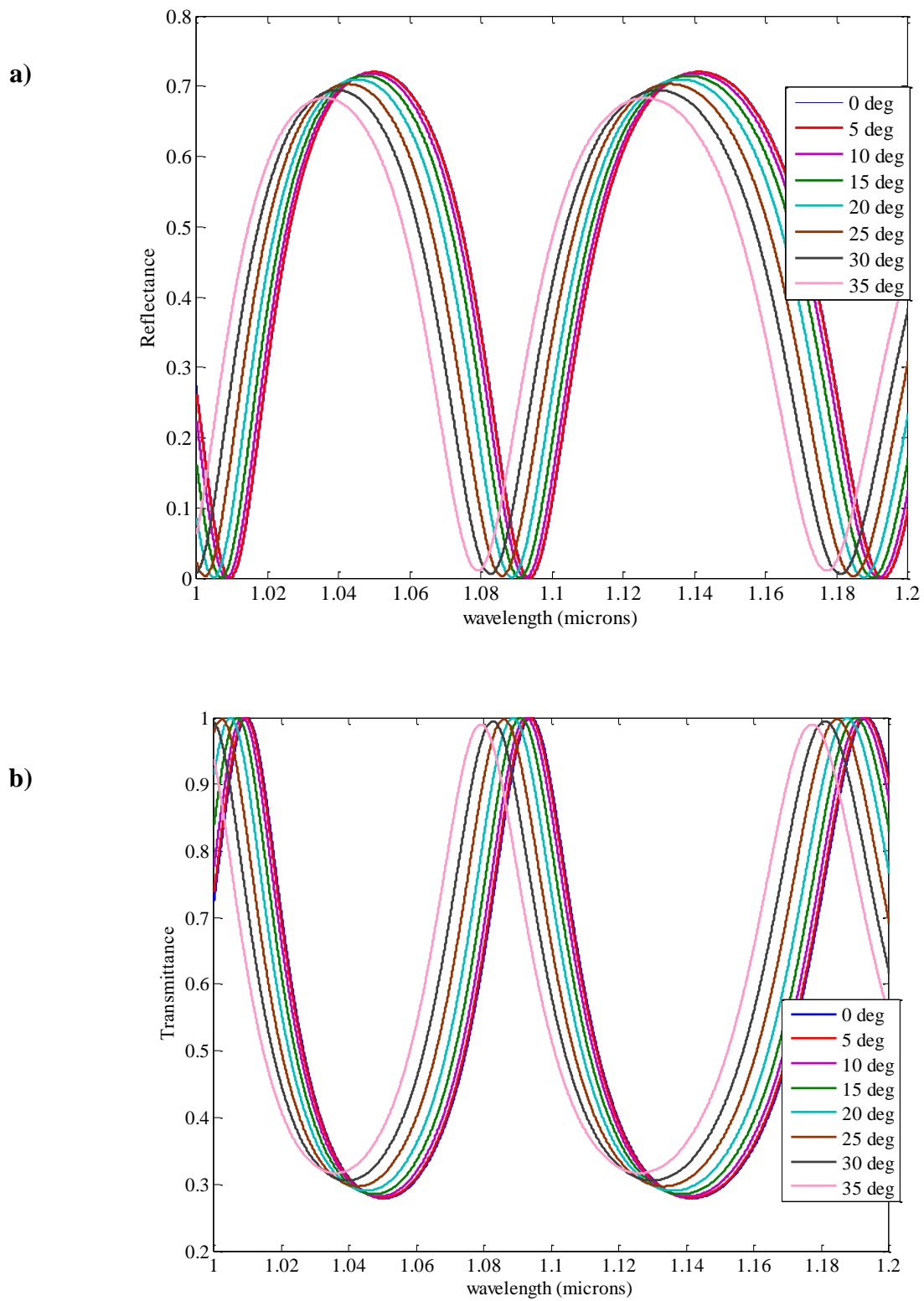


Figure 6.4: a) Reflectance b) Transmittance of a dielectric slab for TM polarization

6.3.2 Metal film

The metal film is assumed to have finite thickness and known material properties. The thickness of the metallic film has been kept as 30 nm in the calculations because the thickness of metallic films in most artificial structures is typically a few tens of nanometres. The material properties of silver film are described by the Drude model with a plasma frequency $\varepsilon_\infty = 1$, $\omega_p = 2175$ THz and a collision frequency $\omega_c = 4.35$ THz [15]. In general, consideration of the reflectance, transmittance and absorption accounts for the entire incident light, with scattering, for example from rough surfaces being neglected. It is well established that if there is no absorption in the spectral range of interest then reflectance and transmittance must equal unity or 100 percent if the values are given in percentages [16, 17].

$$R + T = 1$$

It is possible, from measurements of reflection and transmission, to determine whether a particular sample is losing light energy through a mechanism of absorption by calculating the absorbance as follows

$$1 - (R + T) = A$$

The results are shown in Figure 6.5 and 6.6 for TE and TM polarizations for reflectance, transmittance and absorbance.

6. Angle Resolved Reflection and Transmission Coefficients

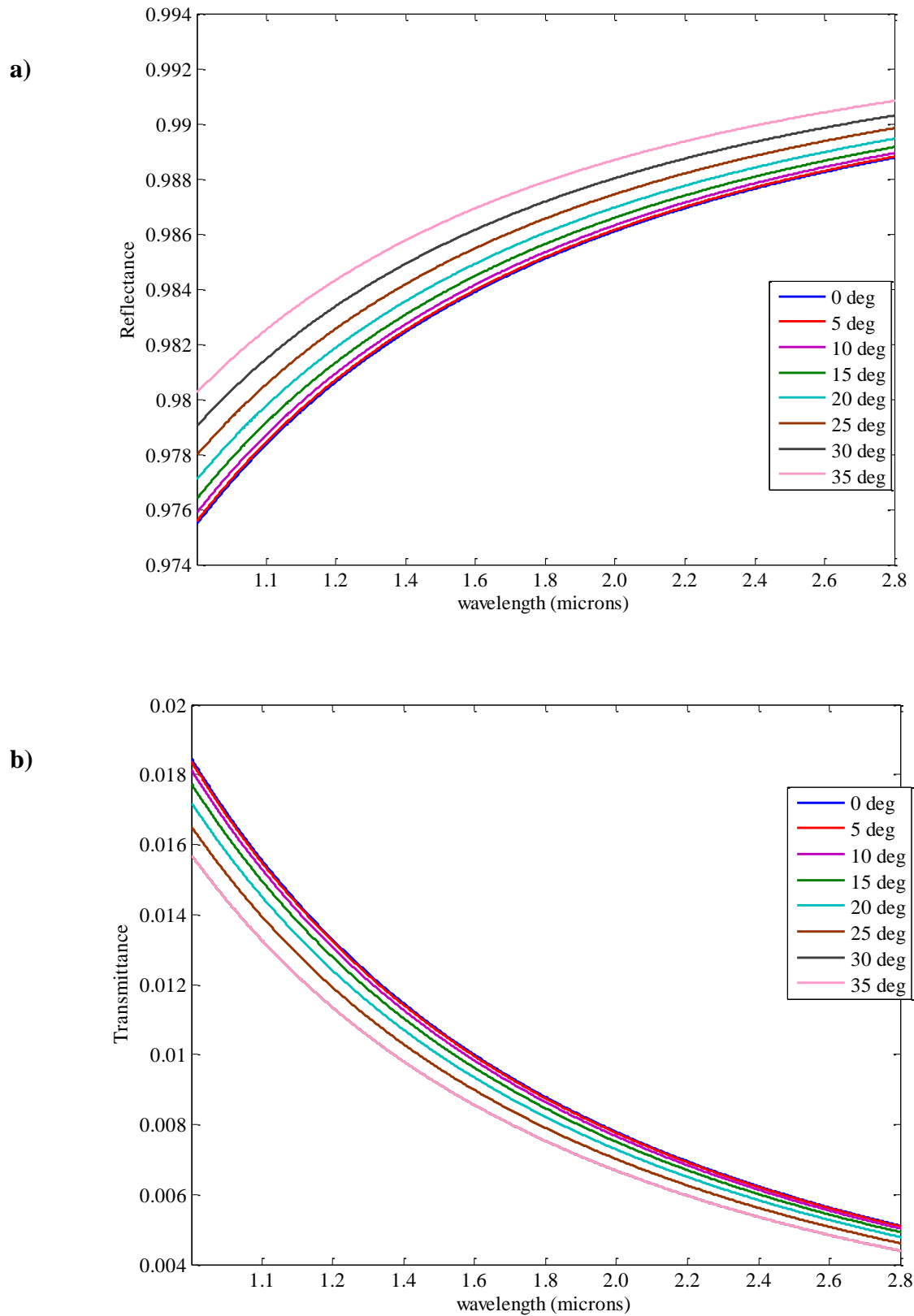


Figure 6.5: a) Reflectance b) Transmittance of a finite thickness metal film as a function of wavelength for TE polarisation.

6. Angle Resolved Reflection and Transmission Coefficients

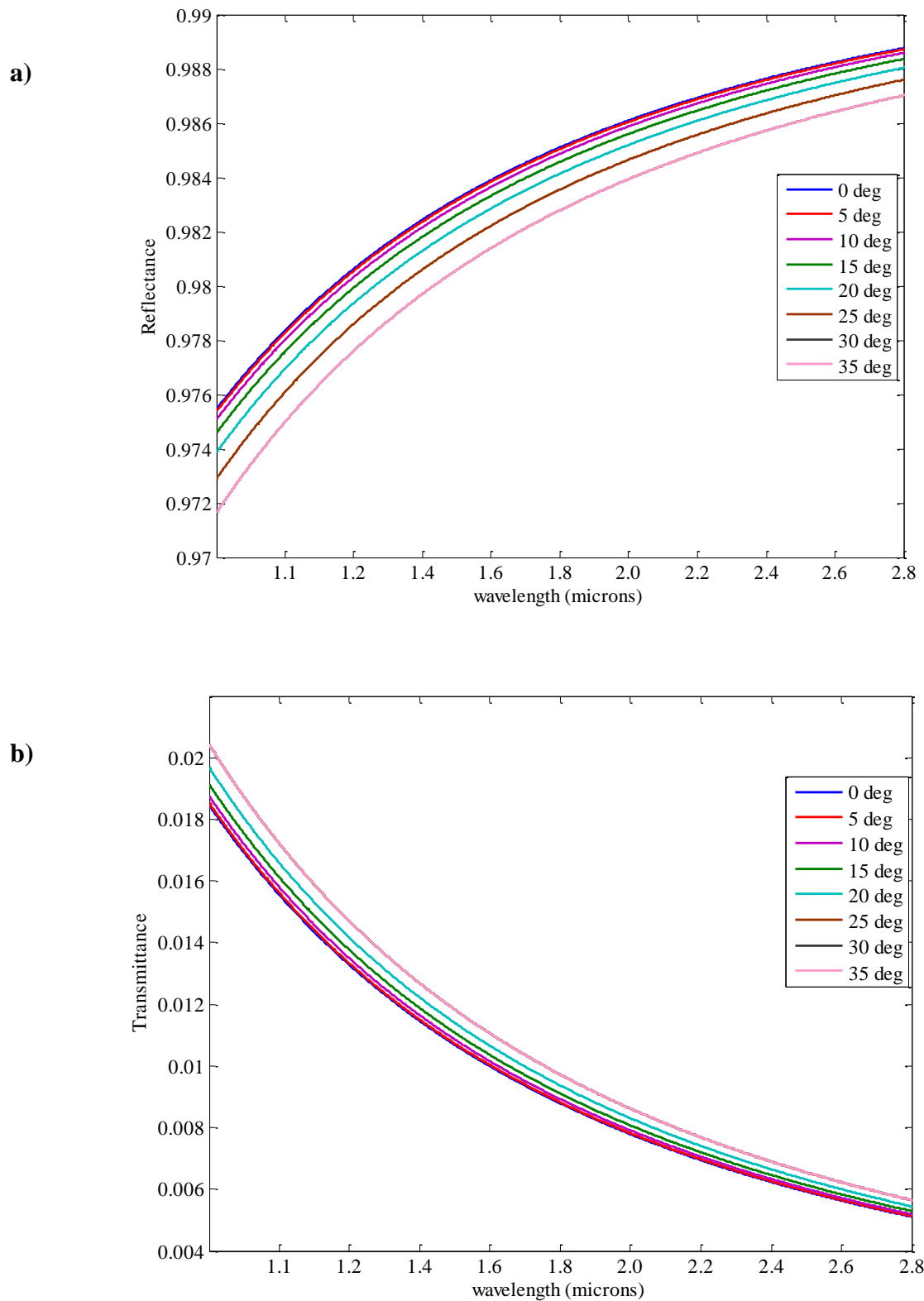


Figure 6.6: a) Reflectance b) Transmittance of a finite thickness metal film as a function of wavelength for TM polarisation.

6.4 **Validity of results at normal incidence**

The reflectance and transmittance obtained for the dielectric slab or metal film by using analytical expression can be verified by using Lumerical Solutions.

Dielectric Slab

The reflectance and transmittance of a dielectric slab can be obtained by simulating a finite area of the slab. The thickness and refractive index of the dielectric slab are kept as $1.865 \mu\text{m}$ and 3.5 respectively. The dielectric slab is illuminated by a plane wave source over the wavelength range from $1 \mu\text{m}$ to $2 \mu\text{m}$. The direction of propagation of the light is the negative- z direction. The structure is periodic in the x and y directions. Antisymmetric/symmetric boundary conditions are used depending upon the polarisation of source. A perfectly matched layer is imposed on the edge-planes of the simulation area and perpendicular to the direction of propagation of source. The reflectance and transmittance obtained from a dielectric slab are shown in Figure 6.7. There is a good agreement between the simulation results and the results obtained from the analytical expressions.

6. Angle Resolved Reflection and Transmission Coefficients

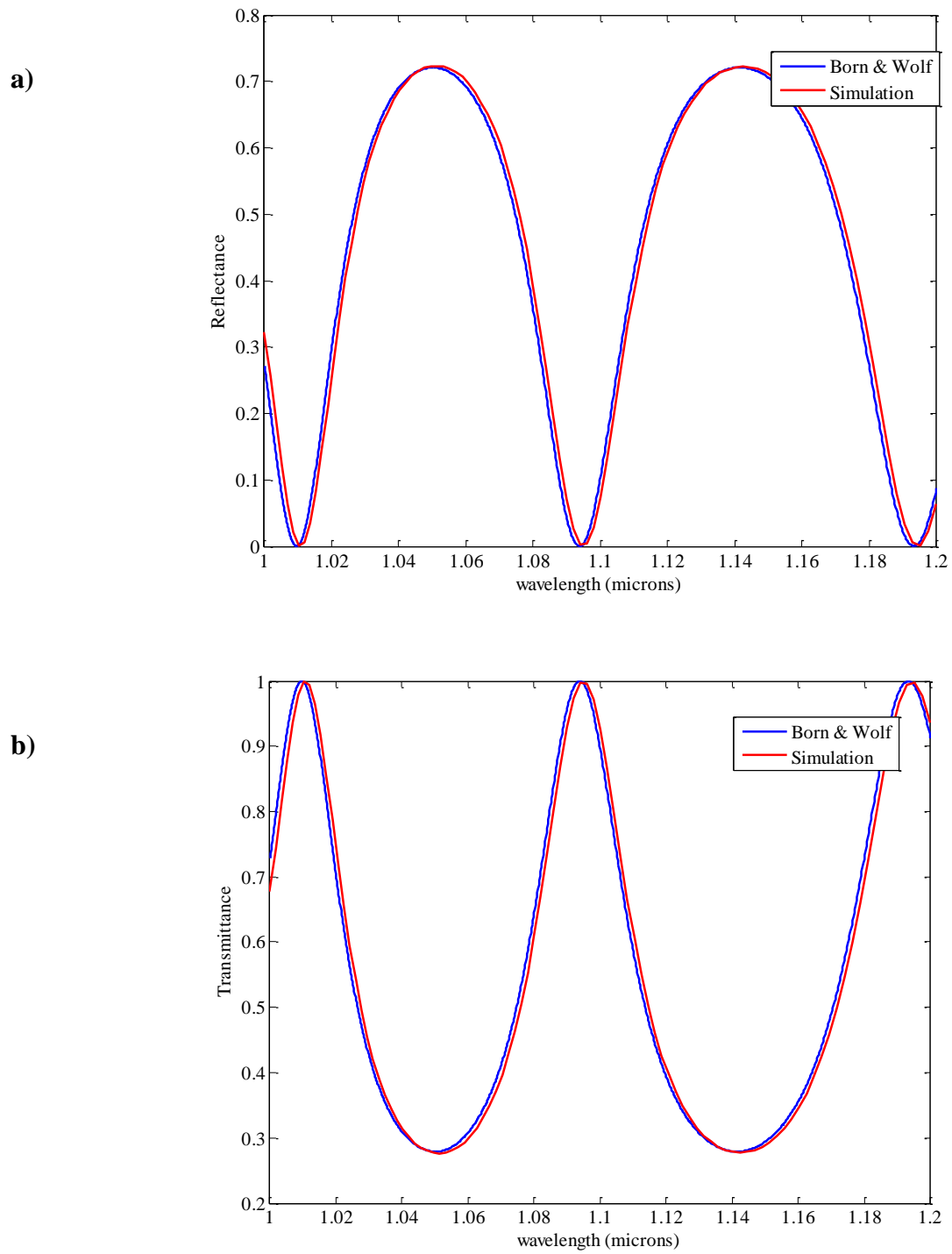


Figure 6.7: a) Reflectance b) Transmittance of a dielectric slab for normal incidence as a function of wavelength.

Metal film

The reflectance and transmittance of a thin metal film has been obtained by using Lumerical Solutions simulation software to validate the analytical results. The thickness of the metallic film is kept as 30nm. The material properties of the silver film are described by the Drude model with the plasma frequency $\epsilon_\infty = 1$, $\omega_p = 2175$ THz and a collision frequency $\omega_c = 4.35$ THz [15]. The metallic film is illuminated over the wavelength range between 1 μ m and 2 μ m. The direction of propagation is the negative-z direction. The structure is periodic in the x and y directions. Antisymmetric/symmetric boundary conditions are used depending upon the polarisation of source. A perfectly matched layer is imposed on the edge planes of the simulation area perpendicular to the direction of propagation of source. A very fine inner mesh size of 0.3 nm is used in the z-direction over the metal layer and seems to adequate for convergence of the simulation. The reflectance, transmittance and absorbance obtained from a metallic film are shown in Figure 6.8.

6. Angle Resolved Reflection and Transmission Coefficients

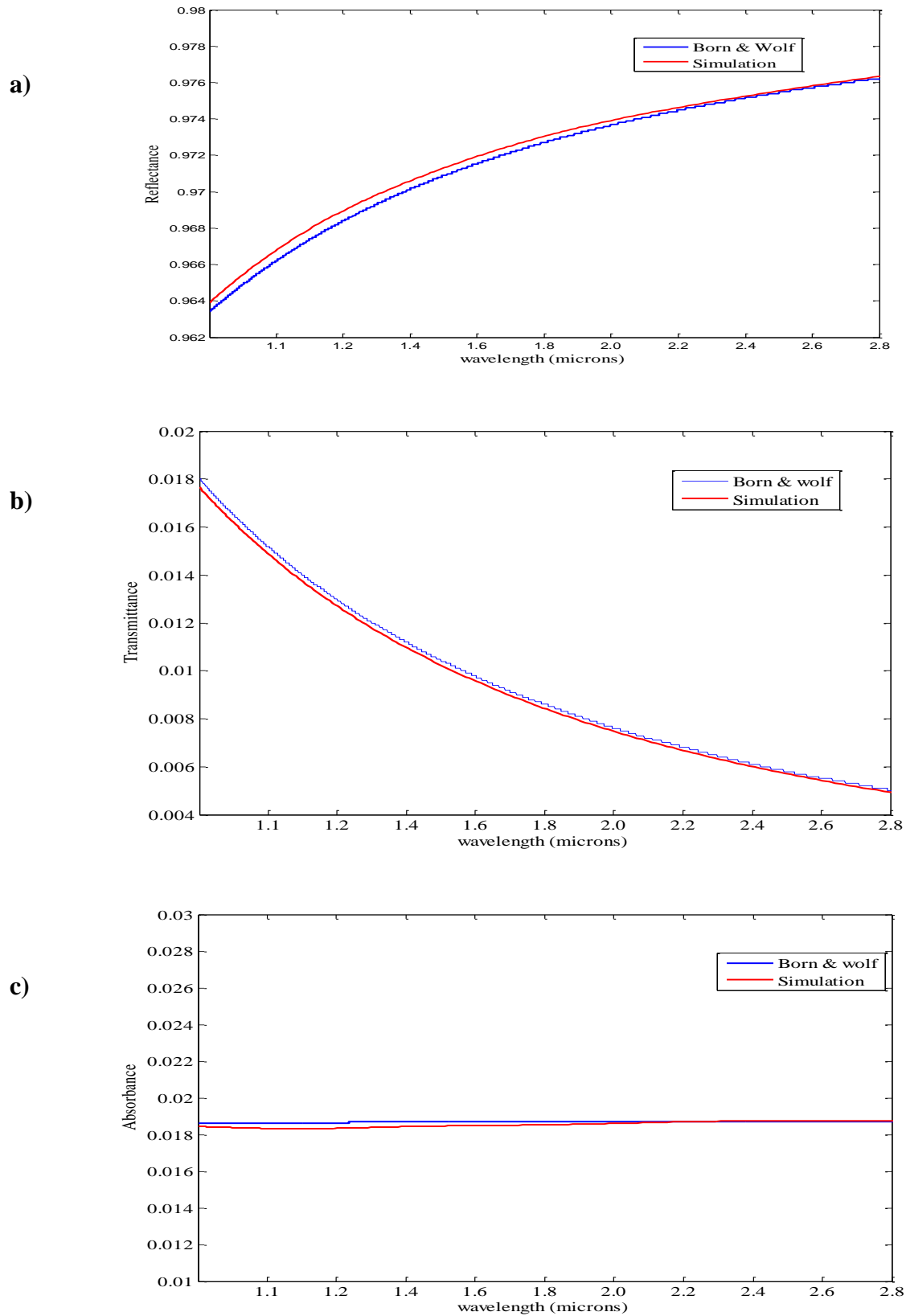


Figure 6.8: a) Reflectance b) Transmittance c) Absorbance of a metal film for normal incidence as a function of wavelength.

There is a good agreement between the simulation results and results obtained from the analytical expression which demonstrate the validity of the analytical expressions. It is not necessary to achieve simulation results with an error of less than 1%, since it is reasonable to assume that the error in the results of a simulation diminish with decreasing grid size. There are other sources of error that need to be considered. The results can be improved by applying the convergence testing [18]. The accuracy of the results depend upon the simulation objects for instance, the distance of PML boundary from the structure, PML reflectivity, multi-coefficient model (MCM) fits, Inner mesh and increasing the number of PML layers. The results presented in Figure 6.8 are obtained by increasing the PML distance to approximately $2\mu\text{m}$ from the metal film and increasing the PML layers, decreasing the PML reflectivity and using the minimum mesh size of 0.3 nm. The FDTD can give almost accurate answers with enough computer resources and results presented in Figure 6.8 can be further improved by repeating the steps for convergence testing [18]. There is also a chance of numerical error for the results obtained by analytical expression using matlab [19].

6.4.1 Validity of results at oblique incidence

The determination of angularly resolved reflection and transmission coefficients for metamaterials is complicated; it requires considerable CPU and memory resources. The reflection and transmission coefficients can be obtained by using the parameter sweep method. This method can also be used to obtain the reflectance and transmittance of artificial structures but it requires CPU and memory requirements that exceed readily available CPU performance.

Parameter sweep method

Parameter sweeps are useful for finding the optimum value of a parameter or for studying the sensitivity of the design performance to certain parameters or for running a series of simulations with a set of varying parameters [18]. Parameter sweeps execute the same piece of code multiple times with unique sets of input parameters. Possibilities include varying one parameter over a range of values or varying multiple parameters over a large multidimensional space.

Parameter sweep jobs are extremely amenable to parallelization. In parameter sweeps each individual simulation runs independently of all other simulations. This property is important

6. *Angle Resolved Reflection and Transmission Coefficients*

for parallelizing parameter sweep jobs because it is possible to formulate this type of problem so that none of these jobs communicate with each other and, they only communicate their results back when computing has finished. Because each job is independent, it does not matter which job completed first. It is only important that each job is completed and its results are recorded.

Parameter sweep simulations run with the help of serial code. It runs a command for a specified number of times (indicated by start, end and incremental values) generally across indexed input and output files. A typical parameter sweep application consists of a ‘for’ loop which repeatedly executes the same code, usually in a function. A unique set of arguments is supplied to the function in each iteration. Since the loop iterator has a unique value for each iteration, it can be used to compute the set of arguments. A more advanced parameter sweep job may nest multiple ‘for’ loops and use multiple iterators to compute the input arguments. Each iteration is computed entirely on one processor and, different loop iterations are processed on different processors.

In the study of metamaterials, it is often necessary to solve several variations of a model to find its optimal properties. Instead of manually changing these property values and resolving each time, one can perform parametric sweep tasks which allow changes to be made in the parameter values through a specified range.

Nested parameter sweeps allow parametric sweeps to be performed using more than one parameter. In this type of parameter sweep every combination of parameter is utilized and the parameter lists do not need to be of the same length.

In order to obtain broadband results at a certain angle, a parameter sweep task can be set up to run a series of single frequency simulations that sweep over the frequency range of interest. To obtain broadband results over a range of injection angles, a nested sweep can be set up to sweep over the range of injection angles and source frequencies. The reflectance and transmittance characteristics at oblique incidence can be calculated for a section of dielectric slab, or metal film or for an artificial structure. The results obtained from a piece of dielectric slab are provided in appendix. If the structure is periodic in both the x and y directions, Bloch boundary conditions are used in the x and y directions. These boundary conditions are used in simulations of periodic structures that are illuminated with a plane-wave source propagating at an angle. Bloch boundary condition can be understood as a more general form of periodic

boundary conditions. Simulations that use Bloch boundary conditions required as much as twice the memory and time compared with an equivalent simulation without Bloch boundary conditions. These boundary conditions take into account the phase change across each period. Nested parameter sweep tasks can provide the reflectance and transmittance of different structures and also they can be used to obtain complex reflection and transmission coefficients at oblique incidence. In order to obtain the complex reflection and transmission coefficients using the parameter sweep task, it is necessary to generalize the phase of complex reflection and transmission coefficients.

It is possible to calculate the complex reflection and transmission coefficients for geometrically complex structures by using FDTD simulation softwares. The calculation of the Poynting vector at oblique incidence on a single layer NIM slab consisting of a hexagonal array of sub-wavelength coaxial waveguide structures, as shown in reference [20], indicates that it is possible to calculate the complex reflection and transmission coefficients of a metamaterials structure at oblique incidence for both polarizations using FDTD softwares.

6.4.2 Numerical Example

The reflectance and transmittance of a single thin metal film in air have been obtained by using Lumerical Solutions simulation software in order to demonstrate the applicability of the FDTD method for the situation of obliquely incident optical waves on a medium with a mathematically complex dielectric function and refractive index. The thickness of the metallic film was chosen as 30 nm and silver was chosen as the metal for this test because of its well established characteristics and its application in the realisation of metamaterials structures. The material properties of the silver film are described by the Drude model with the plasma frequency $\epsilon_{\infty} = 1$, $\omega_p = 2175$ THz and a collision frequency $\omega_c = 4.35$ THz [15]. The metallic film is illuminated over the wavelength range between 1 μ m and 2 μ m. The direction of the z-component of propagation is the negative-z direction. The structure is periodic in the x and y directions. Bloch boundary conditions are used that depend upon the polarisation of source. A parameter sweep set up has been used to obtain reflectance and transmittance at oblique incidence over a range of angle of incidence. A perfectly matched layer is imposed on all of the edge planes of the simulation area that are perpendicular to the direction of propagation of the source. A very fine inner mesh size of 0.3 nm is used in the z-direction over the metal layer and seems to be adequate for convergence of the simulation. The reflectance and transmittance obtained are shown in Figure 6.9.

6. Angle Resolved Reflection and Transmission Coefficients

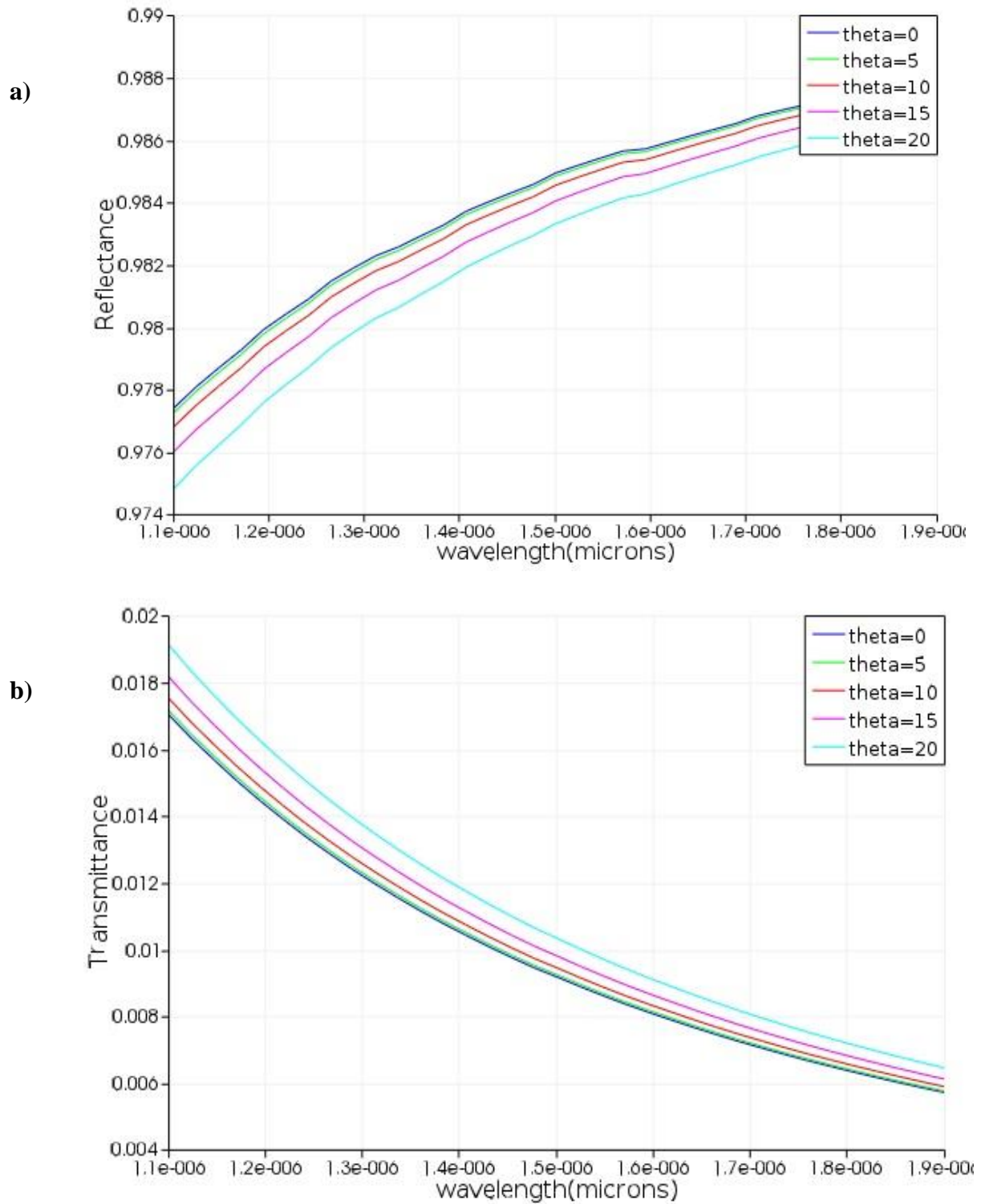


Figure 6.9: a) Reflectance b) Transmittance of a metal film of a finite thickness metal film as a function of wavelength.

6.5 Summary and concluding remarks

Measurement of the reflectance and transmittance or the complex reflection and transmission coefficients of a thin metal film is a common method for obtaining the optical constants n and κ of the metal. The same approach may be used to characterize metamaterials and the material parameters have been retrieved. In the past, the measurements of complex reflection and transmission coefficients for metamaterials have usually been made at normal incidence. A general procedure for analysing measurements made at oblique incidence has been proposed in this chapter. The analytical expression for an absorbing medium are taken from the literature and rewritten for an alternative definition of complex refractive index. The expressions are validated for finite thickness and the known material properties of a dielectric slab and a metal film. Simulations were performed to obtain results at normal incidence for a dielectric slab and a metal film. The results are in good agreement with the analytical results. Convergence testing has been applied in the metal film case and close agreement was obtained. The discrepancies in the reflectance and transmittance of a metal film with the analytical results are well explained.

Reflectance and transmittance estimates at oblique incidence can be obtained by simulation and use of the parameter sweep method, but excessively large computational resources are required. The author has not been able to compute the complex reflection and transmission coefficients from artificial structures by using Lumerical Solutions. The reasons are explained in this chapter. It is possible to obtain complex reflection and transmission coefficients for metamaterials for instance the fishnet structure by embedding its complex refractive index using the methods given in Chapter 6 of this thesis in the analytical expressions written for an absorbing medium. These expressions are in principle valid for oblique incidence, as well as a general definition of complex refractive index, but the author has so far not been able to carry through the computer calculations for the case of artificial structures. Therefore the equivalent complex refractive index and thickness representation of the metal-dielectric-metal fishnet structure have not been verified. One possible reason for this algorithm not working for metamaterials is that these expressions do not address the possibility of negative material parameters. Also there is no reliable refractive index data available for complex refractive index for these geometrically more complex structures [9]. The data for complex refractive index can be obtained using the retrieval approach which has been widely used to obtain the equivalent material parameters for the metamaterials. But the results obtained for

the dielectric slab, the metal film and their validity provide the possibility that this proposal may yield a general algorithm for obtaining the complex reflection and transmission coefficients for artificial structures.

6.6 References

- [1] A. M. Nicholson and G.F. Ross, "The measurement of the intrinsic properties of materials by time-domain techniques," *IEEE Trans. Instrum. Meas.* 17 395 (1968)
- [2] W. Weir, "Automatic measurement of the complex dielectric constant and permeability at microwave frequencies," *Proc. IEEE* 62 33
- [3] D. R. Smith, S. Schultz, P. Markos, C. M. Soukoulis, "Transmission properties and effective electromagnetic parameters of double negative metamaterials," *Phys. Rev B.* 65, 195104 (2002)
- [4] C. Menzel, C. Rockstuhl, T. Paul, F. Lederer and T. Perttch, "Retrieving effective parameters for metamaterials at oblique incidence," *Phys. Rev B.* 77 195328 (2008)
- [5] L.Li, "New formulation of fourier modal method for crossed surface relief gratings," *J. Opt. Soc. Am. A.* 14 2758 (1997).
- [6] Harland. G. Tompkins, Eugene. A. Irne, *Handbook of Ellipsometry*, Springer- Verlag Gmbh & Co. KG (2005)
- [7] T. Koschny, P. Markos, D. R. Smith, and C. M. Soukoulis, "Resonant and antiresonant frequency dependence of the effective parameters of metamaterials," *Phys. Rev. E* 68, 065602 (2003)
- [8] D. R. Smith, D. C. Vier, T. Koschny, C. M. Soukoulis, "Electromagnetic parameter retrieval from inhomogeneous metamaterials", *Phys. Rev. E* 71 036617 (2005).
- [9] T. Koschny, P. Markos, E. N. Economou, D.R. Smith, D.C. Vier, C. M. Soukoulis, "Determination of effective parameters from reflection and transmission coefficients," *Phys. Rev. B* 71 245105 (2005).

6. Angle Resolved Reflection and Transmission Coefficients

- [10] X. Chen, T. M. Grzegorzcyk, B. I. Wu, J. Pacheco, J.A. Kong, “Robust method to retrieve the constitutive effective parameters of metamaterials,” *Phys. Rev. E*, 70, 016608 (2004).
- [11] S. A. Tretyakov, C. R. Simovski. M. Hudlicka. “Bianisotropic route to the realization and matching of backward wave metamaterials slabs,” *Phys. Rev. B*, 75, 151304 (2007).
- [12] S. I. Khan, R. M. De La Rue, T. D. Drysdale, N. P. Johnson, “Electromagnetic parameter retrieval at oblique incidence,” *Proc. Of SPIE* 8771, 87718 (2013)
- [13] S. I. Khan, G. J. Sharp, R. M. De La Rue, T. D. Drysdale, N. P. Johnson, “Angle resolved reflection and transmission coefficients from the fishnet structure formed from nanoimprint lithography,” *Proc. Of SPIE* (2014).
- [14] Max Born, Emil Wolf, *Principles Of Optics*, Pergamon Press, (1959)
- [15] I.E. Kadly, M. M. Sigalas, R. Biswas, K. M. Ho, and C. M. Soukoulis, “Metallic photonic crystals at optical wavelengths,” *Phys. Rev. B*, 62, 299 (2000)
- [16] L. N. Hadley and D. M. Dennison, “Reflection and transmission interference filters, Part I: Theory,” *J. Opt. Soc. Am. A*. 37, 451 (1947)
- [17] L. N. Hadley and D. M. Dennison, “Reflection and transmission interference filters, Part II: Experimental, Comparison with theory, Results” *J. Opt. Soc. Am. A*. 37, 451 (1947)
- [18] Lumerical Solutions Inc.
- [19] www.mathworks.co.uk
- [20] S. Burgos, R. Waele, A. Polman, H. A. Atwater, “A single layer wide angle negative index metamaterial at visible frequencies,” *Nature Materials*, 9, (2010).

7. Conclusions and Future Work

7.1 Thesis Summary:

A summary of the main conclusions obtained from the previous chapters is as follows:

- A general overview of metamaterials and recent interest in metamaterials is presented in the introductory chapter of this thesis.
- The interaction of light in metamaterials is often described in a simplified form by means of effective material parameters. They simplify the description and characterisation considerably. An understanding of these material parameters is established and their physical meaning is accessed. The limits for the applicability of material parameters are discussed in a preliminary chapter (Chapter 2) of the thesis.
- The main driving force for the investigation of metamaterials is the artificial magnetic response of the structures in frequency domains where naturally available materials do not possess an intrinsic magnetic response. Once such an artificial magnetic response of considerable strength is achieved, materials may be fabricated that possess a negative refractive index in a certain frequency range by combining the magnetic constituents with elements that have negative effective permittivity. The explanation in terms of LC resonance is usually applied to describe the electromagnetic response of such structures. The first and most widely investigated meta-atoms is split ring resonator (SRR). But the (SRR) cannot be arbitrarily small because of the saturation of the magnetic response of the (SRR) at optical frequencies. To increase the resonance frequency further and to achieve structures that are optically small the geometry must be modified. The simplest and best way is to remove the base of the (SRR) which results into a structure called a cut-wire pair. A concise overview of these structures and rules for their optimization has been given in Chapter 3.

- The performance of the fishnet structure is investigated comprehensively and necessary explanation of this structure is recapitulated in Chapter 4 of the thesis. The fishnet metamaterial is often preferred in the optical domain due to its superior performance in terms of figure of merit. The larger the figure of merit the more negative the refractive index and the less absorptive the material is. The fishnet is biaxially anisotropic, due to its geometry and it is sensitive to polarization, even for normal incidence. However, this polarization sensitivity is an undesirable property of metamaterials for many purposes. Parametric investigation of the structure in the infrared region has shown that, by changing the geometrical parameters, there is a strong influence on the frequency of the resonances. This effect is naturally exploited when scaling up the spectral domain of operation. The retrieved effective material parameters suggest that the artificial magnetic resonance of the fishnet structure is quite strong and that the real part of the permeability can achieve negative values there by making the fishnet become doubly negative medium. The unit cell of fishnet structure consists of two perforated metallic layers separated by a dielectric spacer. This three layer system is usually called a single functional layer. These functional layers are stacked to form multi-layer metamaterials, which can be considered as a step towards the formation of bulk metamaterials. The convergence of the effective material parameters, most importantly, the convergence of negative refractive index has been shown. Since a single functional layer will behave significantly different compared to a sequence of functional layers or even an infinite structure.
- The theory of the interaction of light with metamaterials has been described in the previous chapters. But it has been challenging to fabricate metamaterials that are large enough to be practical. Fishnet metamaterials usually have several vertically stacked repeat units spread out over much larger lateral dimensions. Because they are structured both vertically and laterally, they are called three dimensional materials. The usual fabrication techniques suffer from difficulties of which the most important is that the final metamaterial structure, for currently available fabrication methods is limited to critical dimensions of tens of nanometres which restricts the frequencies of resonances that can be achieved, and in turn, the functionality of the final structure. The fishnet structure has been fabricated using nanoimprint lithography. The details of the fabrication technique and characterization of the structure are explained in

Chapter 5 of this thesis. Two different structures with different sets of dimensions have been fabricated by this method. The transmission properties of the structures have been measured experimentally over part of the infrared frequency region (1 μm - 3 μm). The results are complemented by simulations that show good agreement. The effective refractive index for the structure has been retrieved by using The NRW method and taking into account the effects of the substrate and the patterned poly-methyl-meth-acrylate (PMMA) layer that forms part of the complete structure. A comparison of this effective refractive index has been made with the case where the single functional layer of the fishnet has been embedded in the effective medium. The difference in the magnitude of the effective refractive index for the two cases has been clearly shown indicating the effect of the substrate on the properties of metamaterials. This difference is usually masked in the available literature because the negative effective refractive index is reduced in the presence of a substrate and is usually not taken into account.

- A wide variety of publications has been dedicated to the investigations of metamaterials either by identifying suitable geometries or by characterizing their properties. However the investigations made with respect to metamaterials has raised fundamental questions on the characterization of metamaterials that have only been partially answered. However some issues still need to be addressed, for instance characterization of metamaterials at oblique incidence. The structures that are responsible for providing negative refractive index may possess identical optical properties along the principal propagation direction. But their overall response may not be optically isotropic. Investigations carried out on particular structures are often performed only for certain high symmetry directions i-e. they do not cover all possible directions. It is therefore necessary to obtain the complex reflection and transmission coefficients for a range of angles of incidence for both TE and TM polarisation to completely understand the behaviour of structure. In the previous chapters The NRW method has been applied to characterize metamaterials at normal incidence. This method has the potential to be extended towards the case of oblique incidence. In this method, analytical expressions for an isotropic dielectric medium have been utilized to characterize metamaterials at normal incidence.

An obvious advantage of a fast-microprocessor is the ability to use advanced numerical techniques on a laptop computer and this has accelerated developments in the field of numerical simulation models. But simulations of artificial structures require huge CPU and memory requirements that exceed, by far, the current single CPU performance. Therefore an analytical approach has been suggested to obtain the complex reflection and transmission coefficients at oblique incidence for artificial structures in Chapter 6 of the thesis. It is possible to obtain the complex reflection and transmission coefficients at oblique incidence by embedding the complex refractive index data obtained at normal incidence in the analytical expressions for an absorbing film. The analytical expressions for an absorbing film may be rewritten for an alternative definition of refractive index to match the simulation results. These expressions have been validated for the cases of dielectric slab and metal film. These results provide with the basis that this algorithm may be used to obtain complex reflection and transmission coefficients from metamaterials slab for both polarizations and for oblique angles of incidence.

7.2 Conclusions

The work contained in this thesis aimed to study and model metamaterials operating at visible and near-infrared frequencies. An emphasis is given to the fishnet structure and its characterization. The optical behaviour of the structure is modelled using Lumerical solutions which use FDTD method. Results are obtained using the simulation software and compared with the experimentally measured results. Field plots are generated where the electric field distribution is of interest.

The work contained in this thesis is based on the modelling of the fishnet structure formed from nanoimprint lithography, which is a valuable technique in the fabrication of metamaterials. The refractive index of as fabricated structure has been obtained by using retrieval method and compared with the available literature. It has been established that it may not be possible to detach these structures from the substrate therefore retrieval has been performed by taking into account the effect of polymer and substrate beneath it.

An analytical approach has been suggested to obtain the complex reflection and transmission coefficients at oblique angles for artificial structures. It is established that these structures are

bianisotropic, this approach has the potential to take into account the effects of bianisotropy at oblique angles thus completely specifying the properties of these structures.

7.3 Future work

This present research work is anticipated as a significant step forward towards obtaining angle resolved complex reflection and transmission coefficients for artificial structures. It is believed that the basis has now been set, that will allow it to be expanded in several directions. The author hopes that these suggestions offered for further research will result in interesting material for future contributions. The following may provide a way forward and some potentially important directions are suggested:

- The NIL technique presented in this thesis can be adapted for imprinting on flexible substrates such as ones made of poly-di-methyl-siloxane (PDMS), as well as for use in pattern transfer, by lifting the imprinted fishnet from a sacrificial layer. Imprinting into a greater number of metal-dielectric-multi layers, so as to increase the magnitude of the negative refractive index and improve the figure of merit also remains feasible.
- It has been shown that the substrate and cladding layer have a significant effect on the effective properties of metamaterials. The effective refractive index of the fishnet structure formed from nanoimprint lithography has been retrieved by taking into account the effect of substrate which shows a reduction in the magnitude of the negative refractive index obtained by comparison with an unsupported structure. The author suggests that the effect of the substrate or cladding layers should always be taken into account while retrieving negative refractive index and calculating the figure of merit for all the structures providing negative refractive index.
- The determination of angularly-resolved complex reflection and transmission coefficient for a metamaterials slab is complicated. The reasons for the difficulty of obtaining these results from electromagnetic solvers have been indicated. Therefore, an algorithm based on analytical expressions has been proposed to obtain complex reflection and transmission coefficients for range of angles and polarization. The foundation for this formulation has been set by considering separately a dielectric slab

and a metal film of known thickness and material properties. This work has the potential to be extended for the artificial structures.

- An extension of the well-known parameter retrieval procedure toward oblique incidence has been introduced. This provides the opportunity to straightforwardly characterize the optical properties of metamaterials by effective parameters. In order to completely characterize the metamaterials it is necessary to consider bianisotropy at oblique incidence and completely specify all the elements of the tensors for range of angles and polarization.
- For the purpose of experimentally characterizing the fishnet in air, it is feasible that the structure be detached from the substrate allowing it to be suspended in air. This enables the fishnet to be characterized without a conjoining substrate. This is of particular benefit in performing angular resolved reflection and transmission measurements with the aim of experimentally determining the refractive index.

Appendix

Reflectivity and transmissivity results for a dielectric slab with the help of nested parameter sweep are shown. This method can be used to obtain reflectivity and transmissivity of a dielectric slab, metal film or for an artificial structures but it requires huge CPU and memory requirements.

Simulation setup

The dielectric slab is illuminated by a plane wave source over the frequency range from 5 THz to 15 THz. The direction of propagation of source is in negative z direction. The simulation area is a rectangular parallelepiped shape. The calculation region is $100\text{nm} \times 100\text{nm} \times 1000\text{nm}^3$ with a conformal mesh region self-adapted to the structure. A perfectly matched layer is imposed on the edge planes of the simulation area perpendicular to the direction of propagation of source. This boundary condition is an absorbing boundary condition and ideally it should produce zero reflections but in practice there will always be small reflections. These boundary conditions are optimized to absorb light at normal incidence. At grazing angles of incidence, large PML reflections can reduce the accuracy of simulation results. The reflections from this boundary can be reduced by increasing the number of perfectly matched layers. So the steeper injection angles require more PML layers.

6.4.3 Reflection and Transmission coefficients of a dielectric slab

To simplify the problem, a simulation is performed using Lumerical solutions initially for a dielectric slab at oblique incidence by using the parameter sweep method. A nested parameter sweep method is used to achieve these results.

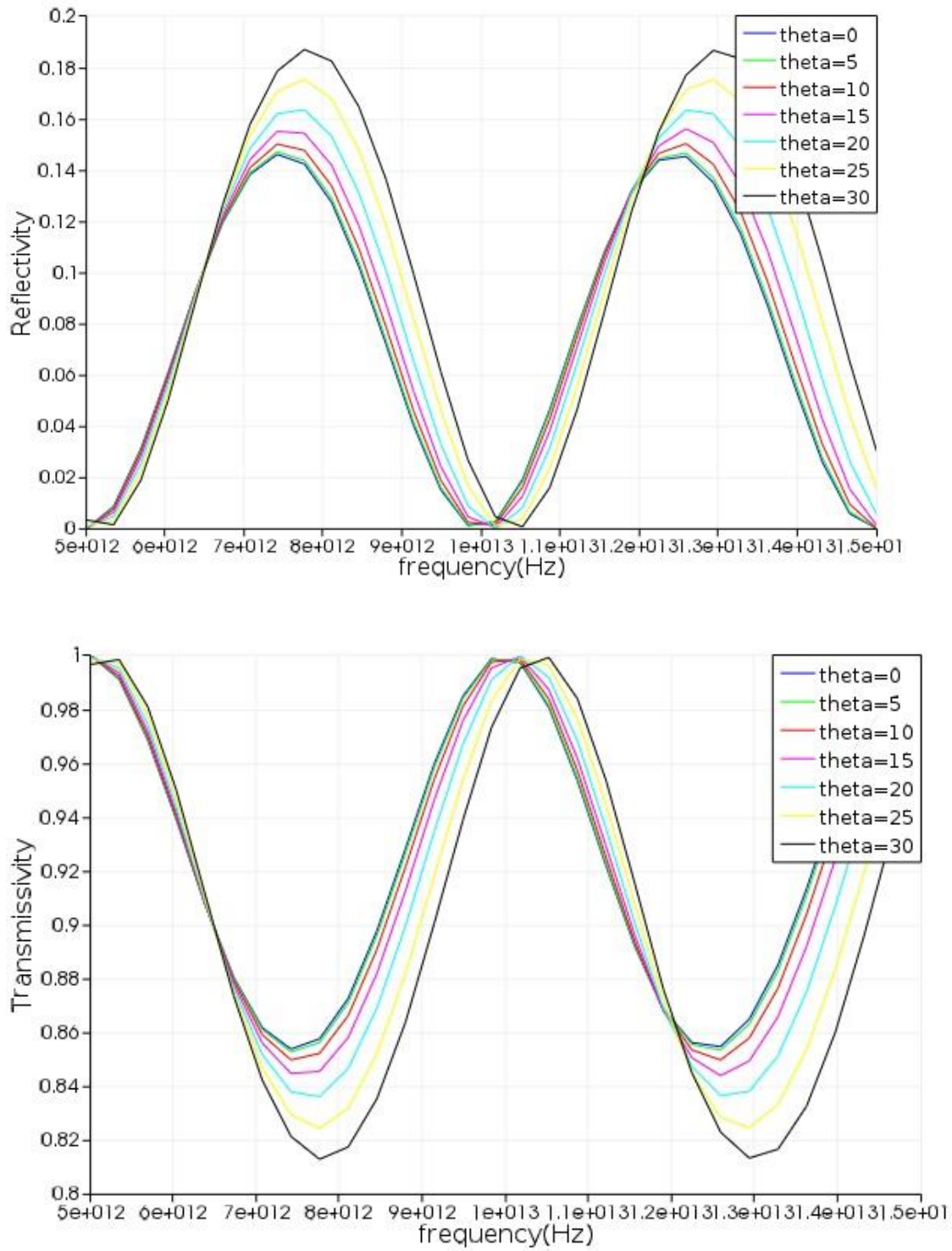


Figure A: a) Reflectivity and b) Transmissivity of a dielectric slab for TE polarization obtained from simulations using parameter sweep method

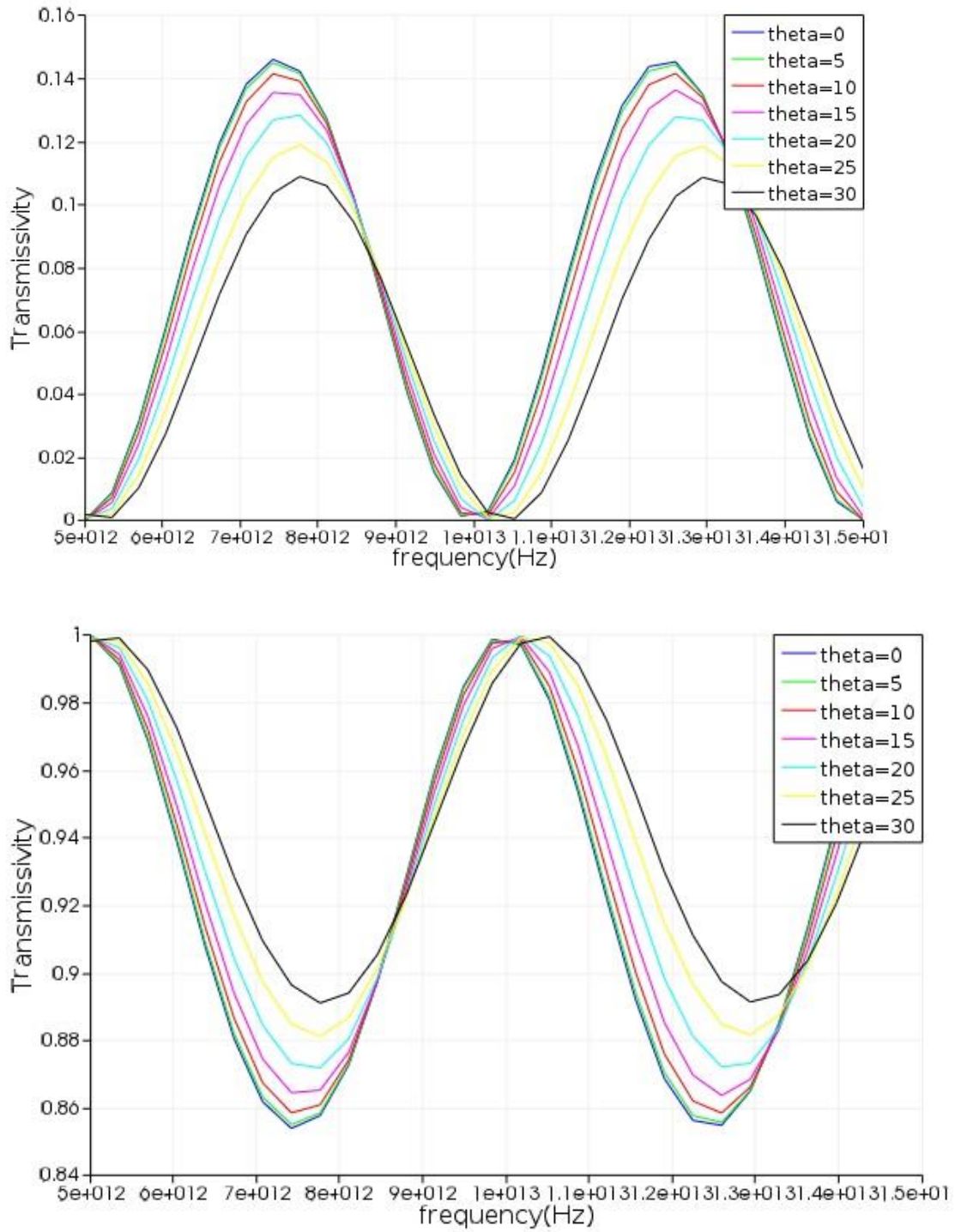


Figure B: Reflectivity and Transmissivity of a dielectric slab for TM polarization obtained from simulations using parameter sweep method.